NPS 67-83-001

NAVAL POSTGRADUATE SCHOOL
Monterey, California

THESIS

PRELIMINARY INVESTIGATION OF ALUMINUM COMBUSTION
IN
AIR AND STEAM

by

Amos Edward Hallenbeck, Jr.

March 1983

Thesis Advisor: Allen E. Fuhs

Prepared for:
Naval Surface Weapons Center
Silver Spring, Maryland

NAVAL POSTGRADUATE SCHOOL
Monterey, California

Rear Admiral J. J. Ekelund
Superintendent

David A. Schrady
Provost

This thesis is prepared in conjunction with research supported in part by Naval Surface Weapons Center under project number N6092183WRW0142.

REPORT DOCUMENTATION PAGE

READ INSTRUCTIONS BEFORE COMPLETING FORM

1. REPORT NUMBER: NPS 67-83-001
2. GOVT ACCESSION NO.:
3. RECIPIENT'S CATALOG NUMBER:

4. TITLE (and Subtitle): Preliminary Investigation of Aluminum Combustion in Air and Steam
5. TYPE OF REPORT & PERIOD COVERED: Master's Thesis; March 1983
6. PERFORMING ORG. REPORT NUMBER: NPS 67-83-001

7. AUTHOR(s): Amos Edward Hallenbeck, Jr.
8. CONTRACT OR GRANT NUMBER(s):

9. PERFORMING ORGANIZATION NAME AND ADDRESS: Naval Postgraduate School, Monterey, California 93940
10. PROGRAM ELEMENT, PROJECT, TASK AREA & WORK UNIT NUMBERS: 62633N, N6092183WRW0142

11. CONTROLLING OFFICE NAME AND ADDRESS: Naval Postgraduate School, Monterey, California 93940
12. REPORT DATE: March 1983
13. NUMBER OF PAGES: 123

14. MONITORING AGENCY NAME & ADDRESS (if different from Controlling Office): Mr. Donald Phillips, Code R102, Naval Surface Weapons Center, Silver Spring, Maryland 20910
15. SECURITY CLASS. (of this report): Unclassified
15a. DECLASSIFICATION/DOWNGRADING SCHEDULE:

16. DISTRIBUTION STATEMENT (of this Report): Approved for public release; distribution unlimited.

17. DISTRIBUTION STATEMENT (of the abstract entered in Block 20, if different from Report):

18. SUPPLEMENTARY NOTES:

19. KEY WORDS (Continue on reverse side if necessary and identify by block number): Aluminum Combustion; Air and Steam; Underwater shaped charges

20. ABSTRACT (Continue on reverse side if necessary and identify by block number):

The goal of the experiment is to understand the role of metal-steam combustion in the explosion of underwater shaped charges. An apparatus was constructed to investigate combustion of aluminum in steam. For background information, aluminum wires (1 mm diameter, 50 mm length) were ignited in air by high current (480 amperes). Tests in air and steam were photographed using 35 mm color slides and 16 mm movies (4300 frames/sec).

Two types of diffusion flames associated with the complete wire were observed, one type of diffusion flame had diffuse pale blue radiation centered on the wire, and another type of flame had intense yellow radiation above the wire. Also, radiation from the wires was measured using Photomultiplier Tubes. Ejected aluminum particles exhibit different combustion properties depending on the environment, air or steam. Particles in air attain velocities of 7 to 11 meters/second and exhibit erratic trajectories before burn out. Particles in steam move at slower speed (2 to 4 m/sec); the particles burn out and re-ignite.

Approved for public release; distribution unlimited.

Preliminary Investigation of Aluminum Combustion in Air and Steam

by

Amos Edward Hallenbeck, Jr.
Lieutenant Commander, United States Navy
B.A., State University of New York at Oneonta, 1966
M.S.A., George Washington University, 1977

Submitted in partial fulfillment of the requirements
for the degree of

MASTER OF SCIENCE IN AERONAUTICAL ENGINEERING

from the

NAVAL POSTGRADUATE SCHOOL
March 1983

ABSTRACT

The goal of the experiment is to understand the role of metal-steam combustion in the explosion of underwater shaped charges. An apparatus was constructed to investigate combustion of aluminum in steam. For background information, aluminum wires (1 mm diameter, 50 mm length) were ignited in air by high current (480 amperes). Tests in air and steam were photographed using 35 mm color slides and 16 mm movies (4300 frames/sec). Two types of diffusion flames associated with the complete wire were observed, one type of diffusion flame had diffuse pale blue radiation centered on the wire, and another type of flame had intense yellow radiation above the wire. Also, radiation from the wires was measured using Photomultiplier Tubes. Ejected aluminum particles exhibit different combustion properties depending on the environment, air or steam. Particles in air attain velocities of 7 to 11 meters/second and exhibit erratic trajectories before burn out. Particles in steam move at slower speed (2 to 4 m/sec); the particles burn out and re-ignite.

TABLE OF CONTENTS

LIST OF TABLES

LIST OF FIGURES

I. INTRODUCTION

Research in the explosion underwater of shaped charges containing aluminum liners has indicated the combustion of aluminum. Simulation of underwater detonation of shaped charges requires duplication of several conditions in order to obtain valid results. Many different physical phenomena occur during the explosion of an underwater shaped charge including shock waves from the explosion, shock waves from the metal jet and reflected shock waves; see, for example, Hains [Ref. 1]. The penetration of the metal jet involves a wide range of pressure extending from 100 kilobars to near vacuum. Many of these phenomena are discussed by Strott and Buck [Ref. 2]. To provide a foundation for the interpretation of the extensive experimental results of Strott and Buck [Ref. 2], and other experimental results, information is needed on combustion of aluminum in water or steam. The information which is desired includes ignition temperature as a function of aluminum particle size, particle temperature, and steam temperature and pressure. Also, the rate and extent of combustion is needed as a function of aluminum particle size, etc. In order to play a significant role in the behavior of underwater shaped charges, a major fraction of the aluminum must be burned.

Research using exploding wire techniques has been conducted for several years. Baker and Liimatainen [Ref. 3]

compiled the results of research conducted on aluminum, zirconium, stainless steel, and uranium. The research involved the investigation of metal-water and metal-air explosive reactions which could occur during nuclear reactor accidents. Wilson and Martin [Ref. 4] heated pellets of aluminum in flowing steam and observed the burning rate and ignition temperature of the aluminum. Aluminum ignition was achieved at various times, ranging from 18 to 0 minutes at temperatures from 1600 to 1750 C, respectively, with immediate ignition occurring at 1750 C.

Webb, Hilton, Levine, and Tollestrup [Ref. 5] conducted research involving silver, gold, copper, aluminum, tin, cadmium, zinc, molybdenum, titanium, platinum, nickel, iron, and tungsten wires in air, vacuum, and oil environments. Their research involved the rapid exploding of the test wires using high voltage capacitor discharges under normal temperature and pressure conditions. Explosions in the wires occurred within several nanoseconds of capacitor discharge.

To achieve the desired conditions of high temperature and pressure of the steam, a test apparatus was designed and built that would allow the burning of aluminum wire in a pressurized, pure steam atmosphere at temperatures up to 200 C. Aluminum wires were mounted within this device, and sufficient electrical energy to ignite the wires was provided. The events which occurred were recorded on high speed movie film. The current through the wire test specimen and the change in voltage in

the circuit were measured and recorded using a wave-form recorder and dual beam oscilloscope. Two photomultiplier tubes were positioned to measure the intensity of the visible flash and the intensity within a narrow spectral band at which aluminum oxide (AlO) radiates. A narrow band optical filter with a band center at 480.0 nanometers and a half band width of 7.1 nanometers was used. The wavelength occurs in the blue portion of the visible spectrum.

II. THE APPROACH

A. SELECTION OF EXPERIMENTAL METHOD

The purpose of this experiment was to observe the various phenomena which occurred when heated aluminum wire suspended in a pure steam atmosphere at a specified temperature was subjected to rapid electrical heating.

Various experimental methods have been utilized to examine the reactions of heated aluminum in water and/or steam. Long [Ref. 6] discharged 50 pound samples of pure molten aluminum into steel tanks of water and observed violent explosions even though the metal temperature never exceeded 900 C. Higgins [Ref. 7] used blasting caps to disperse molten aluminum streams under water. Precise measurement of the reactions which occurred was not possible with these methods.

The "exploding wire" technique as described by Chace and others [Ref. 8] allows the investigation of metal-water or metal-steam reactions in a more easily controlled environment. Pressure and temperature of the steam can be regulated to establish the desired test conditions. High speed movie cameras and digital recorders can record the reactions. Hence, the exploding wire technique was selected for the tests reported here.

B. HEATING OF THE WIRE

The total energy required to change aluminum at 200 C into vapor at the boiling point of aluminum (2494 C) is determined by the following equation:

$$e = \int_{T_o}^{T_m} c_{p1}\, dT + h_F + \int_{T_m}^{T_b} c_{p2}\, dT + h_V \qquad (1)$$

where e is the total specific energy (J/gm), T_c is the initial temperature of the aluminum, T_m is the melting point of aluminum (660.4 C), T_b is the boiling point of aluminum (2494 C), h_F is the heat of fusion (397 J/gm), h_V is the heat of vaporization (10.78 kJ/gm), c_{p1} is the specific heat of solid Al and c_{p2} is the specific heat of liquid Al. Both c_{p1} and c_{p2} are functions of temperature; however, constant values were used. A value of 0.9 J/gm K was used for c_{p1} which is the value at 25 C. For c_{p2}, a value of 1.18 J/gm K was used which is the magnitude at 660 C, as listed in Ref. 9.

The energy released due to the combustion of aluminum is determined by the equation:

$$E = m h_C \qquad (2)$$

where m is the mass of aluminum burned and h_C is the heat of combustion of aluminum (31.05 kJ/gm), as listed in Ref. 9.

The electrical energy transferred to the wire was determined using the equation:

$$e = \int_o^t VI\, dt \qquad (3)$$

where V is the voltage at the positive post of the test circuit, I is the current through the wire, and t is the time required for the rupture of the wire.

Careful weighing of the sample test wires before and after the experiment allowed determination of the amount of aluminum that disappears. Knowing the mass of aluminum removed from the wire, an estimate of the energy to heat the wire can be made. Comparisons of the amount of energy required from equation (1) to that of equation (3) provided an idea of how much energy was lost in the electrical circuitry of the test apparatus.

Assuming that the specific heat of solid and liquid aluminum remains constant, that the temperature of the entire sample was increased to the melting point, and that all of the missing sample was melted and vaporized, a calculation of the total energy required to vaporize the wire using equation (1) was made. Using a sample test wire 1 mm diameter and 65 mm long, 106.9 Joules were required to (1) heat the entire sample to the melting point, and (2) melt, vaporize, and ignite a 1 mm piece of the aluminum wire; the calculations appear in Appendix A.

Using test data values for the voltage across the wire, current through the wire, and the time for ignition of the wires, the electrical energy required to rupture and ignite the wire was calculated using equation (3). For a typical test in air, the measured voltage, V, was 8 volts; the current, I, as

a function of time, can be expressed as the equation: $I(t) = 480 - 60t/.076$; and the time for ignition was measured to be 76 milliseconds. The electrical energy required to rupture and ignite the aluminum test wire was determined to be 274 Joules.

Comparing the results of equation (3) to those of equation (1) indicates approximately 167 Joules difference in the electrical energy supplied and the energy required to vaporize the aluminum wire. Some of the remaining energy is lost in the resistance of test wire circuitry. Number 1 gauge Copper cable has a resistivity of 16.73 nanoohm-meters, and 304 stainless steel has a resistivity of 72 nanoohm-meters as specified in Ref. 10. 1.3 meters of Copper cable connect the test wire holder assembly to the shunt and 0.48 meters of one-quarter inch stainless steel rod is used for the test wire holder. Calculation of the energy dissipated within the resistance of these materials accounts for an additional 40.6 Joules of energy.

Additional electrical energy losses are the creation and heating of the plasma during the wire rupture and an unknown quantity of kinetic energy imparted to the aluminum particles released at the instant of wire ignition.

C. HEAT RELEASED BY COMBUSTION COMPARED TO THE ELECTRICAL ENERGY

An interesting comparison is that between the energy released by combustion of the small segment of aluminum wire

and the electrical energy transferred to the wire. The energy released by combustion of the missing 1 mm of aluminum was calculated using equation (2) to be 65.8 Joules. The electrical energy of 106.9 Joules applied to the aluminum wire is considerably more than that released by complete combustion of an equivalent mass of wire.

III. THE APPARATUS

A. THE PRESSURE VESSEL

Figure 1 is a photograph of the pressure vessel which consisted of a twelve-inch high stainless steel cylinder, 10.75 inches diameter, with four, evenly spaced, 5 inch diameter observation ports welded into its circumference. One-inch thick, schlieren quality, Borosicalate Crown glass (BK-7) was installed in the ports using Viton gasket material to prevent breakage of the glass and loss of pressure within the vessel. The observation ports have not been installed in Figure 1.

The top and bottom flanges of the vessel were grooved to hold Viton o-rings which prevented loss of pressure during system operation. The top plate was drilled to provide access for two thermocouples, two pressure sensors, a vacuum tube, the test wire holder assembly, and a pressure relief safety valve. Two thermocouple connectors can be seen at the top of Figure 1. The pressure relief safety valve was designed to release pressure at 150 psia. Swagelok, self-seating, fittings were used to provide positive pressure seals wherever required. The bottom plate was drilled to provide access for one thermocouple and a low point water supply/drain valve. The entire pressure vessel and its various fittings were designed to withstand maximum pressures of 200 psia.

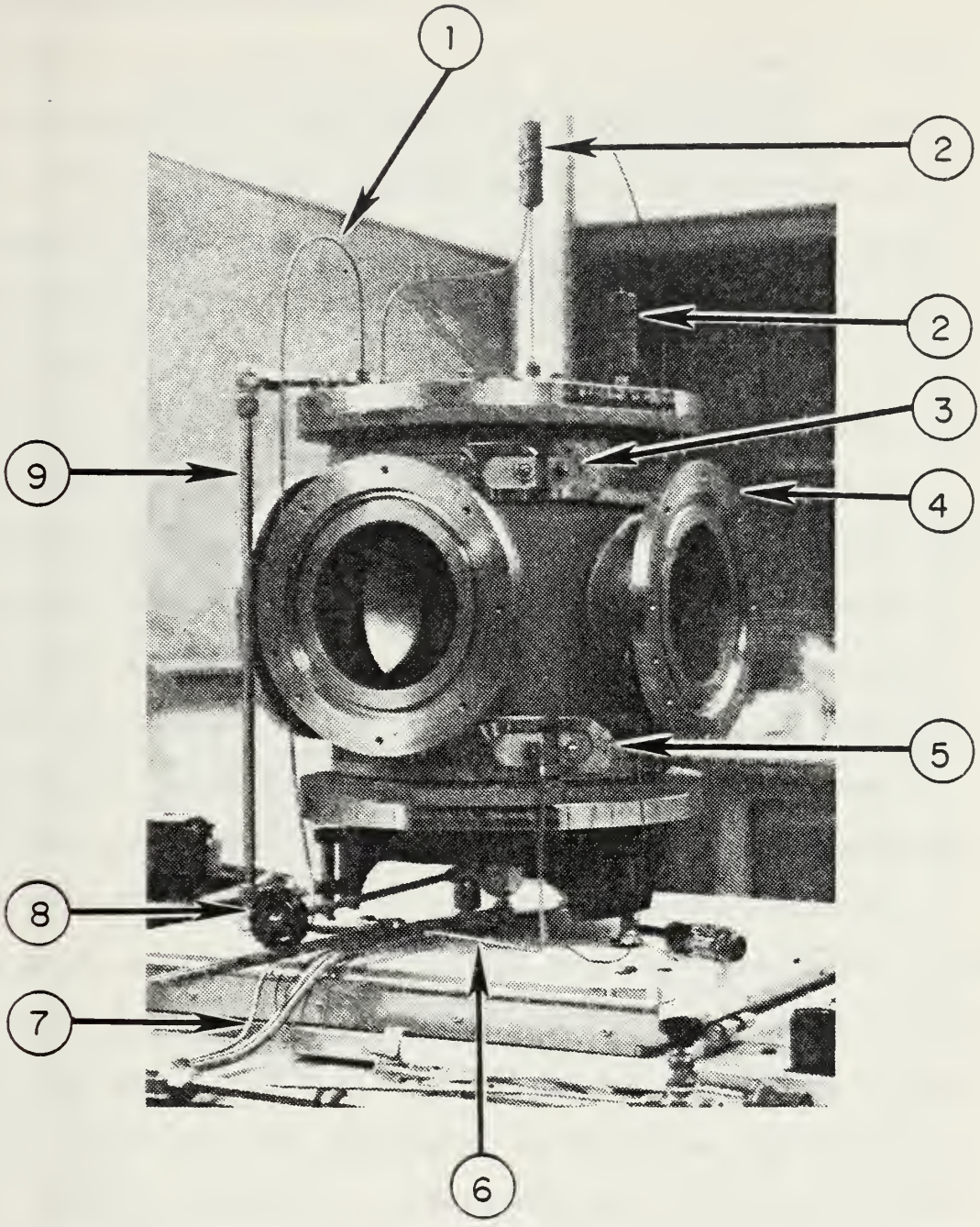

Figure 1. The Pressure Vessel

(1) Tubing for Heise Pressure Gauge, (2) Thermocouple connector, (3) Watlow band heater, (4) Observation port; one of four, (5) Watlow band heater, (6) Power cable for band heaters, (7) Drain and fill pipe for water, (8) Control for Supply/drain Valve, (9) Vacuum tube.

B. THE TEMPERATURE CONTROL SYSTEM

Figure 2 is a photograph of the pressure vessel showing the two Watlow, two-inch wide, 240 volt, 2000 watt, band heaters used to heat the apparatus to operating temperature. The heaters were connected via two, twenty-five amp, solid state relays, as shown in Figure 3, to an Omega, Model 157, two set point, digital controller, shown in Figure 4. The controller allowed rapid heating of the entire assembly with a continuous digital display of the process temperature throughout the heating cycle. Copper-constantin, washer type, thermocouples monitored the temperature of the apparatus at six points on the stainless steel cylinder. Three, copper-constantin, twelve inch, probe type, thermocouples measured the internal temperature of the apparatus at three levels within the cylinder. Figure 5 is a drawing of the pressure vessel with the positions of the thermocouples indicated. Temperature sensing for the heaters was supplied to the digital controller by thermocouple number eight located at the center of the cylinder. Two, Wahl, thermocouple thermometer, digital display units allowed monitoring of all nine thermocouple points, shown in Figure 6. Incidentally, the firing switch also appears in Figure 6. Figure 7 is a drawing of the electrical circuit for the temperature control system.

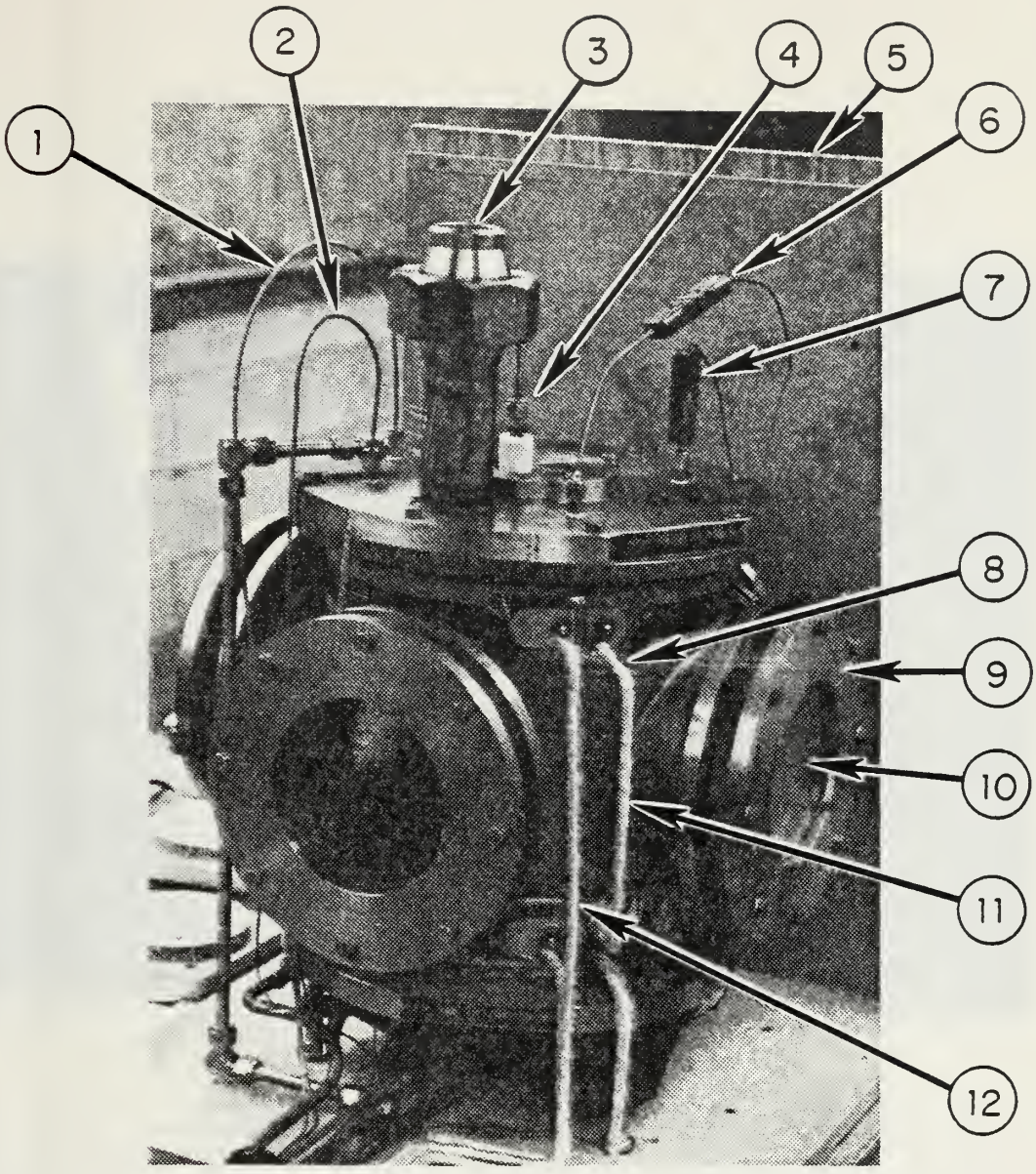

Figure 2. Pressure Vessel with Additional Parts Assembled

(1) Tubing for Heise Pressure Gauge, (2) Tubing for Pressure Transducer, (3) Pressure Relief Valve, (4) Positive Terminal for aluminum wire sample showing teflon insulator, (5) Side of wooden box with NCFR insulation, (6) Thermocouple #9, (7) Thermocouple #8, (8) Upper Watlow band heater, (9) Retaining ring for observation port, (10) Glass port, (11) Ground side of heater circuit, (12) "Hot" side of heater circuit

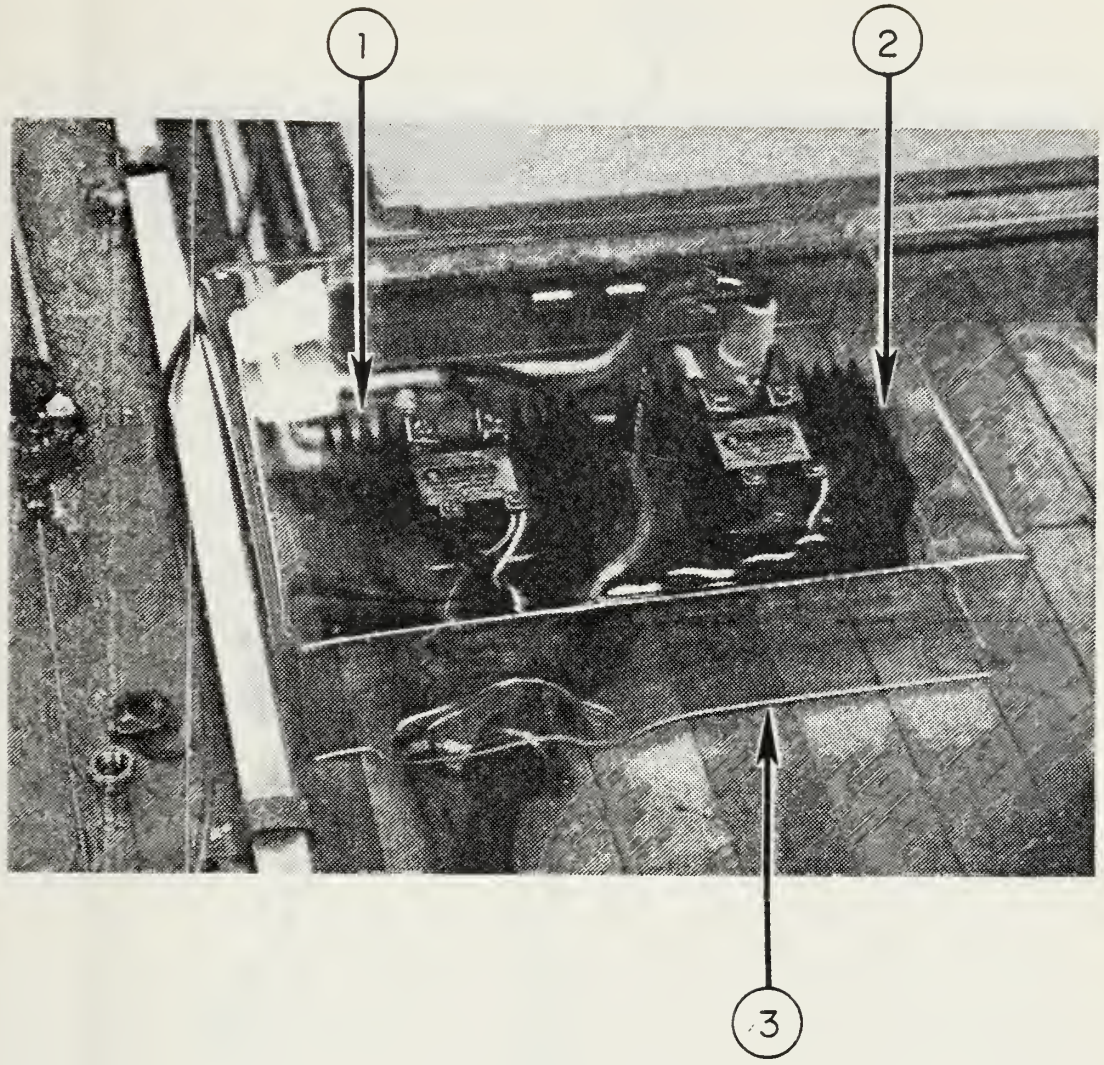

Figure 3. The Solid State Relays

(1) Heat sink for solid state relay, (2) Heat sink for second solid state relay, (3) Plastic safety cover.

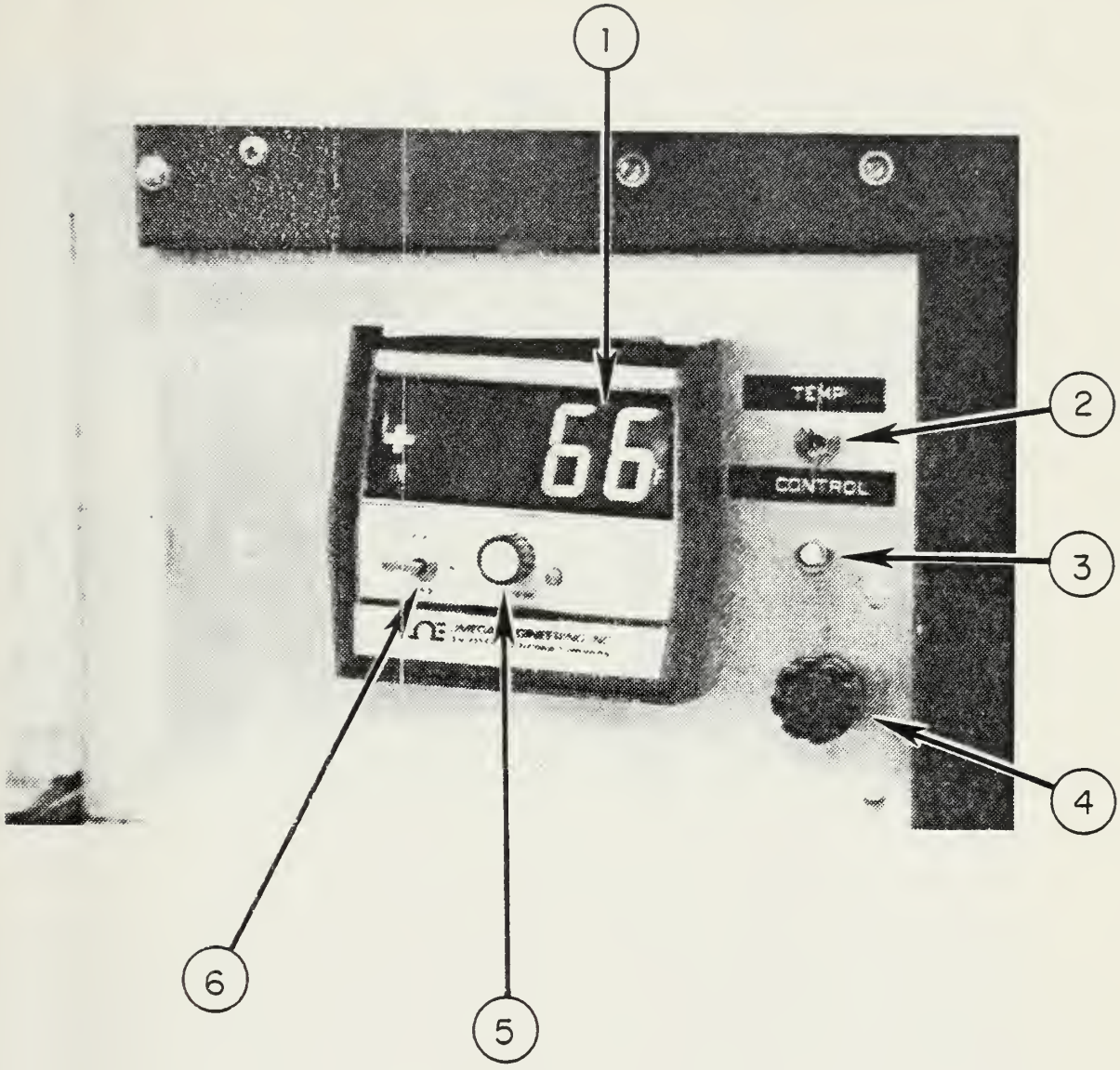

Figure 4. Omega, Model 157, temperature controller

(1) Temperature display showing temperature of thermocouple #8 which was used for control, (2) Switch for temperature controller, (3) Indicator lamp for power switch, (4) Fuze protection for temperature controller, (5) Control knob for setting temperature, (6) Switch for displaying set point temperature.

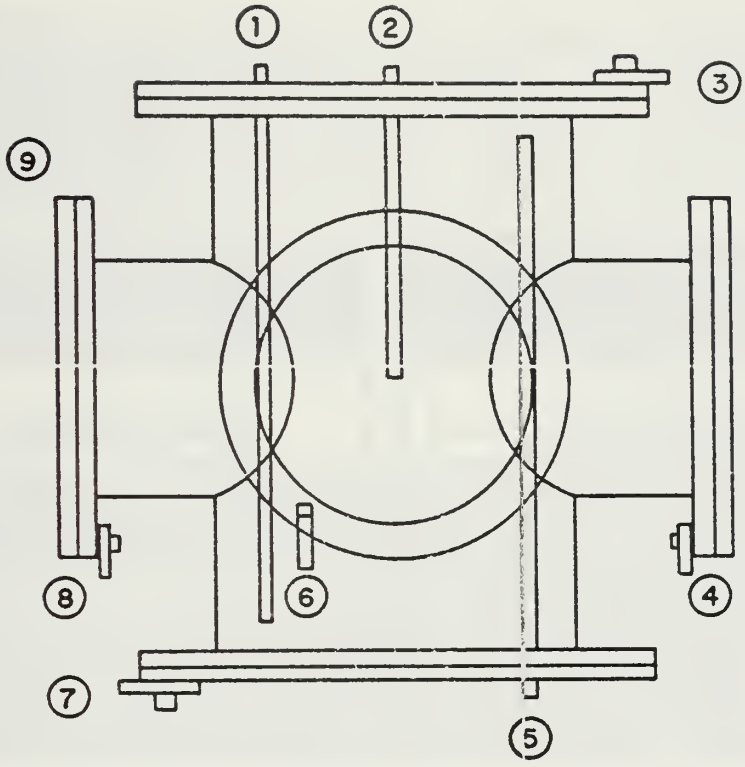

Figure 5. Thermocouple Locations

(1) Internal temperature at bottom of vessel, (2) Internal temperature at center of vessel; also used for temperature control, (3) Top of pressure vessel, (4) Port #3, (5) Internal temperature at top of vessel, (6) Port #4, (7) Base of vessel, (8) Port #1, (9) Port #2; at back of vessel in this position.

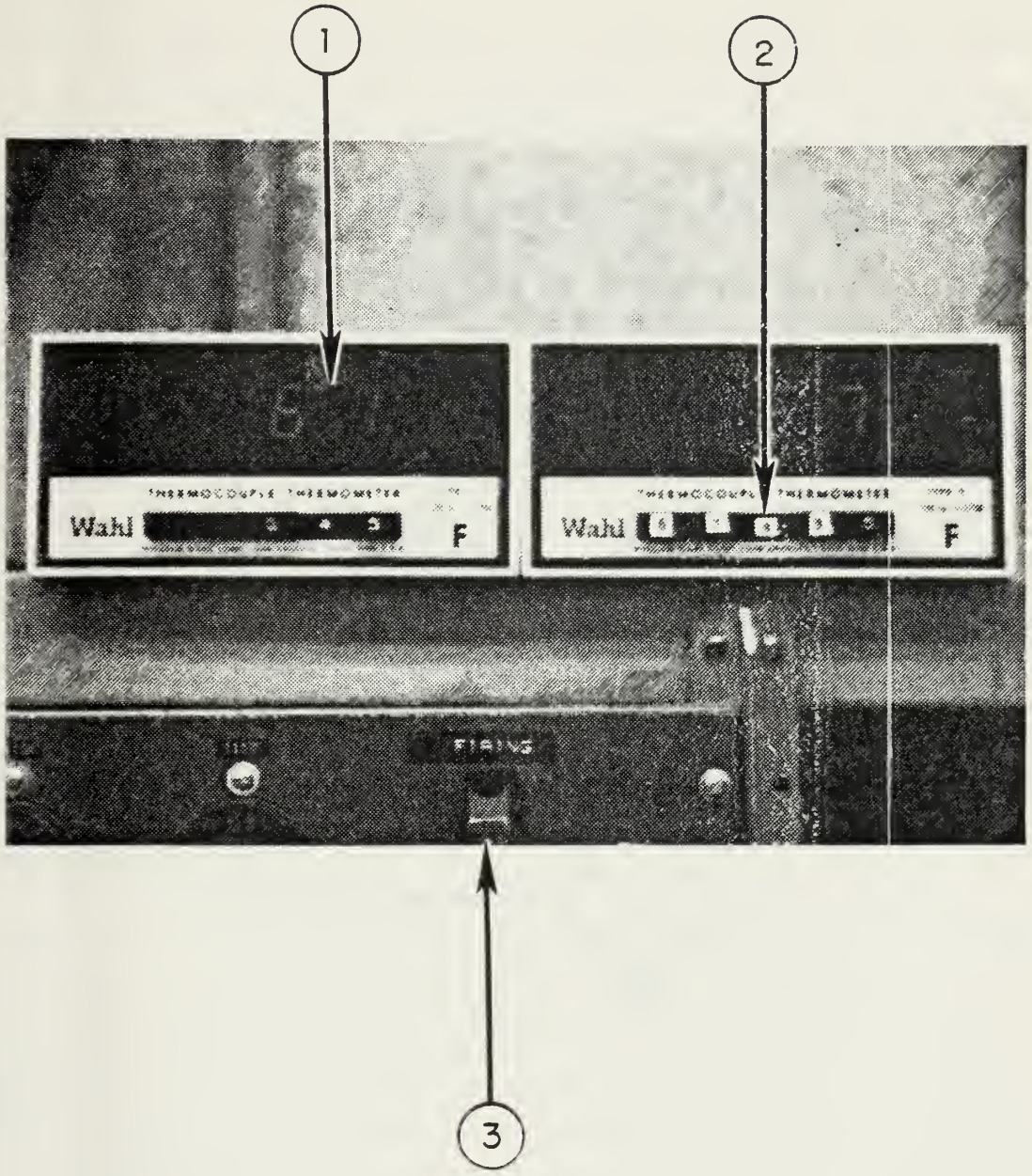

Figure 6. Wahl digital thermocouple thermometers.

(1) Digital display, (2) Channel selector; 5 channels for each thermometer, (3) Firing switch with protective cover.

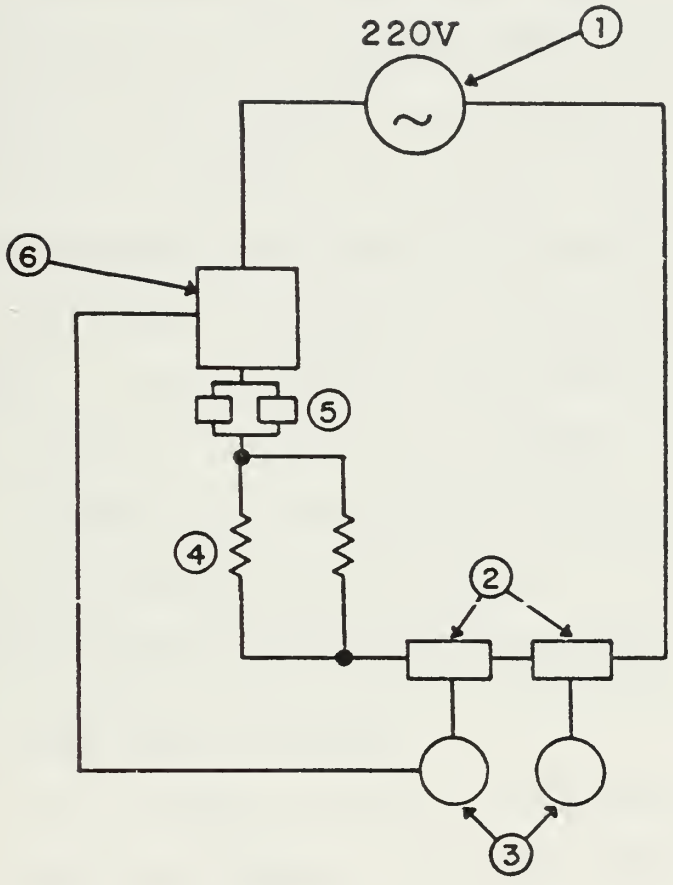

Figure 7. The Temperature Control System

(1) 220 Volt AC Power Supply, (2) Thermocouples, (3) Digital Thermocouple Thermometers, (4) Band Heaters, (5) Solid State Relays, (6) Temperature Controller.

C. THE INSULATION SYSTEM

The apparatus was mounted on a three-legged, steel stand, and the entire assembly was enclosed in an insulated wooden box. The box was hinged on three sides, had a sliding fourth side, and a removable top. Homasote, NCFR insulation board, 15/32 inch thick, with a thermal conductivity of 0.059 BTU/ hr.ft^2 F, was used to reduce heat losses to the surrounding atmosphere. Removable insulated covers provided easy access to all four observation ports and to the removable test wire holder assembly. A small cutout in the sliding side of the box provided access for all wiring, pressure, and water connections. Figure 8 is a photograph of the pressure vessel installed in the insulated box showing the hinged sides and the observation ports with the covers removed.

D. THE TEST WIRE HOLDER ASSEMBLY

The test wire assembly, Figure 9, consisted of a one-half inch thick, five inch diameter, stainless steel plate, drilled every 90 degrees around its circumference; two one-quarter inch stainless steel rods; a Teflon insulation sleeve and assorted bolts, washers, and springs designed to hold two inch long test wire samples. The Teflon sleeve provided electrical insulation for the positive post of the test wire holder. The stainless steel posts were drilled to hold one millimeter diameter test wires. The steel washers, springs, and nuts provided a positive constant pressure on the test wires without creating high resistance areas in the wire

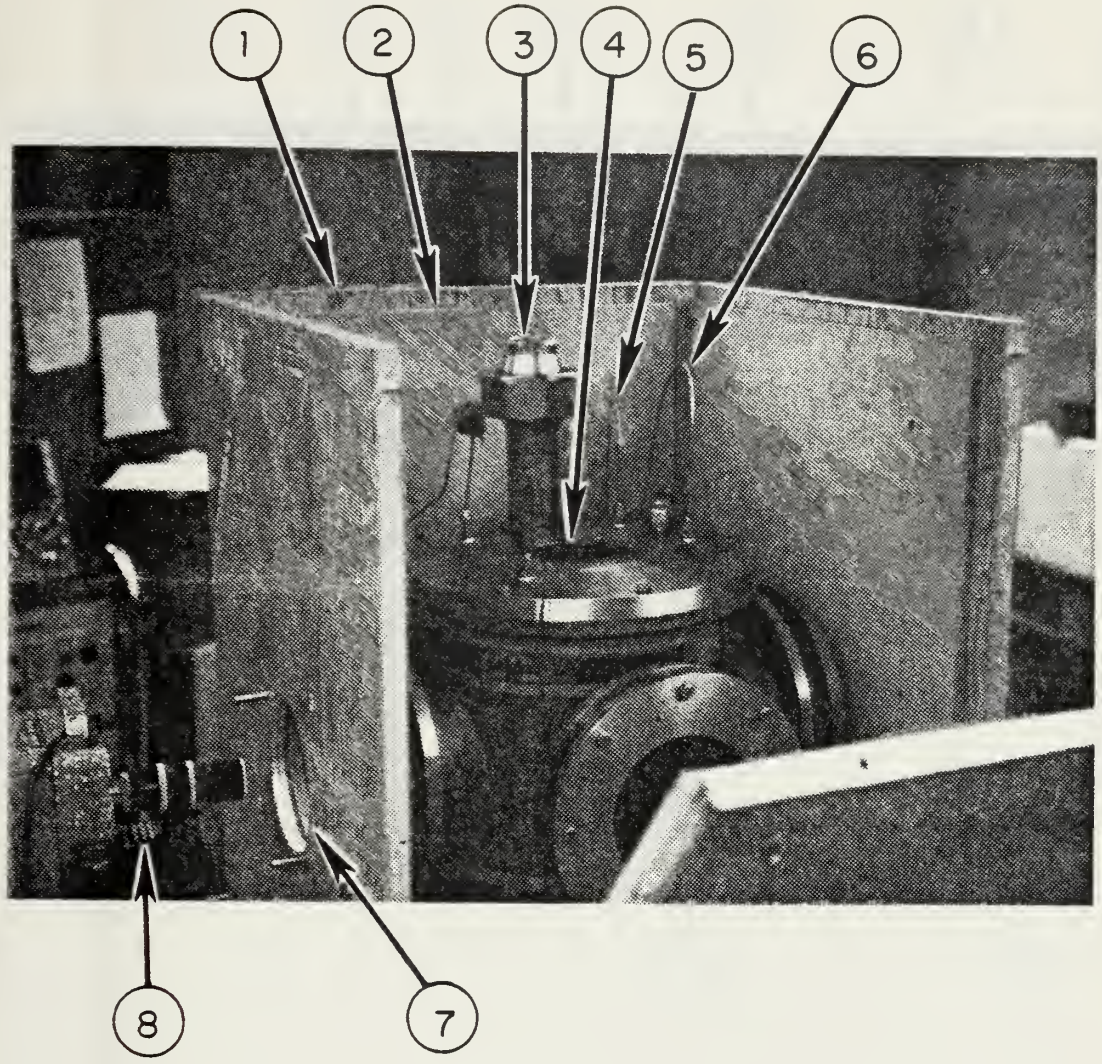

Figure 8. The Insulated Box

(1) Plywood box, (2) Homasote insulation installed on inside of plywood surface, (3) Pressure release valve, (4) Opening for test wire holder assembly (test wire holder assembly is not installed), (5) Tubing for pressure gauge, (6) Tubing for pressure transducer, (7) Observation hole in insulated box normally covered by insulated cover, (8) High speed 16 mm movie camera.

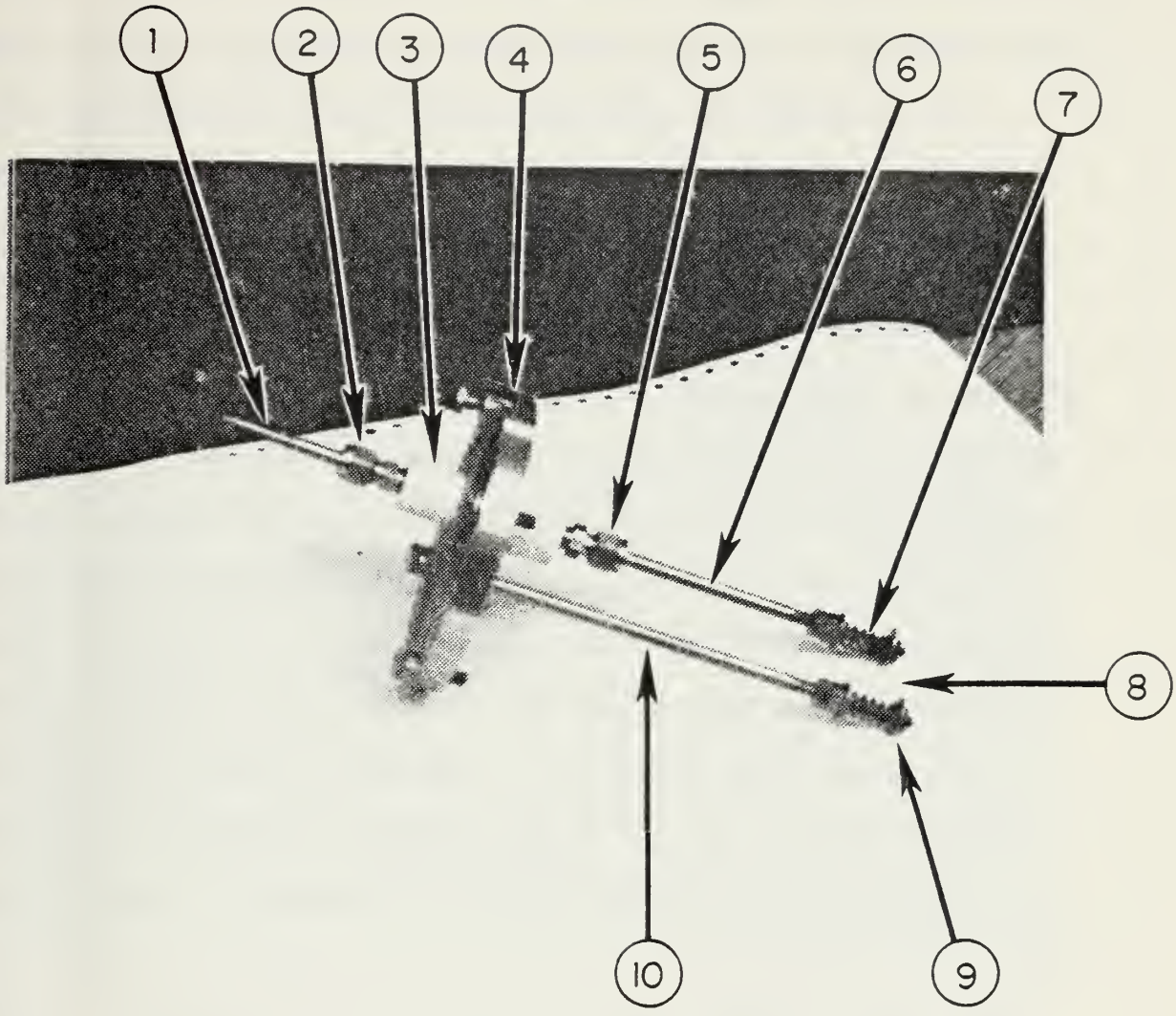

Figure 9. The Test Wire Holder Assembly

(1) Positive electrode of wire holder, (2) Swagelok fitting for pressure seal, (3) Teflon insulator, (4) Cover plate, (5) Swagelok fitting, (6) Portion of the positive electrode within the pressure vessel, (7) Spring for holding test wire, (8) Two inch gap which is spanned by test wire, (9) Washer which contacts test wire, (10) Negative (grounded) electrode.

samples. The top plate of the pressure vessel was drilled and tapped every 45 degrees to allow positioning of the test wire holder assembly in any of four positions relative to any observation port.

E. TEST WIRE ELECTRICAL CIRCUIT

The test wire circuit consisted of the test wire holder assembly, two twelve volt batteries, a twelve volt automobile type starter solenoid, a shunt, battery cables and a firing switch. Figure 10 is a photograph of the batteries, shunt and starter solenoid. AWG 1, battery cable led from the positive terminal of the marine type, heavy duty, twelve volt battery, through the solenoid, to the positive electrode of the test wire holder assembly. The negative lead of the battery was connected through the shunt to a common ground leading from the apparatus. Power for the solenoid was supplied through the firing switch by the second twelve volt battery. Figure 11 is a drawing of the complete test wire electrical circuit. A coaxial cable provided signals from the shunt to a dual-beam oscilloscope or to one channel of a digital recorder which recorded the current in the circuit as the test wire was energized. A second coaxial cable attached to the positive electrode of the test wire holder assembly provided signals for measuring the voltage in the test wire circuit. A third connection to the positive terminal of the solenoid provided the trigger signal for the dual-beam oscilloscopes and digital recorder.

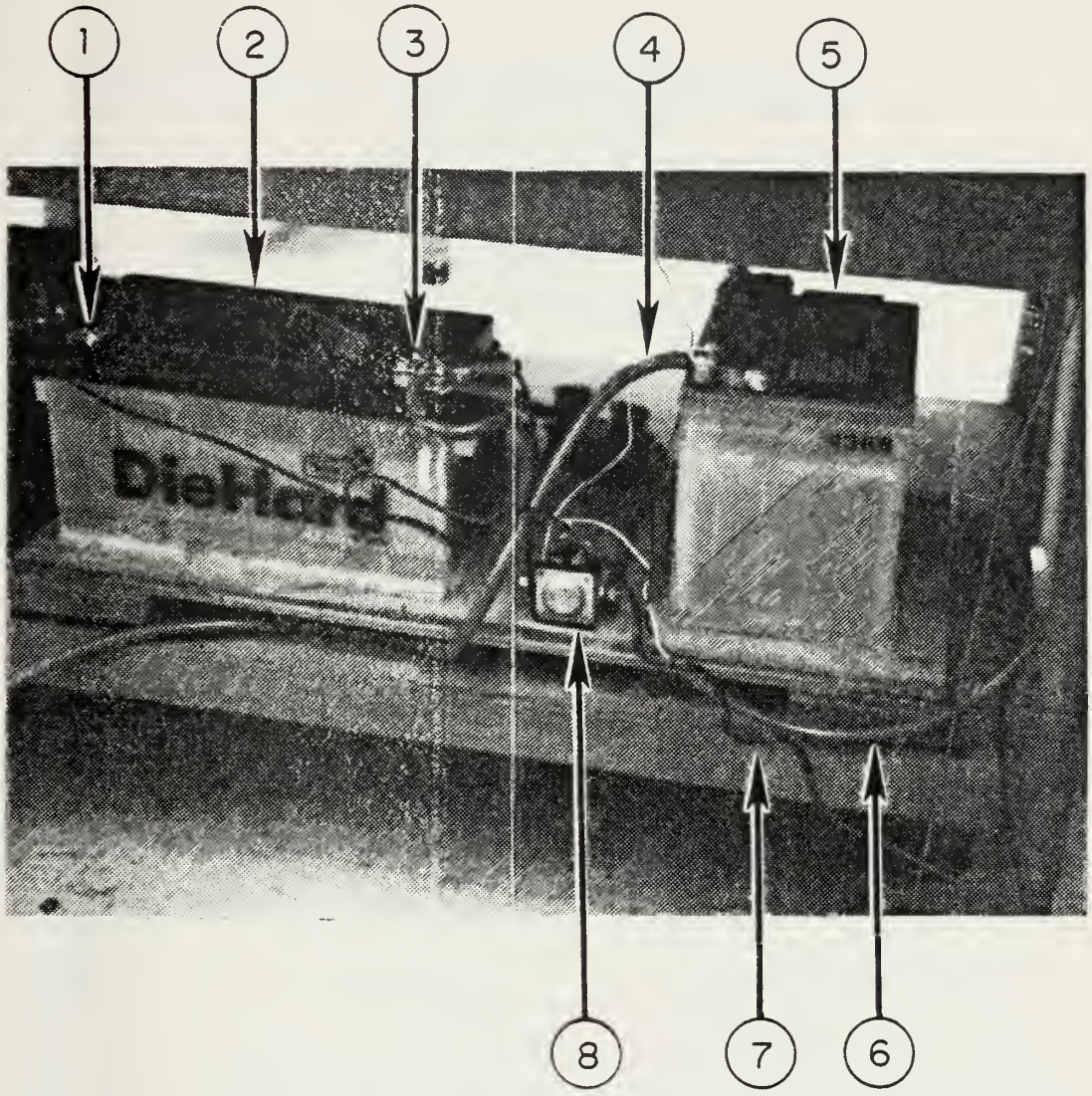

Figure 10. Power Supply for Test Wire Circuit

(1) Negative terminal of battery, (2) Battery supplying energy to the test wire, (3) Positive terminal, (4) Grounding cable from battery supplying energy to starter solenoid, (5) Battery which activates solenoid, (6) Electrical wires attached to solenoid that lead to firing switch, (7) Battery charger cable, (8) Automobile-type starter solenoid.

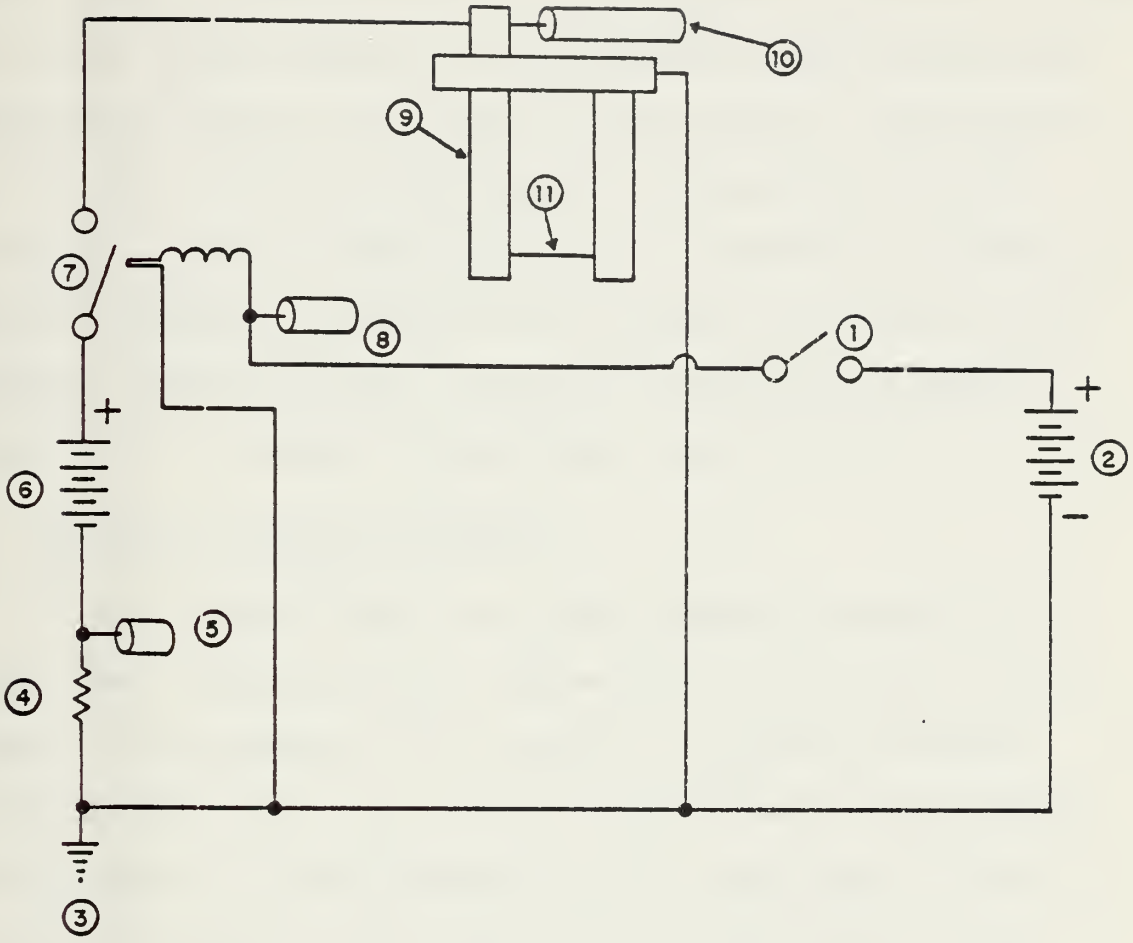

Figure 11. Diagram of Test Wire Circuit

(1) Firing Switch, (2) 12 Volt Battery; provided electrical energy for Firing Switch, (3) Common Ground Point for entire circuit, (4) Shunt, (5) Coaxial Cable to measure current through the wire, (6) 12 Volt Battery; provided electrical energy for test wire, (7) Solenoid, (8) Coaxial Cable to trigger wave-form recorder, (9) Test Wire Holder Assembly, (10) Coaxial Cable to measure voltage across wire, (11) Aluminum Test Wire.

F. THE WATER SUPPLY SYSTEM

A five gallon, plastic, water container provided pure, oxygen free, distilled water by gravity feed, through a stainless steel piping system to the pressure vessel through the supply/drain valve in the base of the vessel. See Figures 1 and 2. Two 50 cc syringes mounted in the piping system provided a means of supplying specific measured quantities of distilled water. A nitrogen flow across the ullage of the reservoir maintained the oxygen free state of the water. Figure 12 is a diagram of the water supply system.

G. THE VACUUM/PRESSURE SYSTEM

Air was removed from the closed pressure vessel by a vacuum pump connected to an access port in the top of the vessel. See component 9 in Figure 1. A Heise pressure gauge allowed monitoring of the system pressure throughout this process. A valve located in the vacuum pump tubing allowed isolation of the vacuum pump during the testing sequence. A similar valve in the Heise pressure gauge tubing prevented accidental damage to the gauge during testing. See component 1 in Figure 1. A fast response pressure transducer connected to a digital voltmeter provided a means of measuring the absolute pressure within the vessel. A minimum pressure of 3.7 psia was achieved using this system with a pumping time of 5 minutes. Table 1 is the results of the calibration of the fast response pressure transducer using the Heise pressure gauge as the standard.

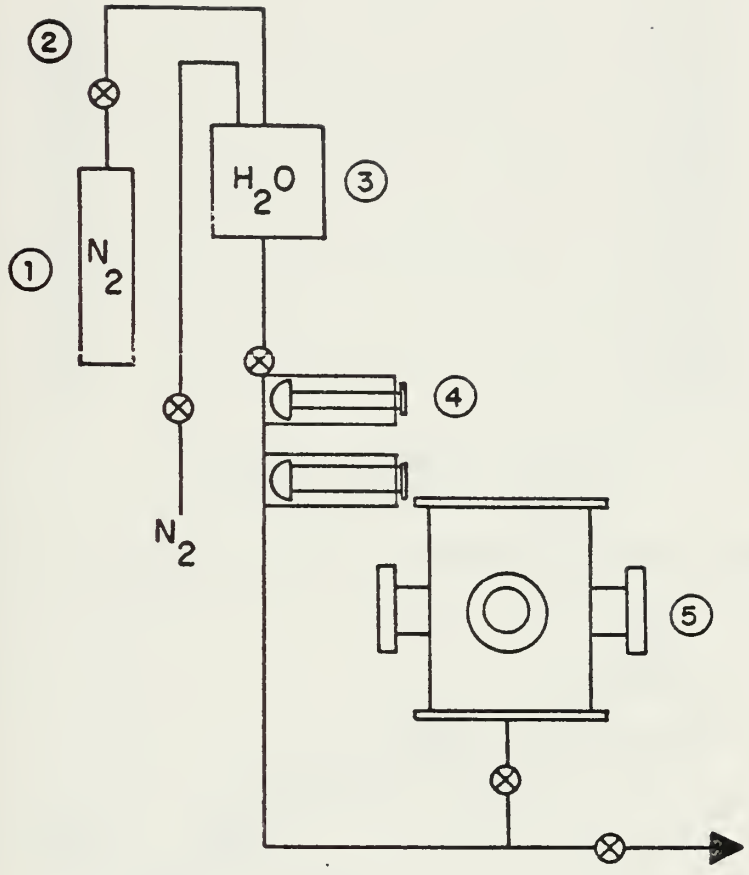

Figure 12. Diagram of Water Supply System

(1) Nitrogen Supply, (2) Shut-Off Valve, (3) Five Gallon Distilled Water Container, (4) Two 50 cc Syringes, (5) Pressure Vessel.

Table 1. Pressure Transducer Calibration

Heise Gauge Pressure (psig)	Digital Voltmeter (volts)
0	0.030
5	0.072
10	0.114
15	0.156
20	0.198
25	0.240
30	0.282
35	0.325
40	0.367
45	0.410
50	0.455
55	0.496
60	0.539

1 psi = 0.00845 volts

Figure 13 is a diagram of the vacuum/pressure system.

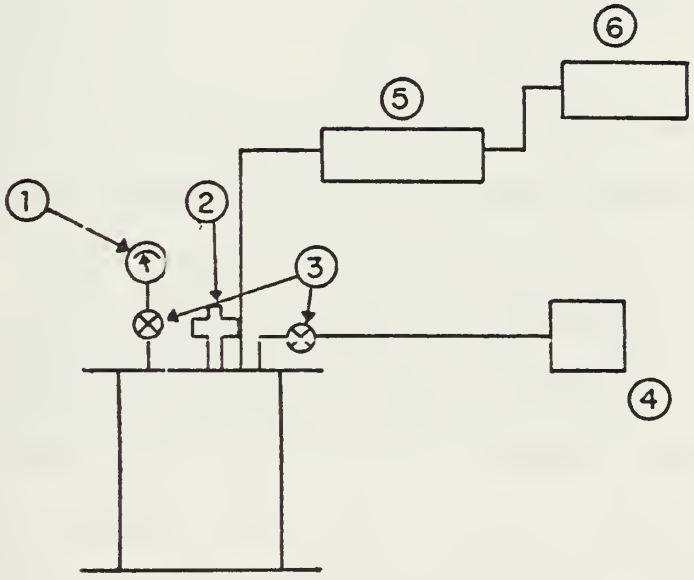

Figure 13. Diagram of Vacuum/Pressure System

(1) Heise Pressure Gauge, (2) Pressure Relief Safety Valve, (3) Isolation Valves, (4) Vacuum Pump, (5) Pressure Transducer, (6) Digital Voltmeter.

IV. INSTRUMENTATION

A. BIOMATION DIGITAL WAVE-FORM RECORDER

A Biomation digital wave-form recorder, shown in Figure 14, containing 4096 words of memory capability, allowed storage and reproduction of the signals received from the photomultiplier tubes and the current and voltage signals from the test wire circuit. The recorder could be used as a one channel/4096 word recorder, a two channel/2048 word recorder, or as a four channel/1024 word recorder. The recorder could be connected to a standard X,Y plotter to provide graphic reproduction of the stored signals. It could also be connected to an oscilloscope with a Polaroid camera attachment for photographic reproduction of the test signals.

The electrical current through the shunt was measured and recorded on one channel of the wave-form recorder. The change in voltage through the test wire was measured and recorded by a second channel of the recorder. The remaining two channels of the recorder were used to record signals from the photomultiplier tubes. For the testing sequence, the recorder was used as a two channel/2048 word, recorder which allowed recording and direct comparison of signals from the photomultiplier tubes. Various voltages were selected for best comparison of the signals from the PMT. A selectable time delay within the recorder allowed selection of the portion of the time interval to be recorded. Since ignition did not occur

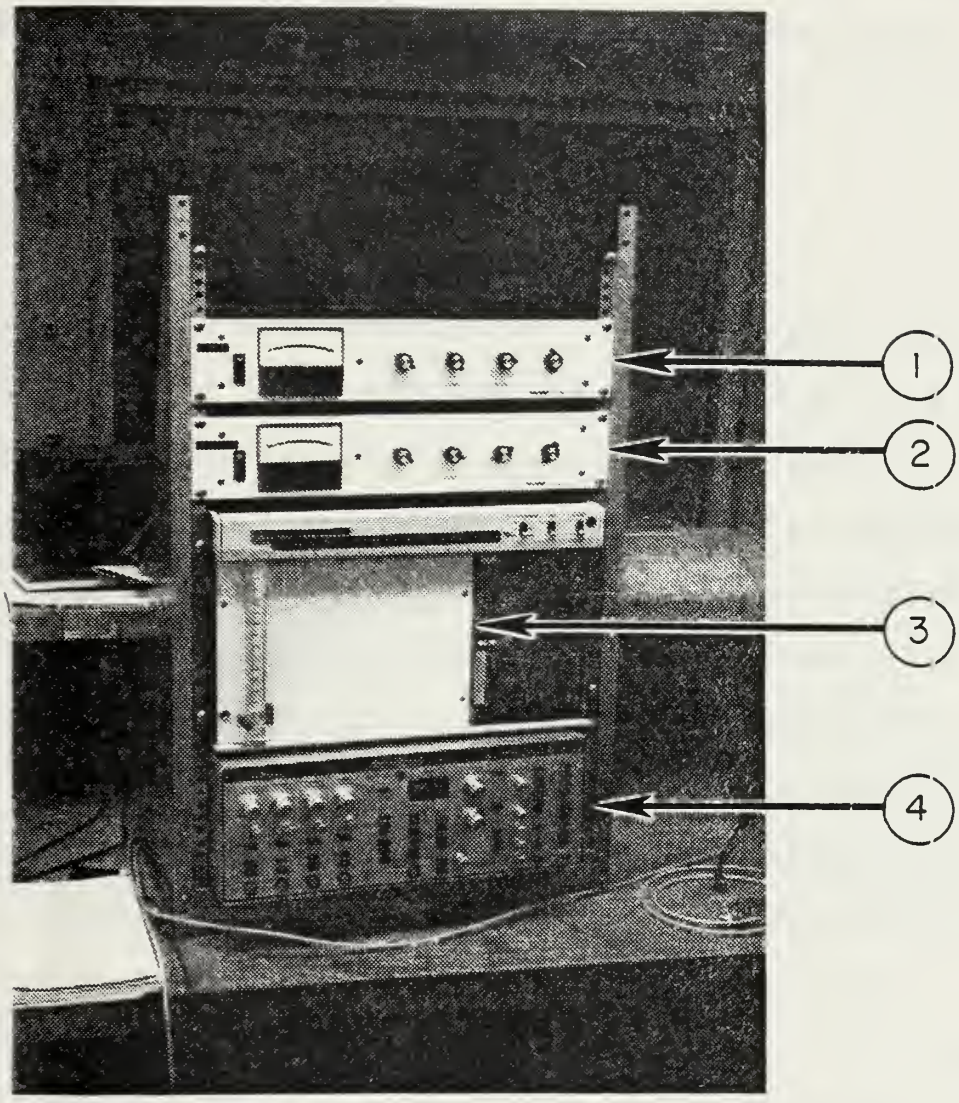

Figure 14. Biomation Digital Wave-Form Recorder

(1) High voltage power supply for the "grey" photomultiplier tube, PMT. The grey PMT used the optical band pass filter. (2) High voltage power supply for the "silver" PMT which was not filtered optically, (3) X-Y recorder, (4) Biomation digital wave-from recorder.

until approximately 80 milliseconds after firing, a delay of 75 milliseconds allowed recording of the desired testing interval. In the two channel mode of operation, 20 milliseconds of the test sequence could be recorded, with a .01 millisecond sampling interval, for close examination of the ignition and burning process.

B. PHOTOMULTIPLIER TUBES

Two RCA, 6199 photomultiplier tubes were positioned at one observation port to measure the visible light emitted by the test wire during the ignition and combustion process. High voltage power supplies provided power to the photomultiplier tubes (see Figure 14) and to the preamplifiers which amplified the output of the photomultiplier tubes to a level that could be recorded and measured on the wave-form recorder and a dual-beam oscilloscope. One photomultiplier tube recorded the wavelength interval within the PMT response range, while the second photomultiplier tube was filtered to record the narrow spectral band at which aluminum oxide (AlO) radiates. Additional details concerning the photomultiplier optical system can be found in the thesis by Strott and Buck [Ref. 2].

C. PENTAX 35 MM CAMERA

A Pentax 35 mm camera with a 55 mm macro lens attached was set at f.1.4 and positioned to photograph each ignition sequence. The shutter was manually opened and closed so that time elapsed pictures of the entire firing sequence were taken. Figure 15 is a close-up picture of a test wire prior to testing.

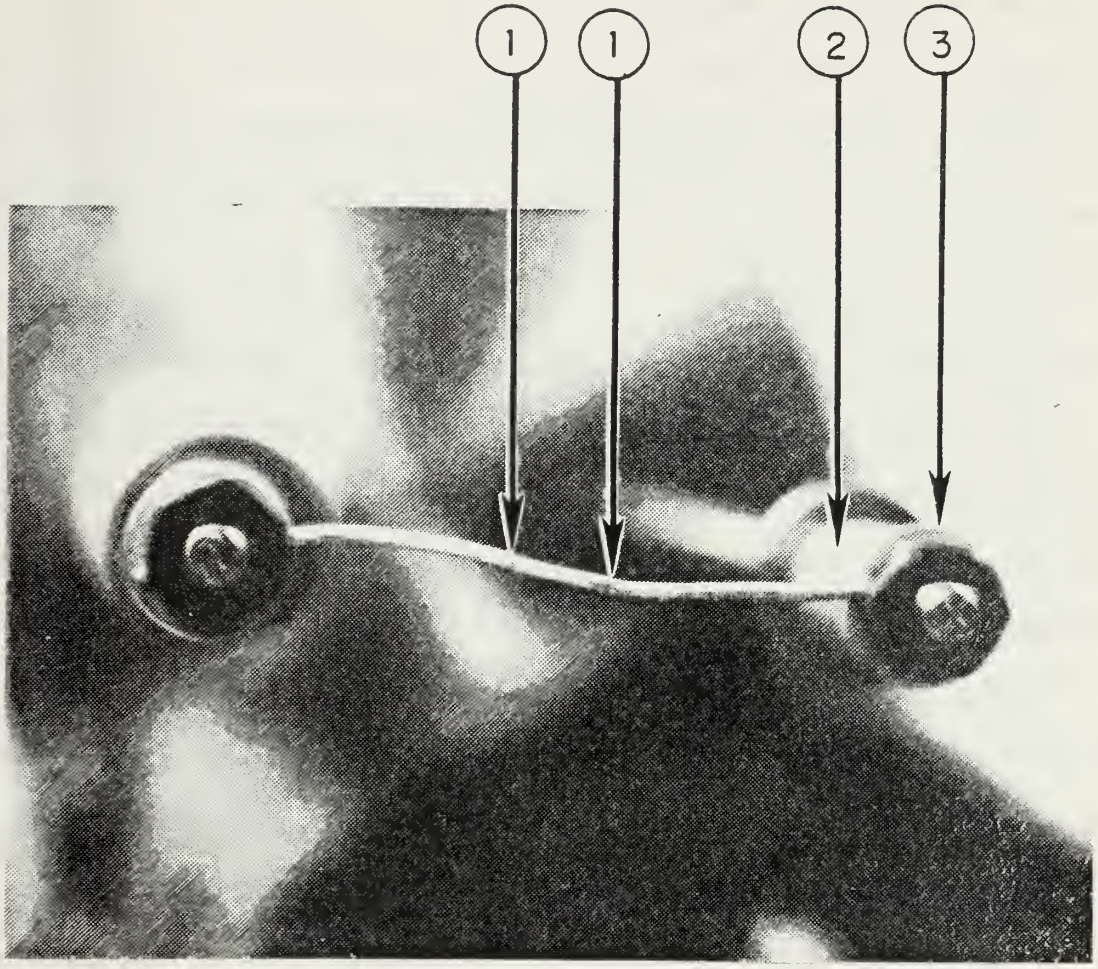

Figure 15. Aluminum Wire Positioned in Holder

(1) Notch in the aluminum test wire; test wire has diameter of 1.0 mm, (2) Spring; see also Figure 9, (3) Washer in contact with end of test wire.

The two notches in the wire were positioned to ensure ignition of the wire occurred near its center and not at one of the posts. The notches in the wire reduced the cross sectional area of the wire and increased its resistivity, thus providing a point at which the wire would ignite first. The reader should also refer to Figure 9.

D. HIGH SPEED MOVIE CAMERA

A Red Lake Labs, variable framing rate, high speed, movie camera was positioned at one observation port to record the entire test sequence. A nominal film speed of 4300 frames per second recorded the entire process from closing of the firing switch until completion of the test wire burning. A triggering switch mounted next to the firing switch was manually closed before the firing sequence started to allow the camera to attain maximum framing speed prior to test wire ignition. Figure 16 is a photograph of the high speed camera as positioned at one of the observation ports. See also Figure 8.

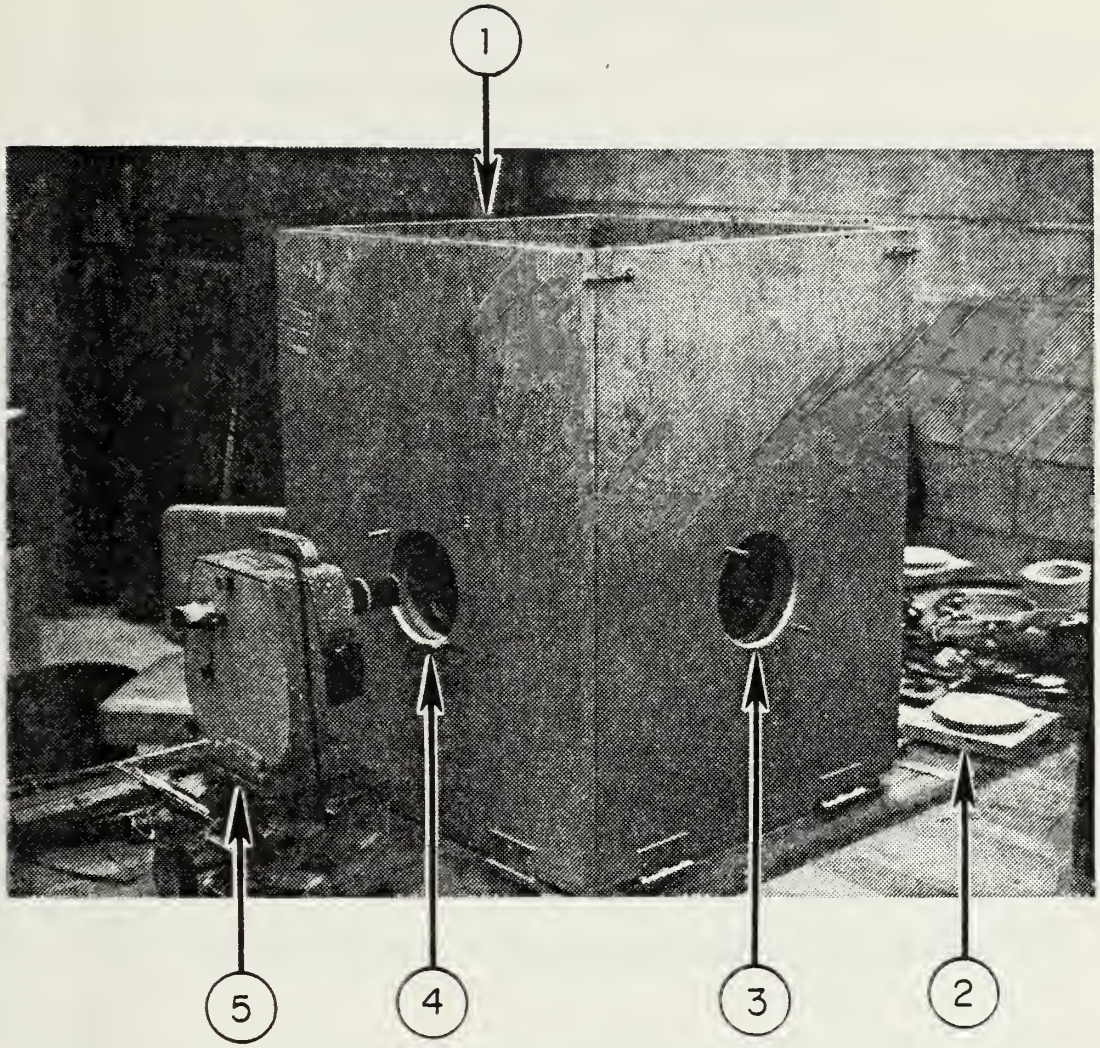

Figure 16. High Speed Movie Camera in Position

(1) Insulated box for pressure vessel, (2) Insulated cover for hole in insulated box, (3) Observation port for PMT system, (4) Observation port for 16mm movie camera, (5) 16mm movie camera.

V. EXPERIMENTAL DATA AND RESULTS

A. ELECTRICAL ENERGY MEASUREMENTS

Numerous samples of aluminum wire were mounted in the test wire holder assembly, connected to the test wire circuit, and exploded in air. Figure 11 shows the test wire circuit. The signals from coaxial cables 5 and 10 were recorded by the Biomation digital recorder. The signal from coaxial cable 8 of Figure 11 was used to trigger the recorder. In addition, the signals from the two photomultiplier tubes were also recorded. A total of four signals were recorded as follows: (1) voltage at the positive terminal of the test wire holder, (2) the voltage across the shunt (see Figure 11) from which current in the wire is determined, (3) signal from the PMT with the optical bandpass filter, and (4) signal from the PMT without an optical filter. The four signals are shown in Figure 17.

Signal 1 in Figure 17 shows constant voltage in the time interval 55 to 77 milliseconds. At 77.5 milliseconds the wire begins to rupture, and the voltage increases from 8 volts to approximately 10 volts. The sinusoidal oscillations in the interval 77 to 80 milliseconds are a result of the melting, ignition, and burning process to which the test wire is subjected. Plasma formed during this process ejects particles of pure aluminum which break the wire and interrupt the circuit. Complete circuit breakdown does not occur until 80

milliseconds when the voltage stabilizes at approximately 10 volts.

Signal 2 in Figure 17 indicates nearly constant electrical current through the wire of 420 amperes until the rupturing processing begins and the circuit is broken. Again the sinusoidal oscillations are caused by the plasma ejecting particles of pure aluminum which begin to burn. The signal shown is a voltage measured at the shunt and converted into current. The shunt used in the test wire circuit was designed to indicate 50 millivolts for a current of 300 amps; this ratio provides a means of determining the actual current in the wire.

Signal 3 in Figure 17 indicates a constant voltage through the optically filtered PMT until the wire began to rupture and the plasma flash occurred. A small voltage in the circuit is being recorded by the PMT prior to the rupturing process. The PMT signal before wire rupture is due to thermal radiation from the hot wire; see Appendix B for a discussion of wire heating. The signals were recorded using a delay feature of the recorder which did not start recording until 50 milliseconds after the firing switch was closed. The PMT signal was at some level above zero when the digital recorder began to record. As previously discussed, the PMT measures the visible light emitted by the test wire. Aluminum wire has an emissivity of 0.19 while tungsten, commonly used in light bulbs, has an emissivity of 0.10 at the same temperature, as noted in Ref. 12. In the time interval after 81 milliseconds

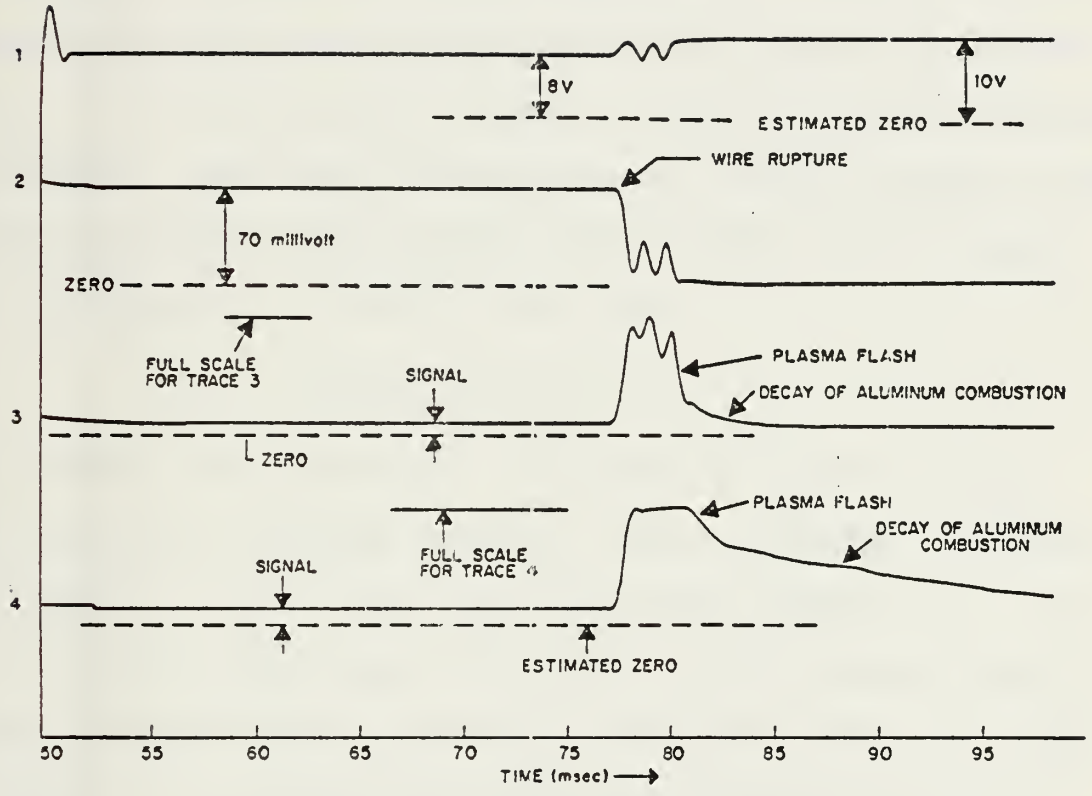

Figure 17. Wave-Form Traces of Voltage, Current and Photomultiplier Tube Signals

(1) Voltage across the wire, (2) Current through the wire, (3) Filtered "Grey" PMT response, (4) Unfiltered "Silver" PMT response; signal was clipped due to scale settings on wave-form recorder.

following the plasma flash, there is a definite change in the shape of the curve indicating either the decay of the plasma or the extinguishment of the aluminum flames. Additional study is needed to clarify the origin of the decay.

Signal 4 in Figure 17 also indicates a constant voltage through the unfiltered PMT until the wire rupturing process begins at 77 milliseconds. Again, a pre-rupture PMT response is present. The shape of the curve for signal 4 after a time of 80.5 ms shows a much slower rate of decay of the plasma than in signal 3. A curve of the form

$$\text{Signal} = \exp(-t/T) \tag{4}$$

was fitted to the curves for the decay of the PMT signals. The values for the decay constant T are as follows: filtered PMT signal, T = 2 ± 0.5ms; unfiltered PMT signal, 13 ± 1.0ms.

It must be noted that information on the actual magnitude of the recorded signals cannot be determined from the traces of Figure 17. Voltage and current amplitudes for signals 1 and 2 were determined from oscilloscope traces. The Biomation recorder is a wave-form recorder which allows comparison of signal wave-forms but does not indicate actual zero values (pen position for zero-signal input) for measuring purposes.

Figure 18 is a wave-form trace of the voltage at the positive terminal of the test wire circuit and the voltage across the shunt for another test run. Signal 1 is the voltage at the positive terminal and signal 2 is the voltage across the shunt. The rupture of the wire did not occur until 83.6

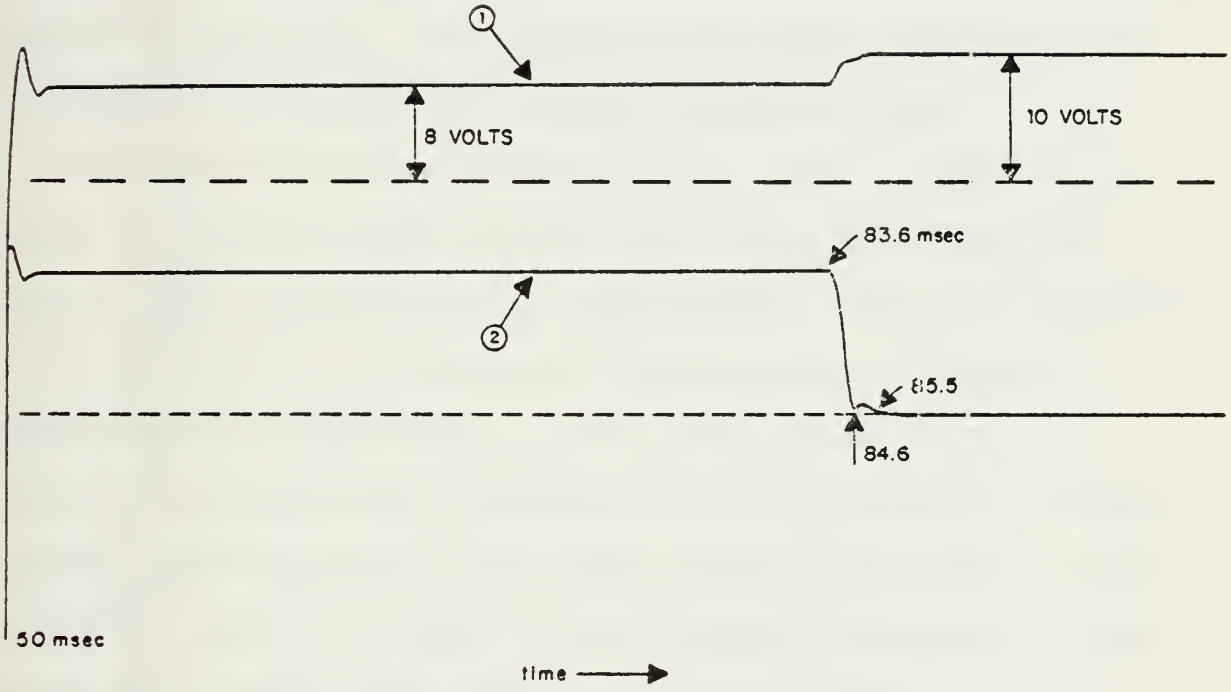

Figure 18. Wave-Form Traces of Voltage and Current

(1) Voltage across the test wire; initially 8 volts, increased to 10 volts after wire ruptured, (2) Current through wire; rupture occurred at 83.6 milliseconds in this test. (Dashed lines indicate zero level.)

milliseconds in this test, and evidence of sinusoidal oscillations is not present. One possible reason for this different response is the point of rupture of the test wire. The wire used in the test for Figure 17 ruptured near its center, while the wire used for Figure 18 ruptured near one of the stainless steel posts. The slight oscillation in signal 2 is attributed to the mechanical response of the pen in the X-Y recorder. The recorder was again configured for a delay of 50 milliseconds before recording began.

The sinusoidal oscillations in the time interval 77 to 80 ms in Figure 17 are a rare event having been observed once in about 20 test runs. Considerable effort was devoted to interpretation of the oscillations shown in Figure 17. One explanation could be that the oscillation is due to digital-to-analog (D/A) conversion by the Biomation recorder. Another possibility could be some unusual occurrence in the recorder. However, after sorting through the possibilities, the most probable cause seems to be the molten aluminum causing a make-break circuit. Note the phase shift in the filtered PMT trace relative to the current trace. During the tests in steam, the high speed movies show a series of plasma flashes. The circuit is being opened and closed by molten aluminum.

Figure 19 is a sketch of the oscilloscope traces of the voltage at the positive terminal of the test wire circuit and the voltage across the shunt. Figures 17 and 18 are traces

for a narrow time interval from 50 to 100 milliseconds. Figure 19 is a sketch of the complete test sequence from closing of the trigger switch until rupture of the test wire has occurred.

Trace A is a sketch of the voltage across the shunt. The voltage reached a maximum of 80 millivolts, decayed to 70 millivolts and dropped to zero as the test wire ruptured and opened the circuit. The voltage did not reach its maximum until 14 milliseconds after closing of the firing switch; the 14 ms delay is attributed to the dynamics of the solenoid switch. The circuit in this test was not broken until 90 milliseconds after the firing switch was energized. Using the ratio of voltage to current for the shunt, as described earlier, the current reached a maximum of 480 amperes and decayed to 420 amperes before the circuit was broken.

Trace B is a sketch of the voltage at the positive terminal of the test wire holder. An initial reading of 8 volts was recorded 14 milliseconds after the firing switch was closed. The voltage remained constant until the wire ruptured and reached a maximum of approximately 10 volts at 90 milliseconds after the firing switch was closed.

These traces provided the initial time and magnitude information which was used to select the proper recording interval and scaling for the digital recorder. These data were also used for estimating wire heating.

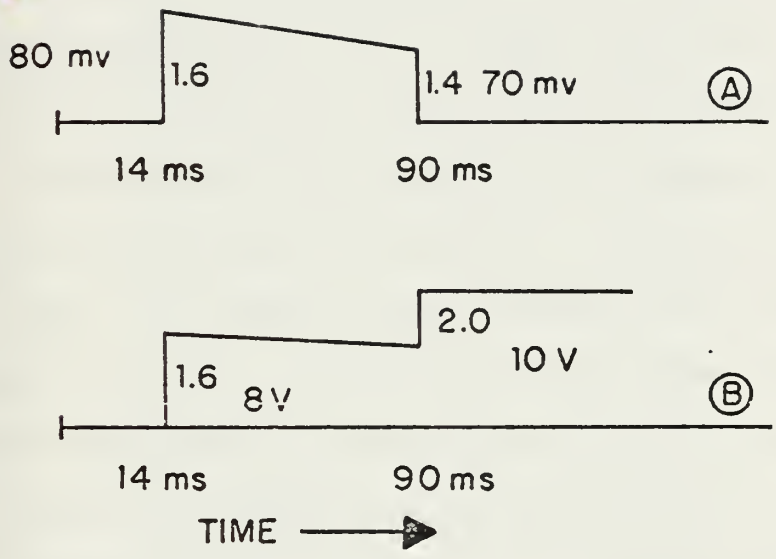

Figure 19. Sketch of Oscilloscope Traces of Voltage and Current

(1) Vertical scale 50 millivolts/division for Trace A.
(2) Vertical scale 5 volts/division for Trace B.

B. PHOTOGRAPHIC RESULTS OF EXPERIMENTS IN AIR AND STEAM

Color slides of the ignition and burning of test wires in both air and steam were taken. Black and white reproductions of these slides were made for inclusion in this report; a tremendous amount of information is lost in the conversion from the original color slides to a half-tone black and white print. Figure 20 is a photograph of the results of one of the test runs conducted in air. After the firing switch was closed, current in the wire heated the wire until ignition occurred. Portions of the wire were red-orange in color indicating this heating; see arrow (1). Brzustowski and Glassman [Ref. 11] observed this glowing wire phenomenon in their research as well. For wires of the same temperature, the the glowing aluminum wire radiates more than a tungsten wire used in light bulb filaments. The emissivity of heated aluminum oxidized at 1100 F is 0.19. Tungsten has an emissivity of approximately 0.10 at the same temperature, as noted in Ref. 14. At the instant of ignition an intense white flash was evident; see arrow (2) in Figure 20. This intense white flash is thought to have occurred as a result of plasma formed from air and the vaporized aluminum. The rupture of the wire and the formation of this plasma ejected burning particles of aluminum at velocities estimated to be as large as 7 meters per second; see Appendix D which discusses results from high speed movies.

The burning particles traveled in straight paths until near the end of the trajectory when sharp bends and erratic

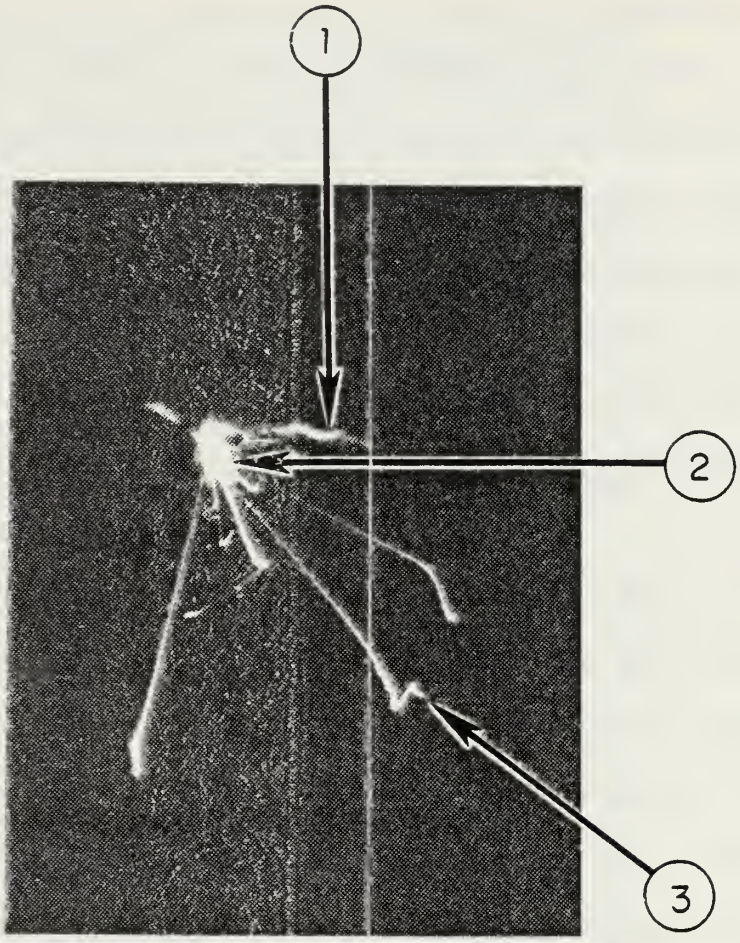

Figure 20. Burning Aluminum Wire in Air

(1) Red-orange (in color slide) glowing wire, (2) Plasma flash, (3) Typical particle trajectory.

spiraling motions became apparent. These motions have been recorded and reported in previous research on burning aluminum particles in oxygen. Macek, Friedman, and Semple [Ref. 13] photographed particles of burning aluminum and observed the same high lateral acceleration turns and the same rotating, erratic trajectories of the burning aluminum particles.

A model to explain the behavior of the burning particles in both steam and air is at the heart of this research. Plausible explanations of the burning particle behavior are presented in Section VI.

Figure 21 shows very similar results for a second test conducted in air. Again, a bright white flash and burning aluminum particles traveling erratic paths are visible. However, in this test, the test wire ruptured at one end near the post of the test wire holder. Rupture of the test wire occurred at a later time, and as a result the entire wire attained a higher temperature before rupture occurred. Visible in this slide was a pale blue diffusion flame, characteristic of burning aluminum, along the entire length of the test wire. The wire is immersed within the flame. In the black and white photography, this is evident as a light shade of gray around the test wire. Brzustowski and Glassman reported this same blue diffusion flame in their work on burning aluminum particles in oxygen; see Ref. 11.

Another phenomenom observed in many of the test runs was the physical displacement of the test wire during the ignition

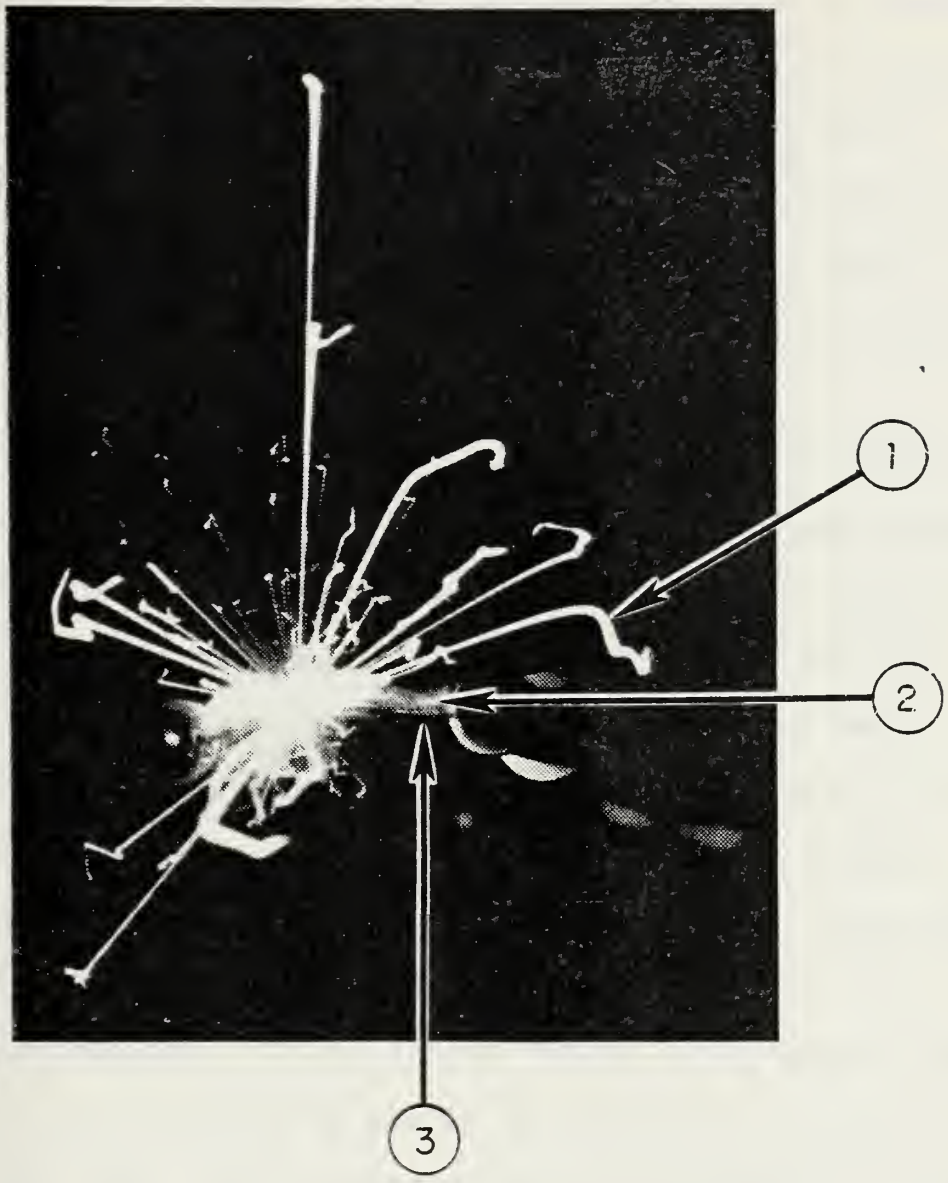

Figure 21. Aluminum Wire in Air

(1) Erratic particle trajectories, (2) Aluminum-air diffusion flame (pale blue in color slide), (3) Glowing Wire.

and burning process. Figure 22 is a photograph which illustrates this displacement. The aluminum test wire is initially positioned directly between the two posts with only slight bends in the wire as shown by arrow (2) in Figure 22(b). The wire is bent by the magnetic forces on the wire during the surge of current; refer to Figure 23. Arrows (3) and (4) in Figure 22 show the bent test wire at the ends of the vibration cycle.

In passing, one should note that the vibration of the test wire is an excellent illustration of a concept from quantum mechanics. In quantum mechanics the probability density function for a harmonic oscillator is developed; see for example, Landshoff and Metherell [Ref. 14]. The camera shutter was open during the event; hence all events are superimposed. When the wire is at rest the reflected ambient light exposed the film. When the wire is moving, the combination of light and time is inadequate to expose the film. Motion from position (2) to (3) in Figure 22(a) is not seen. Likewise, motion between position (3) and (4) in Figure 22(a) is also not seen. At the extremity of the vibration cycle, the wire comes to rest and sufficient time elapses to cause film exposure. The analogy with the probability density function for the harmonic oscillator of quantum mechanics should be apparent.

Figure 23 illustrates the origin of the magnetic force on the wire. The magnetic force on the wire tends to expand the

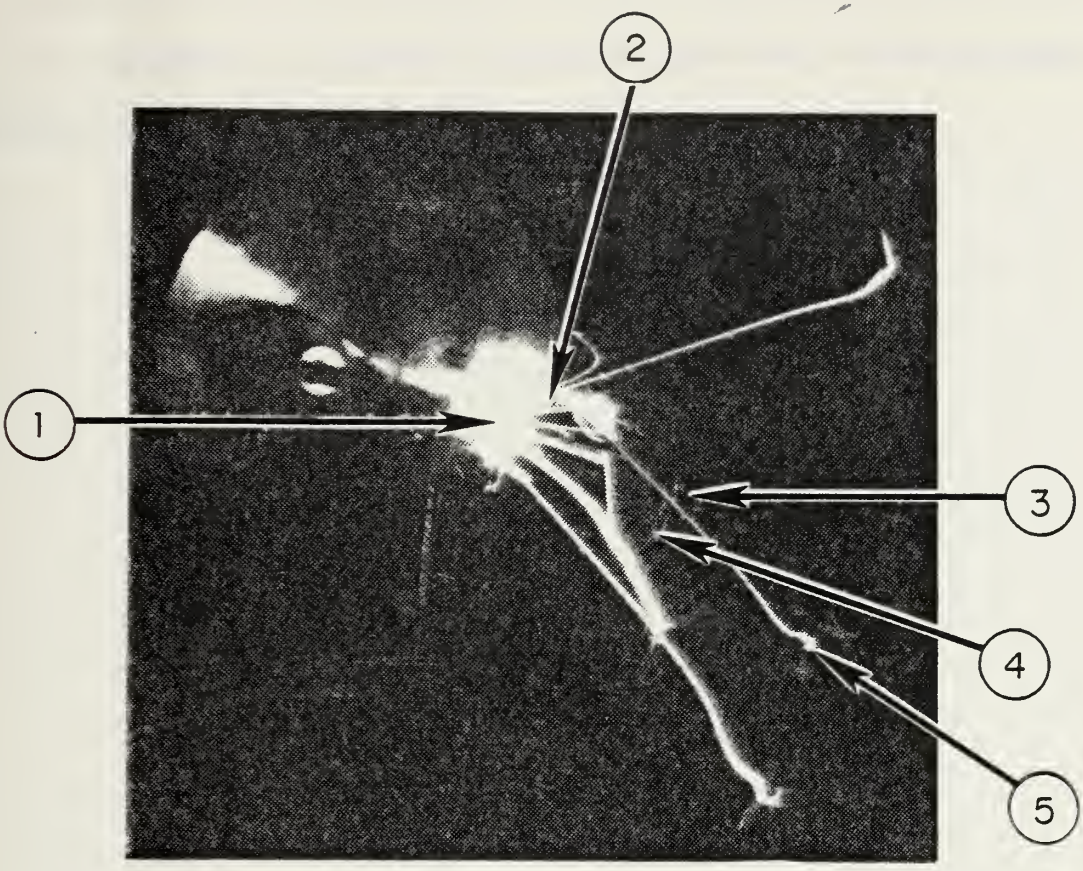

(a) Photograph

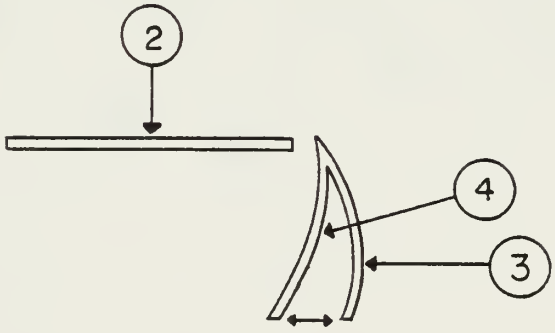

(b) Sketch of wire

Figure 22. Example of test with aluminum wire displacement

(1) Plasma flash, (2) Original wire location, (3) Bent wire at right hand position during vibration cycle, (4) Bent wire at left hand position, (5) Particle showing spiral trajectory

area enclosed by the current loop. The ratio of the magnitude of the magnetic force F to wire weight w is a few hundred. See Appendix C.

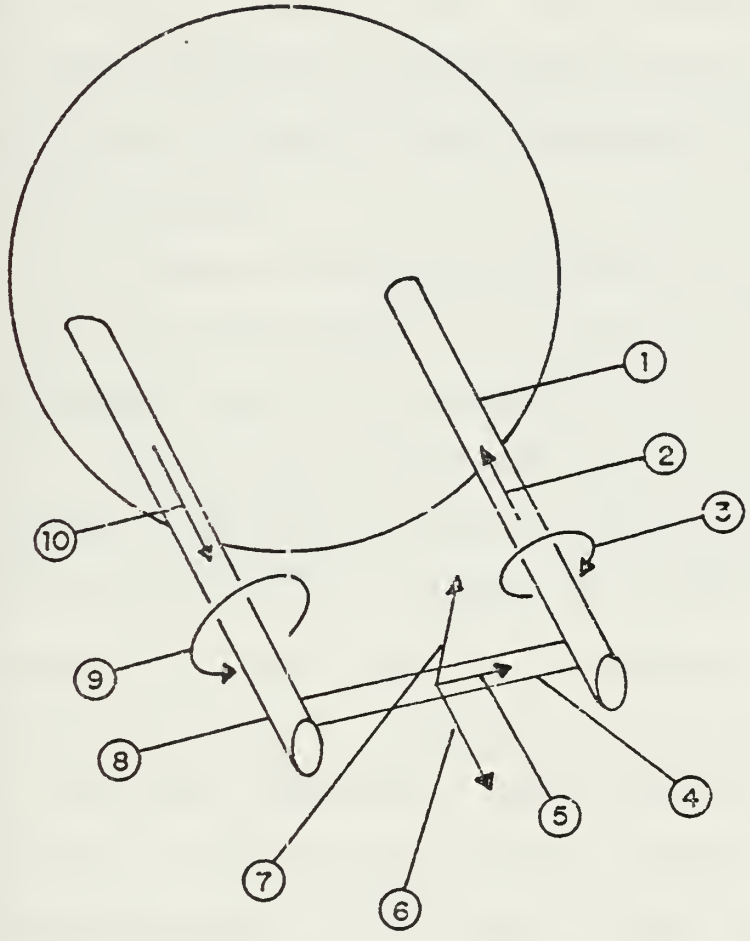

Figure 23. Force on test wire due to current.

(1) Negative electrode of test wire holder, (2) current, (3) magnetic flux density near negative electrode due to current, (4) test wire, (5) current in test wire, (6) force arising from J X B force density, (7) magnetic flux density B at location of wire, (8) positive electrode, (9) magnetic flux density near positive electrode, and (10) current in the positive electrode.

Figure 24 is another photograph of a test conducted in air. A very large, intense, yellow (in color slide), diffusion flame (1) is apparent along the entire length of the test wire. This flame appears to be above the wire which is glowing red in the color slide, (2). The diffusion flame is attributed to the combustion of aluminum with air. The intense blue plasma (3) occurs near the center of the wire at the point of rupture.

Figure 25 is a photograph of the results of a test conducted in nearly pure steam at 131 C and 31.5 psia. The partial pressures of air and steam were 3.6 and 27.9 psia, respectively. The ignition and burning process in steam is markedly different compared to the wires tested in air. The plasma region (see arrow (1) in Figure 24) occurs in the center at the point of wire rupture. Particles of burning aluminum (refer to arrow (3) in Figure 24) are ejected from the wire by the plasma explosion. One of the major differences in results is noted at this point. Evidence of erratic, spiraling particle motion is not seen in this photograph. The particles appear to travel along straight paths while the burning decays. Combustion of each particle (2) appears to cease and reignite at some point near the end of its trajectory. The cause of this flame extinguishment and reignition phenomena is unknown at this time. Further research will be conducted to understand these observations.

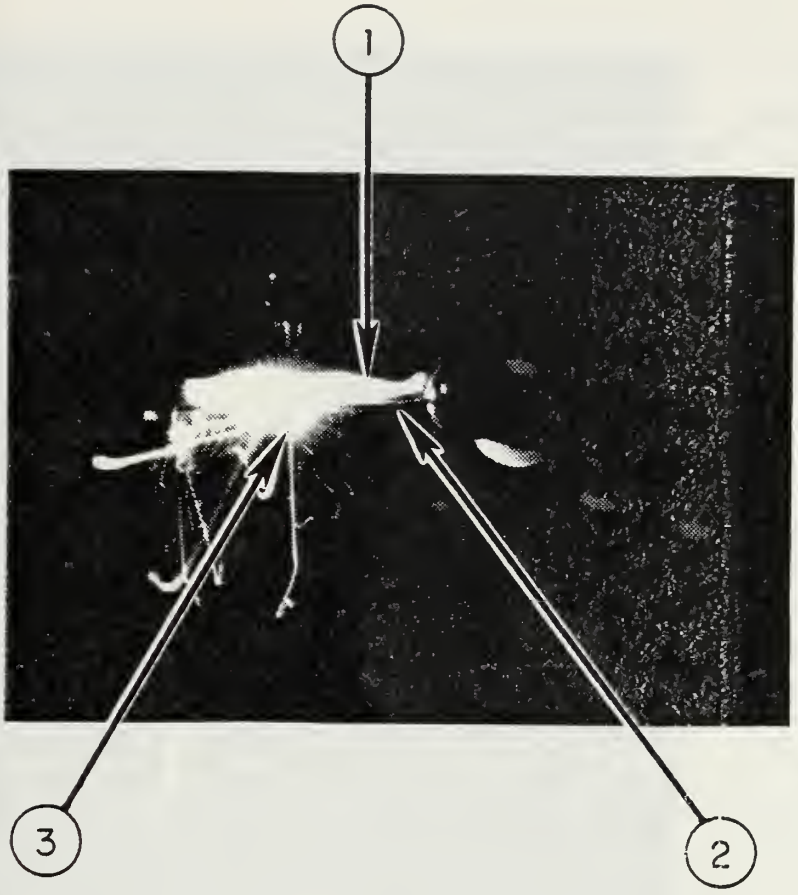

Figure 24. Diffusion Flame Along Wire Burning in Air

(1) Yellow (in color slide) Diffusion Flame above the wire, (2) Glowing Wire, (3) Plasma

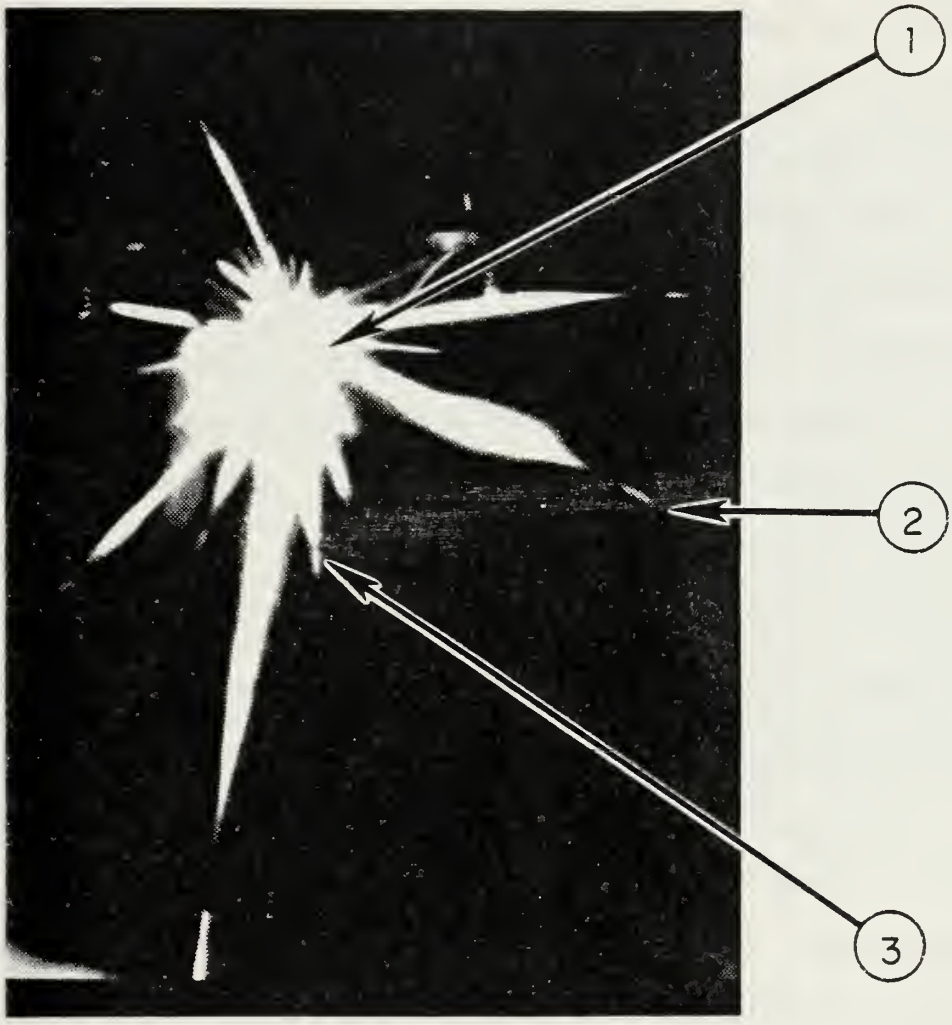

Figure 25. Aluminum Wire Ignited and Burning in Steam at 131 C and 31.5 psia.

(1) Plasma, (2) Reignited Aluminum Particle, (3) Trajectories of Burning Particles

Figure 26 is a photograph of a second test conducted in nearly pure steam. The partial pressure of air was 3.4 psia, and that of steam was 16.9 psia. In this test, the steam temperature was 117 C and the total pressure was 20.3 psia. The plasma (1) forms at the point of wire rupture near the center of the test wire. Burning aluminum particles, (2), are randomly ejected from the wire by the plasma. The cessation of combustion followed by reignition of the burning particles (3) is again quite evident. One burning particle (4) appears to be pulsing after reignition. As seen in the original color slides, the colors for the pulsating combustion of the particle vary from white to red to orange to red. The burning particles in this photograph exhibit one additional phenomenon which must be examined. The particle trajectories (5) curve downward which indicates the influence of gravity on the particles.

The particle trajectory is determined by several forces as follows: inertia, thrust due to combustion, aerodynamic drag and gravity. Considering only inertia (centrifugal acceleration) and gravity one can derive

$$R = V^2/g \qquad (5)$$

where R is the radius of curvature of the particle trajectory, V is the particle velocity, and g is the acceleration of gravity. From analysis of high speed motion pictures, the initial velocity of particles burning in steam is in the range of 2 to 3 meters/second. Using a velocity of 2 meters/second,

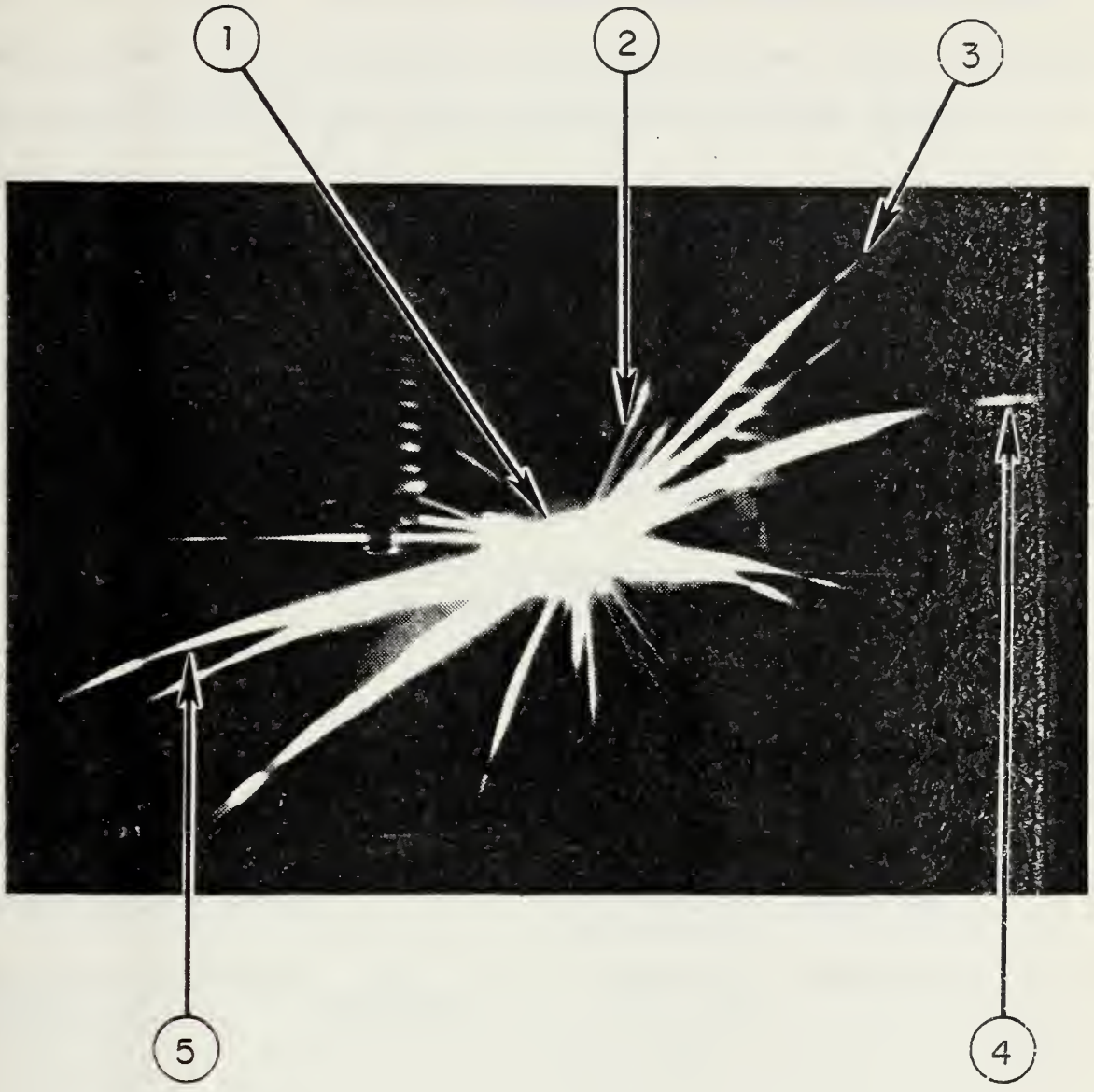

Figure 26. Exploding Aluminum Wire in a Nearly Pure Steam Atmosphere at 117 C and 20.3 psia.

(1) Plasma, (2) Burning Aluminum Particles, (3) Reignition of a Burning Particle, (4) Pulsation of a Burning Particle, (5) Curved Trajectory due to Gravity.

the radius of curvature should be $R = (2 \text{ m/sec})^2/(9.8 \text{ m/sec}) \simeq 0.4 \text{ m} = 400 \text{ mm}$. The wire specimen is 50 mm in length and establishes a length scale in the photographs. The preceding analysis confirms that the trajectory curvature is due to gravity.

Table 2 summarizes the observed results of burning aluminum particles and compares these results with the study of Macek, Friedman, and Semple [Ref. 13]. Tests in air and the flat flame burner of Reference 13 are similar. However, many of the features are missing when burning occurs in steam.

Table 2. Comparison of Observation of Burning Aluminum Particles

Particle Behavior	This Report		Macek, Friedman, and Semple [Ref. 13] Tests in Flat Flame Burner
	Tests in Steam	Tests in Air	
Trajectory with large lateral-acceleration turns	Not observed	Observed near end of particle trajectory	Observed high-g turns following spinning
Particle spinning about C.G.	Not observed	Observed near end of trajectory	Observed
Particle fragmentation	Not Observed	Not observed	Observed in oxygen enriched environment

C. HIGH SPEED MOVIES OF TESTS CONDUCTED IN AIR AND STEAM

A high speed movie camera, described in section IV, was positioned 13 inches from the aluminum test wire, set at 4300 frames per second, and used to record a test wire ruptured in

air. The camera was focused directly on the crimp in the wire. Figure 27 is a series of photographs of the results of the test recorded by the high speed movie camera.

Ignition of the wire and the plasma flash occurs in Frame 1, Figure 27, and the extremely faint images of the burning particles which have been ejected by the plasma are visible in the following frames. The entire sequence of movie frames is completed in 1.0 milliseconds. Arrow 1, in Figure 27, indicates the plasma flash. The "+" sign indicates the center of the plasma flash and was used as a reference mark for measuring the velocity of the burning particles after ejection from the ruptured wire. Arrow 2 indicates the positions of the burning particles 0.2 milliseconds after the plasma flash. Arrows 3, 4, and 5 indicate the positions of the burning particles in the subsequent frames, each 0.2 milliseconds later. Calculation of the particle speed determined that the burning aluminum particles had an average velocity of 8.2 ± 1.9 meters/second; see Appendix D. The camera must be firmly anchored to eliminate vibrations so that sharp images of the burning aluminum particles in motion can be recorded.

The high speed movie camera was positioned at one of the observation ports with the lens 13 inches from the test wire. A high speed movie of an aluminum wire test conducted in steam was taken at the same film speed as the test conducted in air. The steam was at a temperature of 117 C and a pressure of 20.3 psia. Figures 28(a) through 28 (h) are a sequence of photographs of the high speed movie from a test conducted in steam.

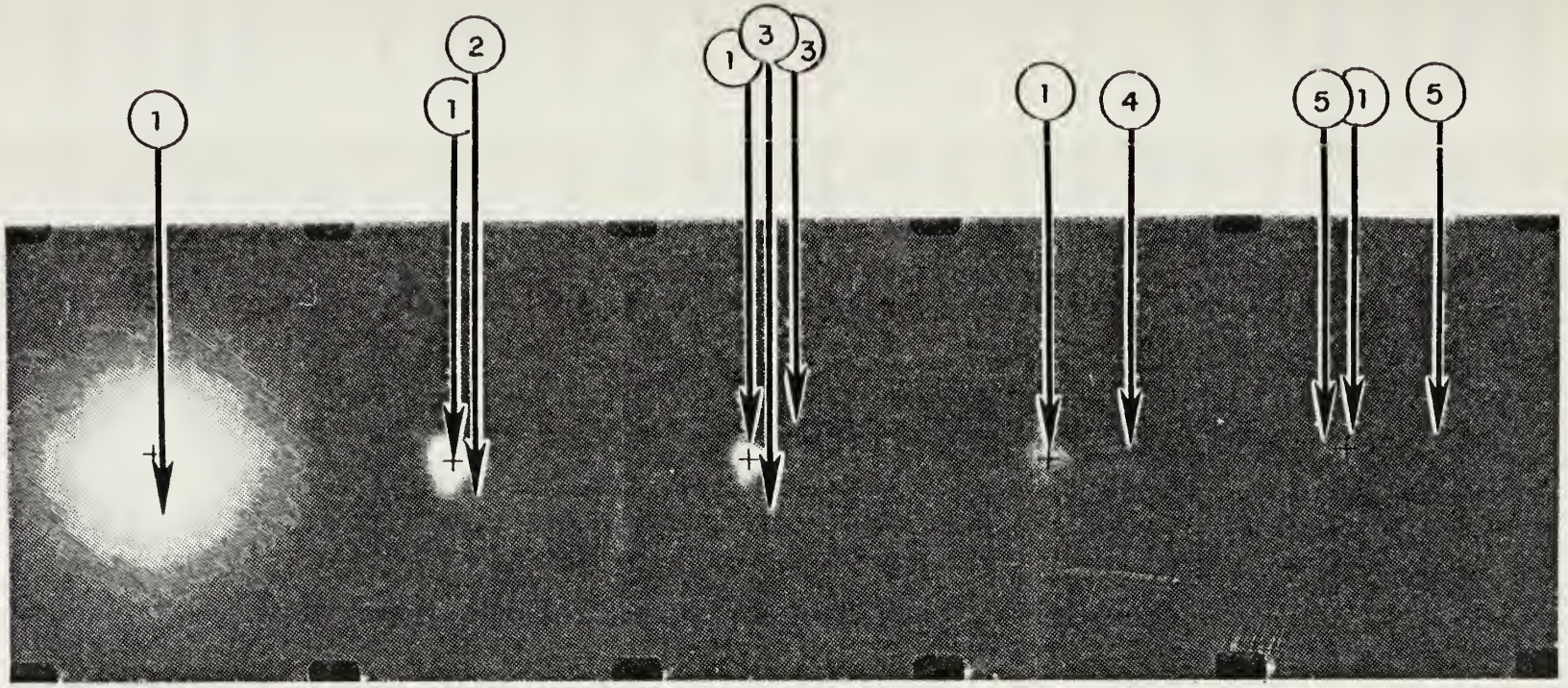

Figure 27. High Speed Film of Test Conducted in Air.

Frames 1 - 5

(1) Plasma Flash, (+) indicating center of the flash, (2) Burning Aluminum Particles (3) Burning Aluminum Particles of 0.5 ms after flash, (4) Burning Particles 0.7 ms after flash, (5) Burning Particles 1.0 ms after flash.

The "+" sign designates the center of the plasma flash and was used as a reference point for determination of particle velocity. Arrow 1, in Figure 28(a), indicates the plasma flash. Arrow 2 indicates the ejection of burning aluminum particles. Arrow 3 indicates the position of the burning particles 0.5 milliseconds after the plasma flash. Arrow 4 indicates the position of the burning particles 1.2 milliseconds after the plasma flash.

Figures 28(b) and 28(c), Frames 6 to 15, show the motion of the burning aluminum particles as movement away from the point of the plasma flash becomes more readily apparent.

Figure 28(d), Frame 16, contains a new, previously unrecorded phenomenon. Arrow 1 indicates the position of a second plasma flash which appears at the point of the original flash. Using the speed of the high speed film as a reference, this second plasma flash occurs 3.7 ms after the initial flash which is shown in Figure 28(a), Frame 1. Evidence of further ejection of burning particles is not seen in this or subsequent frames. The second plasma flash decays within one frame, approximately 0.2 ms. Its intensity is considerably less than that of the original plasma flash.

In Figure 28(e), Frame 22, Arrow 1 indicates a third plasma flash. This flash occurs 5.1 ms after the initial flash. Its magnitude and duration are less than that of the previous flash. Again, there is no evidence of any further ejection of burning aluminum particles.

Figure 28(f), Frame 30, contains a fourth plasma flash. Arrow 1 indicates this flash. The fourth plasma flash occurs 7.0 ms after the initial flash. Its intensity is less than that of the preceding flashes.

Figure 28(g), Frames 31 to 35, depicts the positions of the remaining burning particles 7.2 to 8.1 milliseconds after the original plasma flash. Many of the particles have cooled or are outside the field of view of the camera by this time.

Figure 28(h), Frames 36 to 40, depicts the burning particles 8.4 to 9.3 milliseconds after the rupture of the aluminum wire. Arrow 1, in Frame 39, indicates a fifth plasma flash which occurred 9.1 ms after the initial plasma flash. Its intensity was greater than that of the fourth flash. Explanation of these recurring plasma flashes requires additional research and further understanding of the events which occur in the exploding of aluminum wire in steam. Multiple flashes were also observed for an aluminum wire tested in air. Figure 29 shows the filtered and unfiltered PMT traces. The double plasma flashes are clearly evident.

Calculating the velocity of the aluminum particles for the test conducted in steam, an average velocity of 3.5 meters/second was computed; the calculations are presented in Appendix D. Particle velocities in range from 0.69 m/sec to 4.67 m/sec were observed.

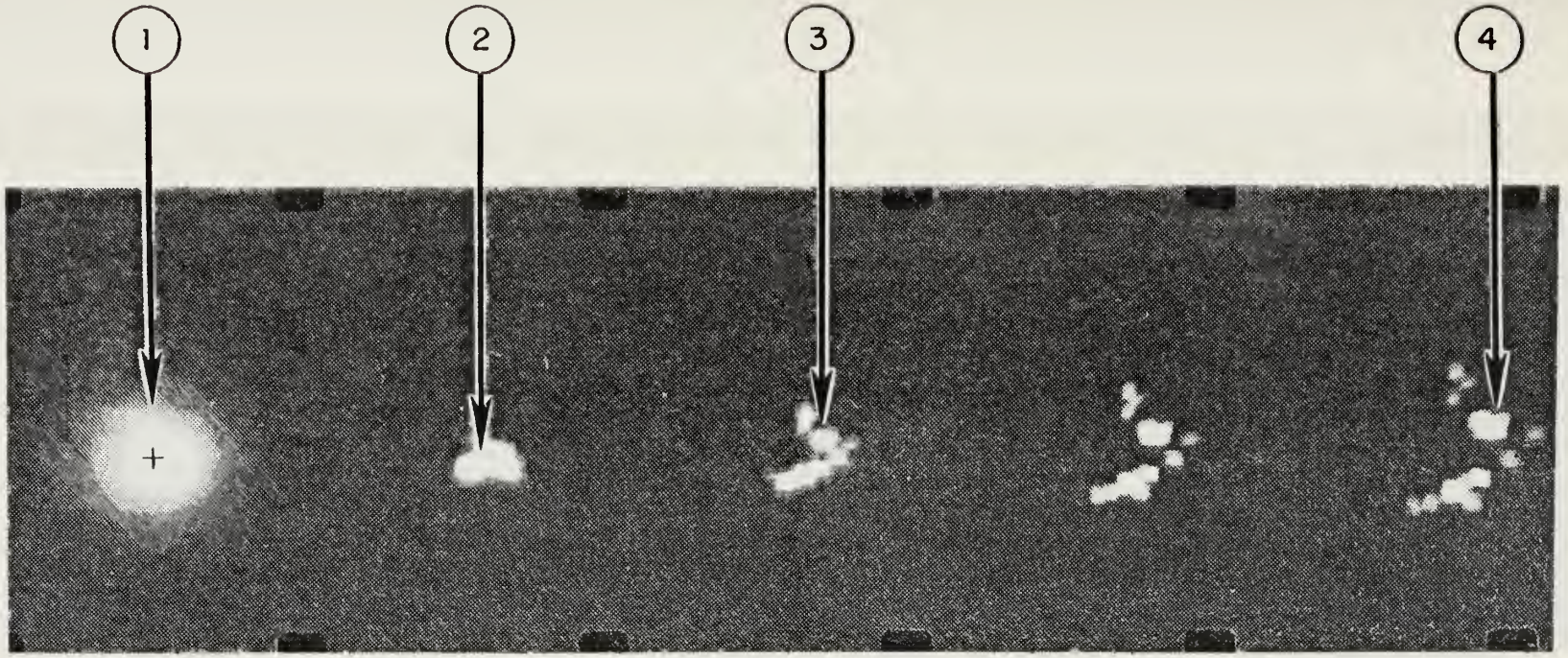

Frame 1 Frame 2 Frame 3 Frame 4 Frame 5

Figure 28(a) Aluminum Test Wire Ruptured in Steam.

Frames 1 - 5

(1) Plasma Flash, (+) indicating center of flash, (2) Ejection of Aluminum Particles, (3) Ejected Particles 0.5 ms after flash, (4) Ejected Particles 1.2 ms after flash.

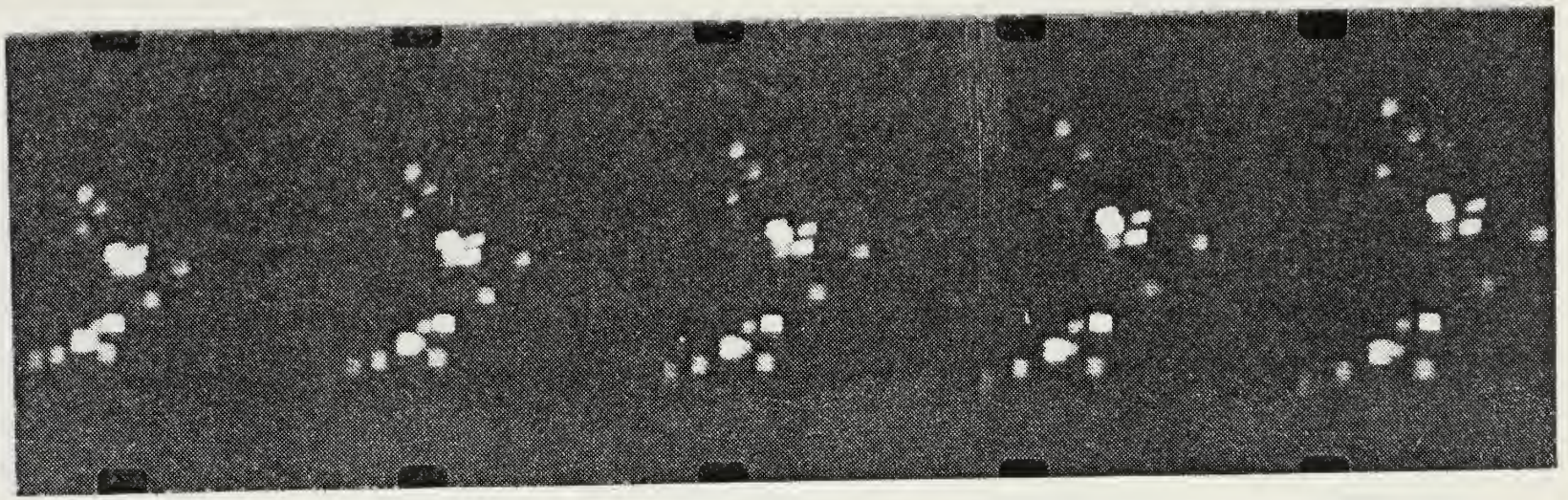

Frame 6 Frame 7 Frame 8 Frame 9 Frame 10

Figure 28(b) Frames 6-10

Burning Aluminum Particles 1.4 to 2.3 ms after plasma flash.

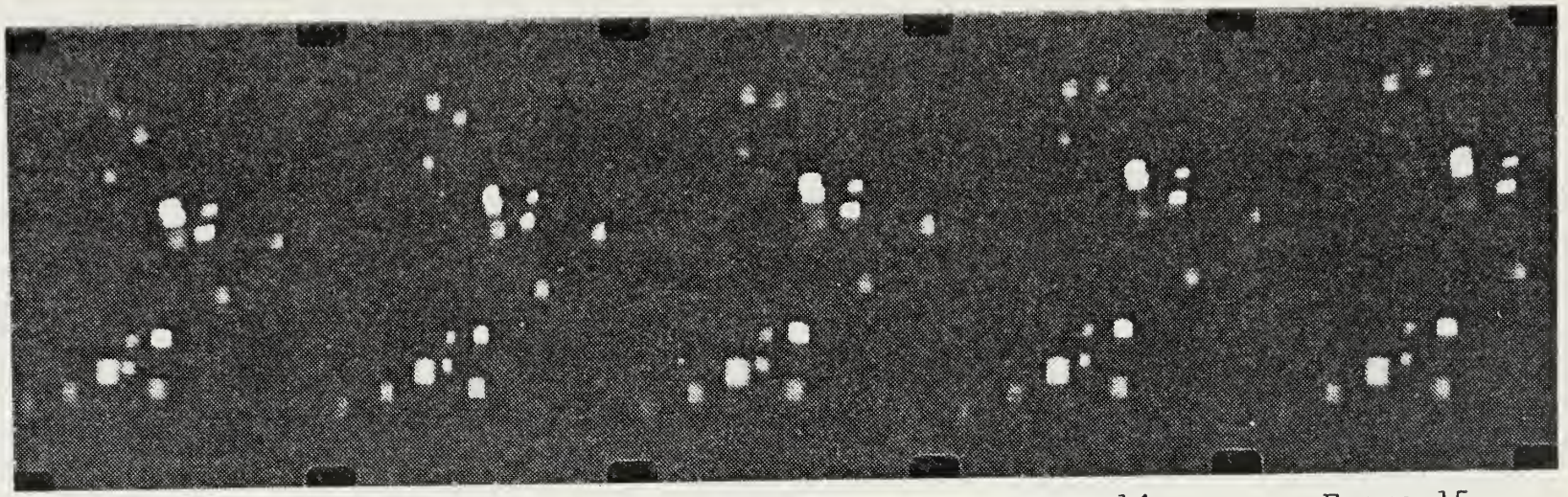

Figure 28(c) Frames 11-15

Burning Aluminum Particles 2.6 to 3.5 ms after plasma flash.

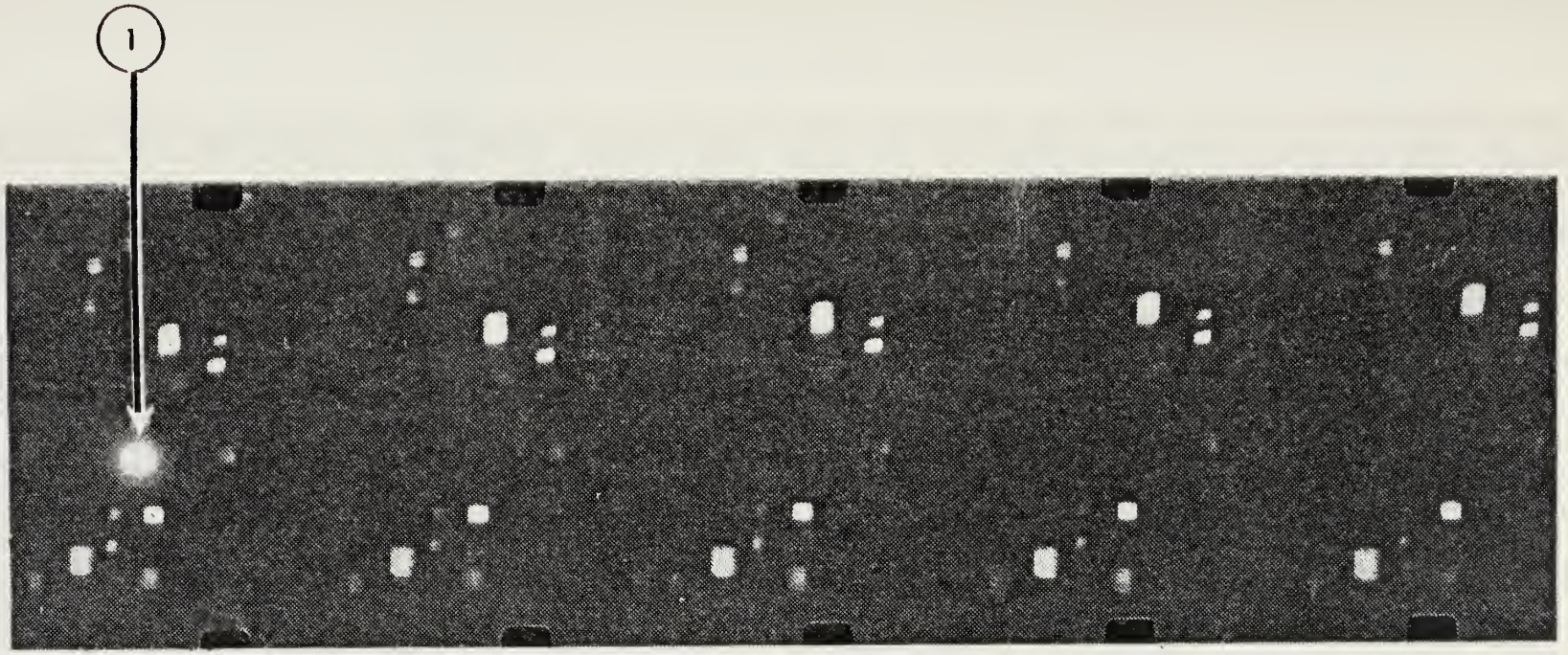

Figure 28(d) Frames 16-20

Burning Aluminum Particles 3.7 to 4.7 ms after initial plasma flash.

(1) Second plasma flash.

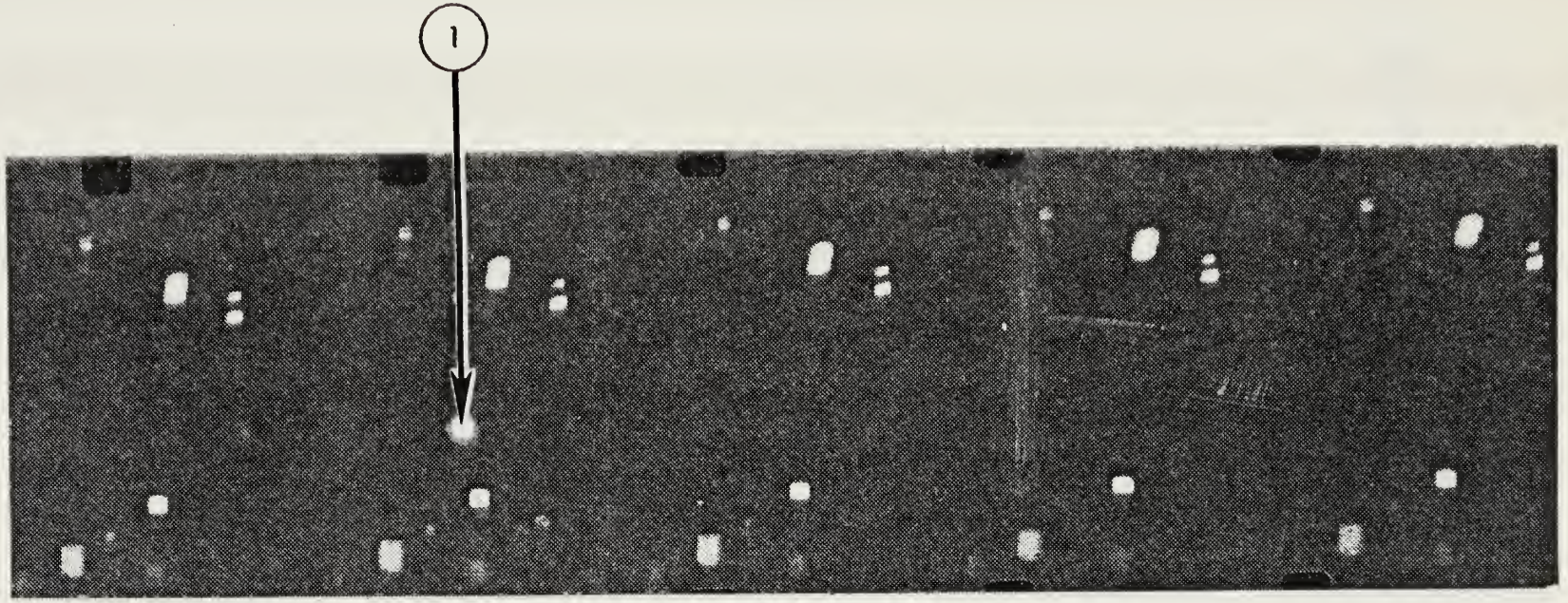

Figure 28(e) Frames 21-25

Burning Aluminum Particles 4.9 to 5.8 ms after initial plasma flash.

(1) Third plasma flash.

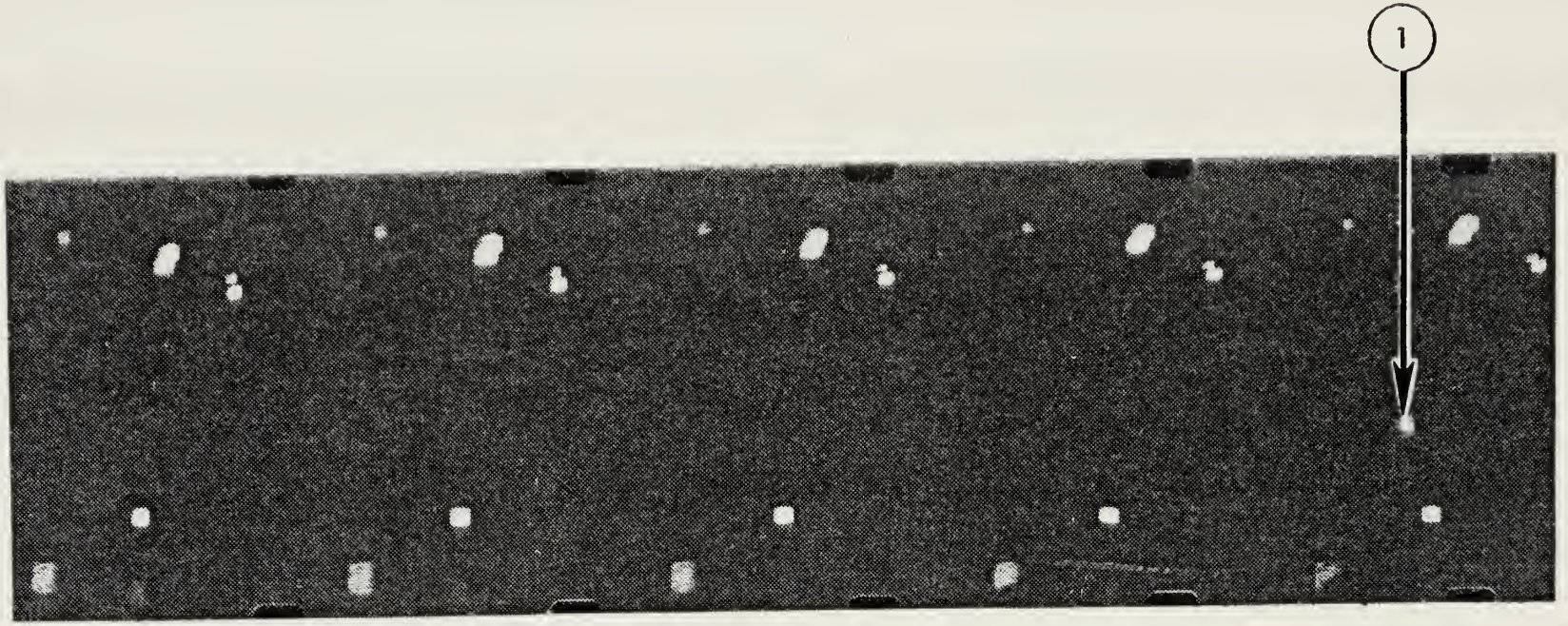

Figure 28(f) Frames 26-30

Burning Aluminum Particles 6.0 to 7.0 ms after initial plasma flash.

(1) Fourth plasma flash.

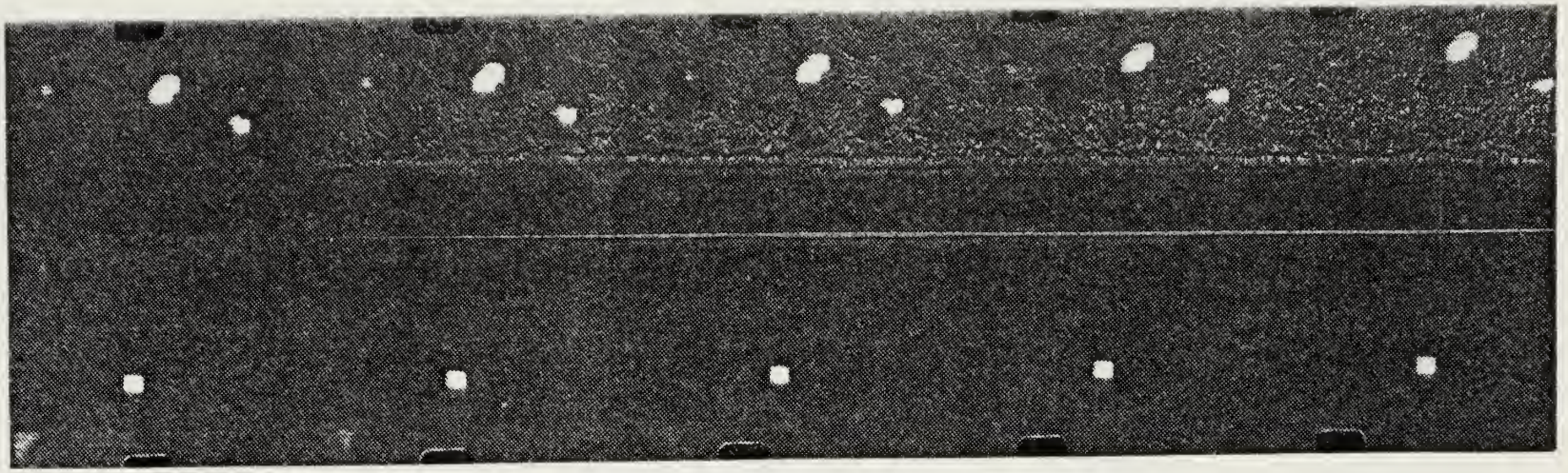

Frame 31 Frame 32 Frame 33 Frame 34 Frame 25

Figure 28(g) Frames 31-35

Burning Aluminum Particles 7.2 to 8.1 ms after initial plasma flash.

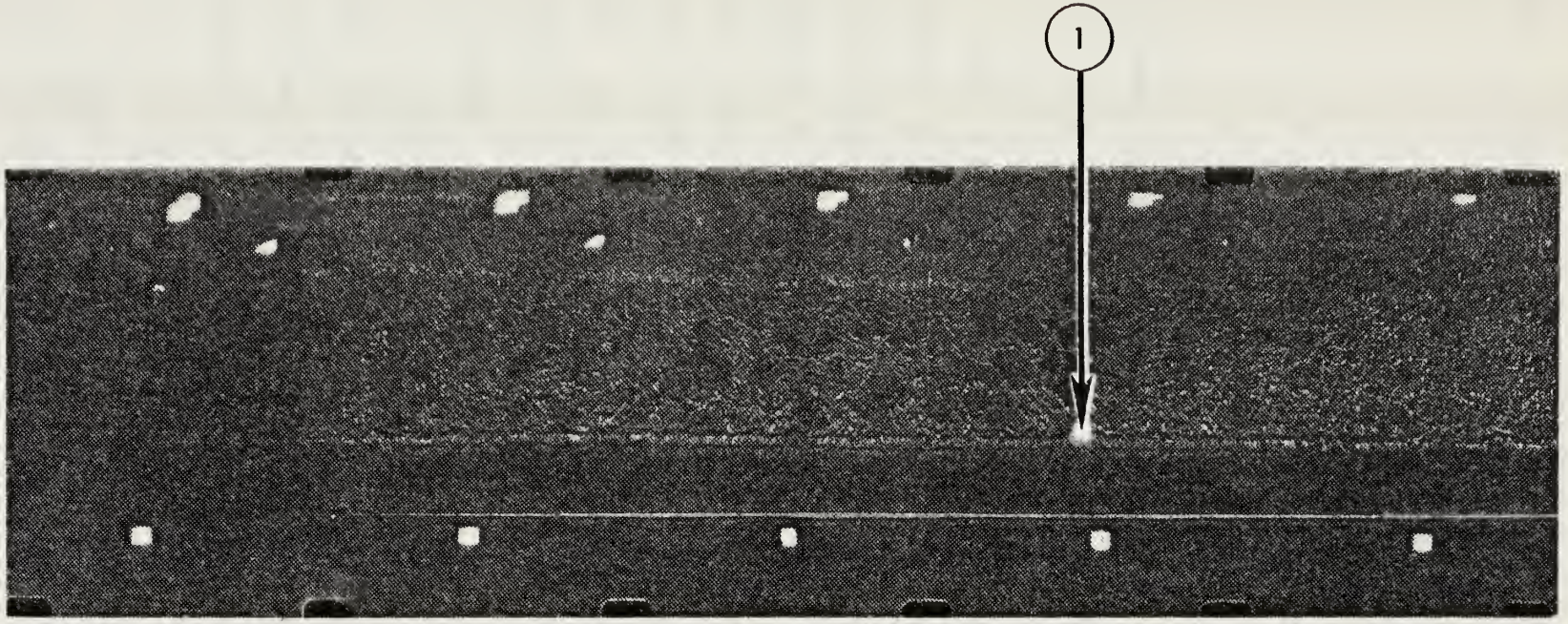

Figure 28(h) Frames 36-40

Burning Aluminum Particles 8.4 to 9.3 ms after initial plasma flash.

Table 3. Summary of Multiple Plasma Flashes

Flash	Time (ms)	Time Interval (ms)	Frequency* (Hz)
1	0		
2	3.7	3.7	270
3	5.1	1.4	714
4	7.0	1.9	526
5	9.1	2.1	476

*Based on time interval

Average frequency = 5 cycles/0.0091 sec = 550 Hz

Table 3 summarizes the time intervals for the five plasma flashes observed for a test in steam. The plasma flashes are accompanied by surges in current in the wire. The average frequency for the flashes is 550 Hz. Figure 17 shows oscillations in current and voltage at a frequency of about 1100 Hz; three oscillations or pulsations are reported here as follows: Figure 17 for test in air, Figure 29 for another test in air, and Figures 28(a) to 28(h) for a test in steam.

The make-break switching action, which leads to the observed phenomenon, may be due to molten aluminum. Figure 30 shows a sequence of events which may lead to multiple plasma flashes; this model is presented as a hypothesis and not as a proven fact.

Figure 29 provides an interesting example of the variation of signals from the filtered and unfiltered PMT. Table 4 contains the data which are interpreted later.

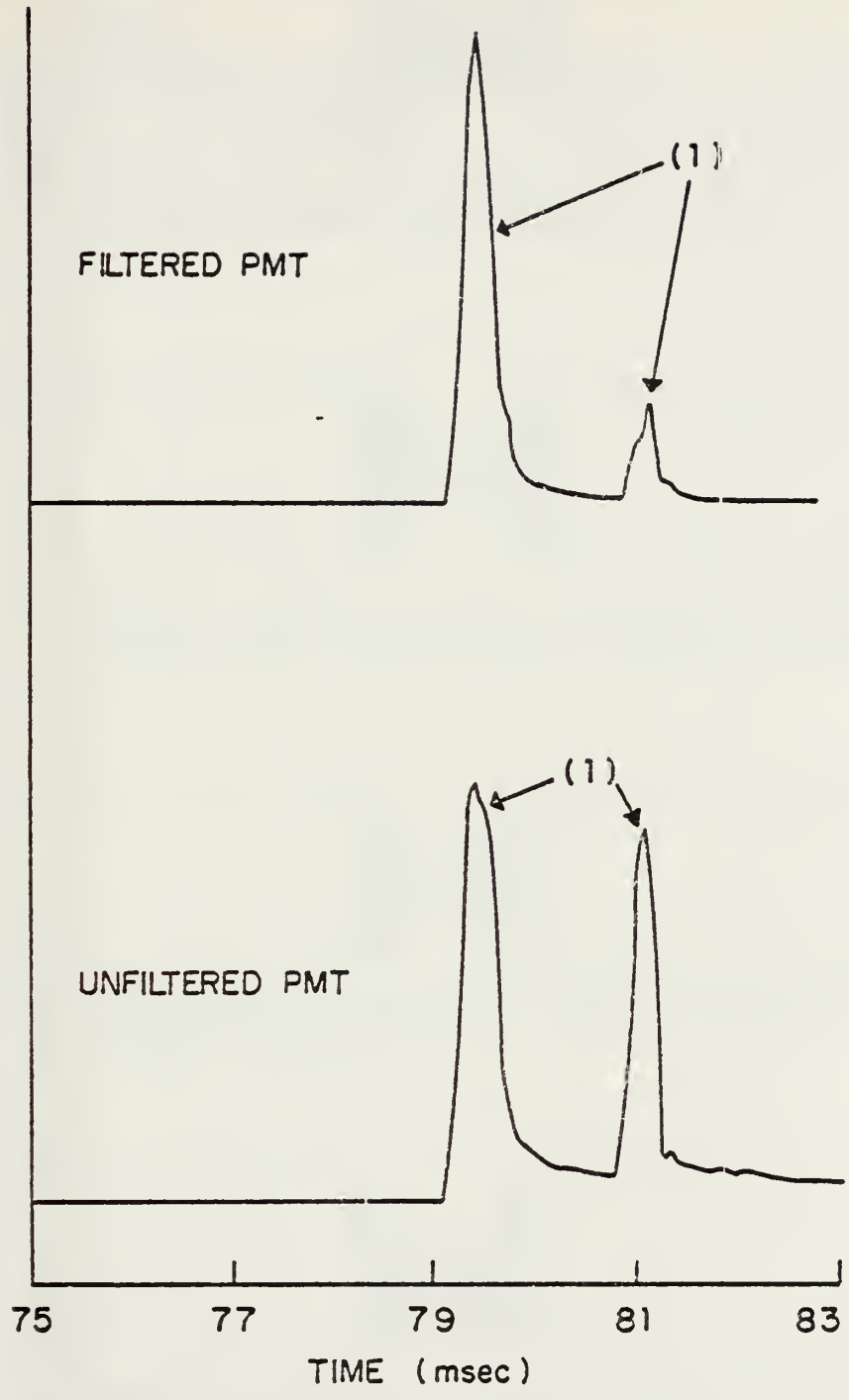

Figure 29. Double Plasma Flash, Test Conducted in Air

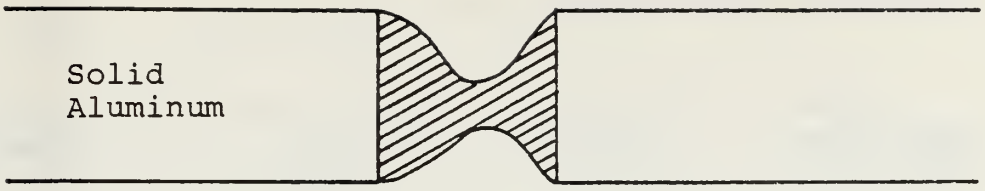

(a) Pinching of molten aluminum due to J X B forces. Molten aluminum shown cross hatched.

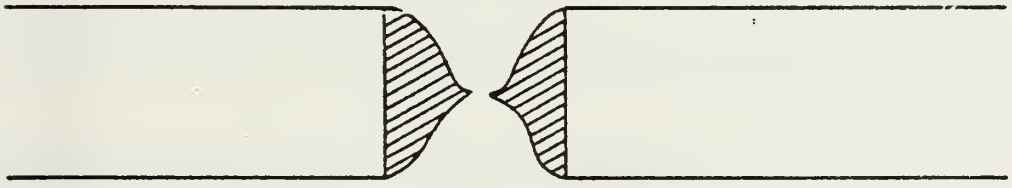

(b) Broken electrical circuit due to magneto-hydrodynamic instability of molten aluminum.

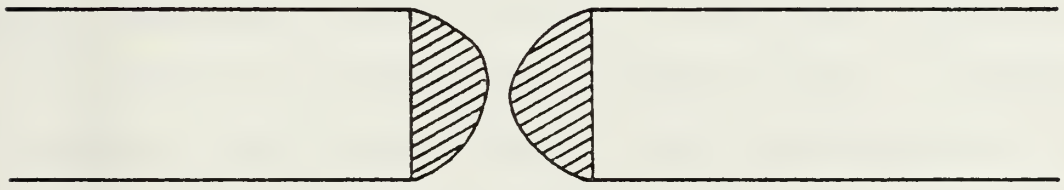

(c) Hemispherical shape of liquid aluminum due to surface tension.

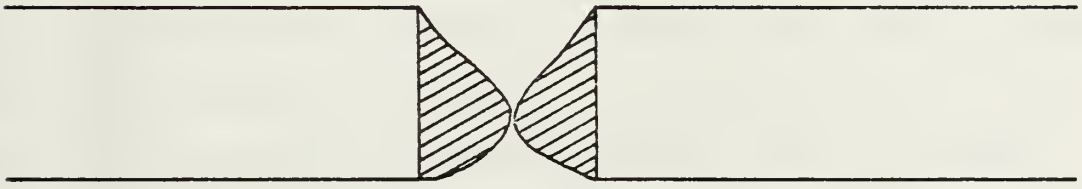

(d) Sagging of liquid aluminum due to gravity and closed electrical circuit. Plasma flash occurs.

Figure 30. Model for explaining multiple plasma flashes.

Table 4. PMT Signals for Multiple Plasma Flashes

Flash Number	Unfiltered PMT Signal*	Filtered PMT Signal*	Ratio $\frac{\text{Unfiltered}}{\text{Filtered}}$
1	2.2	2.4	0.9
2	2.0	0.5	4.0

* Arbitrary Units

D. PHOTOMULTIPLIER TUBE DATA AND RESULTS

A preliminary and simple test was conducted using the optical bandpass filter. The flash from the exploding wire was observed using the human eye without the filter. A judgement was made of the intensity of the flash. The flash was then viewed through the blue bandpass filter. A comparison was made of the flash intensity with and without the bandpass filter. Very small degradation of intensity occurred due to the filter.

The test described in the preceding paragraph is qualitative and judgemental in nature. However, the results indicate a significant amount of energy is in the blue part of the spectrum. To make the test quantitative, PMT are needed.

The PMT system records emitted radiation which is received by the photomultiplier tubes. Emitted radiation from a source is focused on the tubes by a large convex lens. A beam splitter positioned behind the lens splits the emitted light

into two beams, one directed to a mirror which redirects the beam to the filtered, (gray), PMT. The second beam passes directly through the splitter to the unfiltered, (silver), PMT. A more detailed discussion of the PMT system can be found in the thesis by Strott and Buck [Ref. 2].

To develop a baseline for comparison of test wire signals, a 6 volt flashlight bulb was positioned so as to be focused on the PMT, and its emitted radiation was chopped by a variable speed chopper to measure the response of the PMT. The high voltage power supplies, which were connected to the dynodes of the "silver" and "gray" PMT, were set at 370 and 425 volts, respectively. This voltage setting provided adequate signal output without clipping the signal due to radiation emitted by the 6 volt bulb. The voltage to the bulb was then varied from 3.5 to 8 volts, and the resultant response of the PMT was recorded. The high voltage power supply voltages were then changed to 270 volts for the silver PMT and 325 volts for the gray PMT, settings which were used for the aluminum wire tests. Additional tests were then conducted varying the bulb voltage from 6 to 9 volts. A ratio of the response of the unfiltered PMT to the filtered PMT was then tabulated.

Figure 31 is a graph of the ratio of signal from unfiltered PMT to signal from filtered PMT versus the voltage applied to the bulb. Curve 1 is the results of the tests conducted with high voltage power settings set at 370 and 425

volts. Curve 2 is the results for high voltage power supply settings of 270 and 325 volts.

As the temperature of the filment in the bulb (controlled by voltage to the bulb) decreases, the ratio increases indicating the decrease in response of the filtered PMT relative to the unfiltered PMT. The radiation at the center wavelength of the bandpass filter appears as a smaller and smaller part of the total visible radiation.

Using the data from Figure 29 and Table 4, the PMT response ratio was ascertained. The PMT response ratios are plotted in Figure 31(b). The point identified as 1 is for the first flash, etc. The PMT response ratios indicate the first plasma flash yields radiation having a relatively large fraction at blue wavelengths. The first flash is from a higher temperature plasma or else the first flash is accompanied by intense combustion of aluminum.

Figure 32 is a Polaroid photograph of the oscilloscope traces of signals from the PMT for an aluminum wire test conducted in air. The high voltage power supply was set at 325 volts for the gray PMT. The silver PMT high voltage power supply was set at 270 volts. The ratio of the unfiltered signal to the filter signal is approximately 1.05 ± 0.2. Using the graph in Figure 31(a) and interpolating from curve 2, an equivalent "bulb voltage" of approximately 11 volts implies a very hot source.

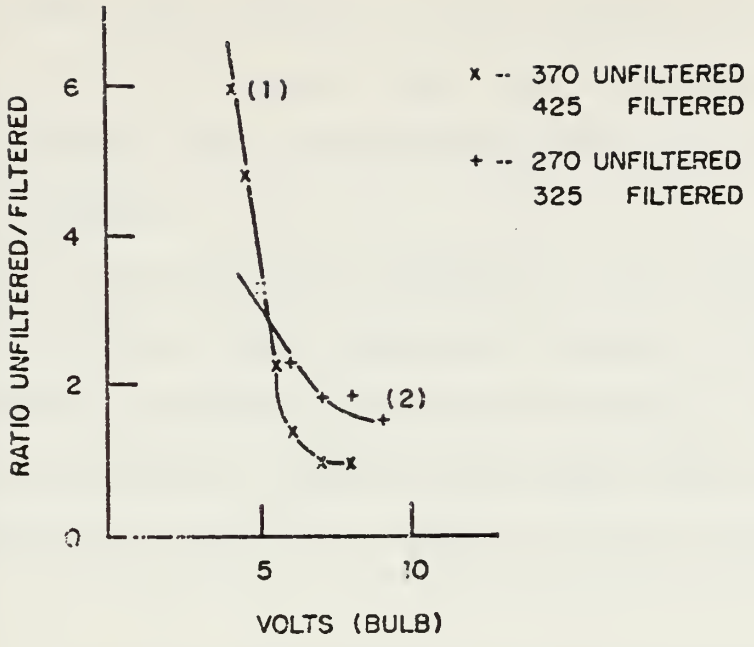

(a) Graph of PMT Reponse Ratio vs Bulb Voltage

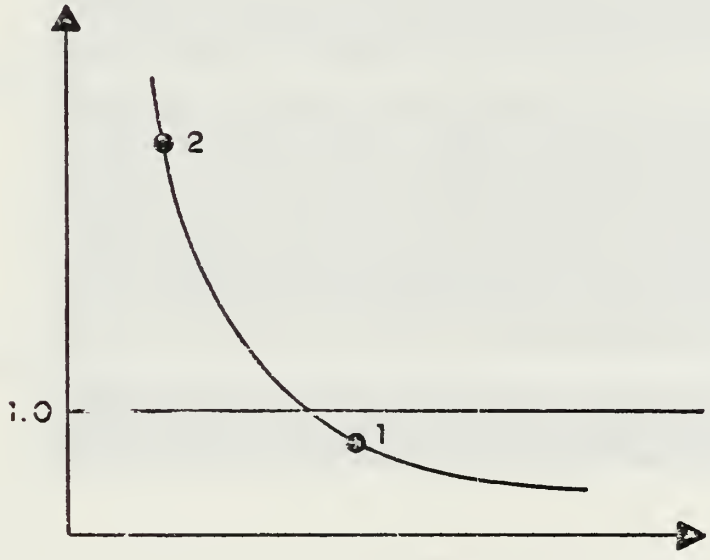

(b) Interpretation of PMT Response Ratio for Multiple Plasma Flashes

(1) High Level of Aluminum Combustion, (2) Low Level of Aluminum Combustion.

Figure 31. Curve of PMT Response Ratio for Calibration and Multiple Plasma Flash

Assuming that the radiation of the aluminum test wire reacts as a true gray or black body, the response of the PMT, as shown in Figure 31(a), is consistent with the theory of black body radiation.

A series of 15 tests were conducted in air using aluminum wire samples which had been accurately weighed. Biomation wave-form traces were made of each test sequence. The Biomation recorder was set at various delay times and various voltage scales in an effort to achieve the best possible

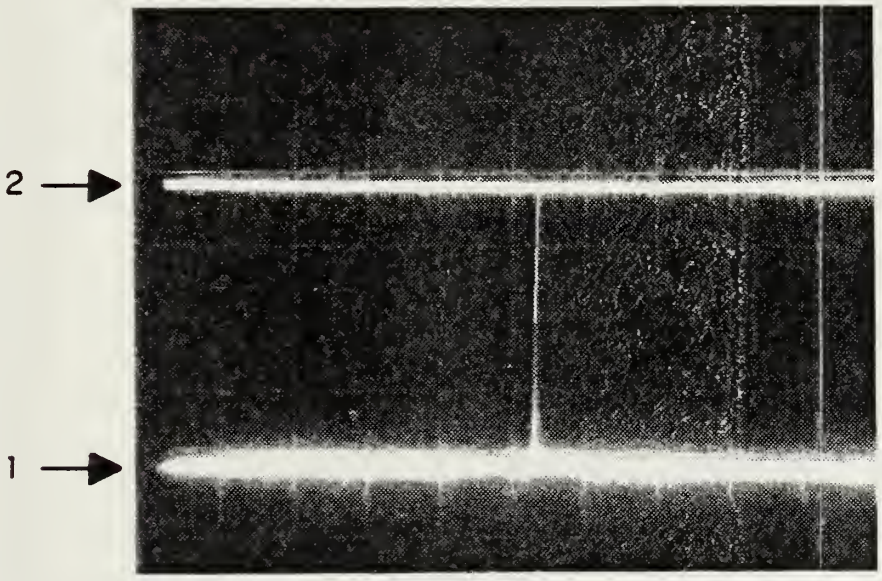

Figure 32. Oscilloscope Traces of PMT Response

(1) Filtered "Grey" PMT, (2) Unfiltered "Silver" PMT; One volt/centimeter Vertical Scale, 20 milliseconds/division Horizontal Scale.

record of the results. Table 5 is a compilation of the results of the test runs. An average time at which the plasma flash begins was calculated to be 81.5 ± 3.9 milliseccnds. The average time at which the signal from the filtered (gray) PMT decayed to zero was calculated to be 86.9 ± 4.2 milliseconds. The time at which the signal for the unfiltered (silver) PMT had decayed to zero could not be determined because, for the recording time used, the signal remained above the zero level.

A calculation was made of the weight and length of the "missing" aluminum sample. The average "missing" sample mass was 0.00056 grams corresponding to 0.283 mm in length. A count of the number of particles observed in a 35 mm slide of a test conducted in steam was used to determine an approximate particle size. Typically, 30 particles can be seen in the slide. An average particle size of 182μ was determined for one of the tests conducted in steam.

The results of the series of test runs provided useful data on the sequence of events which occur when aluminum wire is ruptured in air. The Biomation recorder was not used during the tests conducted in steam. Further research on the reactions in steam using the wave-form recorder should provide considerably more information on the events which occur during combustion of aluminum in steam.

Table 5. Aluminum Wire Tests Conducted in Air

Slide	Run	+	Initial Wt.(gm)	Final Wt.(gm)	Missing Wt.(gm)	Missing Length (mm) NOTE 1	Missing Length (mm) NOTE 2	Start of Flash (ms)	End of Gray PMT Response (ms)	End of Silver PMT Response (ms)	Wire Rupture At Crimp	Wire Rupture At End
3	1		0.1368	0.1362	0.0006	0.283	--	77.3	83.7	96	X	
4	*2		0.1346	0.1336	0.0010	0.472	1.0	--	--	---	X	
5	3		0.1302	0.1288	0.0014	0.660	0.9	81.8	82.9	90	X	
6	**4		0.1372	0.1377	0.0005	---	--	79.85	95.0	95		X
7	5		0.1346	0.1344	0.0002	0.094	1.0	81.45	85.6	97	X	
8	*6		0.1321	0.1315	0.0006	0.283	1.0	---	--	---	X	
9	+7		0.1354	0.1354	0.0000	0.0000	--	90.3	92.0	---		X
10	8		0.1346	0.1342	0.0004	0.189	0.5	84.85	88.0	99	X	
	*9		0.1281	0.1275	0.0006	0.283	--	---	--	---		
	10		0.1289	0.1284	0.0005	0.236	1.0	85.35	91.0	99		
13	11		0.1308	0.1302	0.0006	0.283	--	79	--	99		
14	12		0.1318	0.1308	0.0010	0.472	--	79.25	82.4	99	X	
16	13		0.1375	0.1372	0.0003	0.141	1.0	78.3	86.5	99	X	
17	14		0.1315	0.1311	0.0004	0.189	--	80.65	83.0	99	X	
19	15		0.1371	0.1369	0.0002	0.094	--	78.2	86.2	97	X	
20	16		--	--	--	--	--	---	--	---	X	
21	17		--	--	--	--	--	78.9	81.8	---	X	

* Data were not recorded by Biomation recorder due to equipment malfunction
** Test wire broke and mixed with other samples
\+ Test sample broke at one post not at crimp in center, considerably longer time to start of plasma flash

NOTE 1: Based on missing mass of wire.
NOTE 2: Based on feeler gage measurement of gap.

VI. DISCUSSION OF THE EXPLODING WIRE PROCESS

A. WHAT HAPPENS IN THE WIRE

Figure 33 is a sketch of a wave-form trace of the test sequence for aluminum wires ruptured in air. This wave-form trace can be used to illustrate what happens to the aluminum wire after the firing switch is closed. For the first 75 milliseconds after closing the firing switch, the test wire is heated to a temperature at which the wire begins to glow; see region 1 in Figure 33. The glowing wire emits thermal radiation which excites the PMT and provides an increase in signal level received by the Biomation recorder. The wire continues to heat until the wire ruptures creating the plasma and expelling the liquid aluminum particles; refer to region 2 in Figure 33. These particles ignite and burn in the ambient air. In region 3 of Figure 33, the PMT senses radiation which decays in magnitude. One example is shown in Figure 17. The value of the decay constant, τ, for the unfiltered PMT in Figure 17 was 13 ± 1.0 ms. The decay constant for the unfiltered PMT in Figure 33 is 1.7 ± 0.2 milliseconds. The decay constant varies in magnitudes over a wide range.

What is the origin of the signal in region 3 of Figure 33? Four possibilities exist as follows: (1) decay of plasma flash, (2) radiation from hot glowing wire, (3) luminous bases from combustion of aluminum particles, and (4) thermal radiation from solid or liquid aluminum particles. Results

from high speed movies rule out source (1) above. The plasma flash decays in 200 to 300 microseconds according to the movies. In regard to the hot glowing wire, the results from 35 mm color slides indicate the wire does glow but is relatively dim. Hence, source (2) is not too important in region 3. The burning aluminum particles will leave a wake of luminous combustion products. Immediately surrounding the burning particle is a cloud of luminous gases. The particles of aluminum are hot and radiate. Sources (3) and (4) are probably the cause of the radiation detected by the PMT in region 3.

All experimental evidence indicates the particles move rapidly outward from the origin at the plasma flash and point of wire rupture. The field of view of the optics for the PMT is limited in size. A region of approximately 15 mm in radius centered on the wire crimp is viewed by the PMT. The decay seen in region 3 may be due in part to particles moving out of the field of view of the PMT.

Note the bumps or ripples on the PMT trace in region 3. The bumps are probably caused by ignition and dispersion of the particles within the field of view.

Figure 34 illustrates the reason why rupture of the wire occurs at the crimp. Define R' as resistance per unit length, ohms/mm. The crimp causes a local peak in R' due to mechanical stress and reduced cross sectional area; see Figure 34(a). The energy per unit length E' Joule/mm, added to the wire due to electrical current is

$$E' = I^2 R' \qquad (6)$$

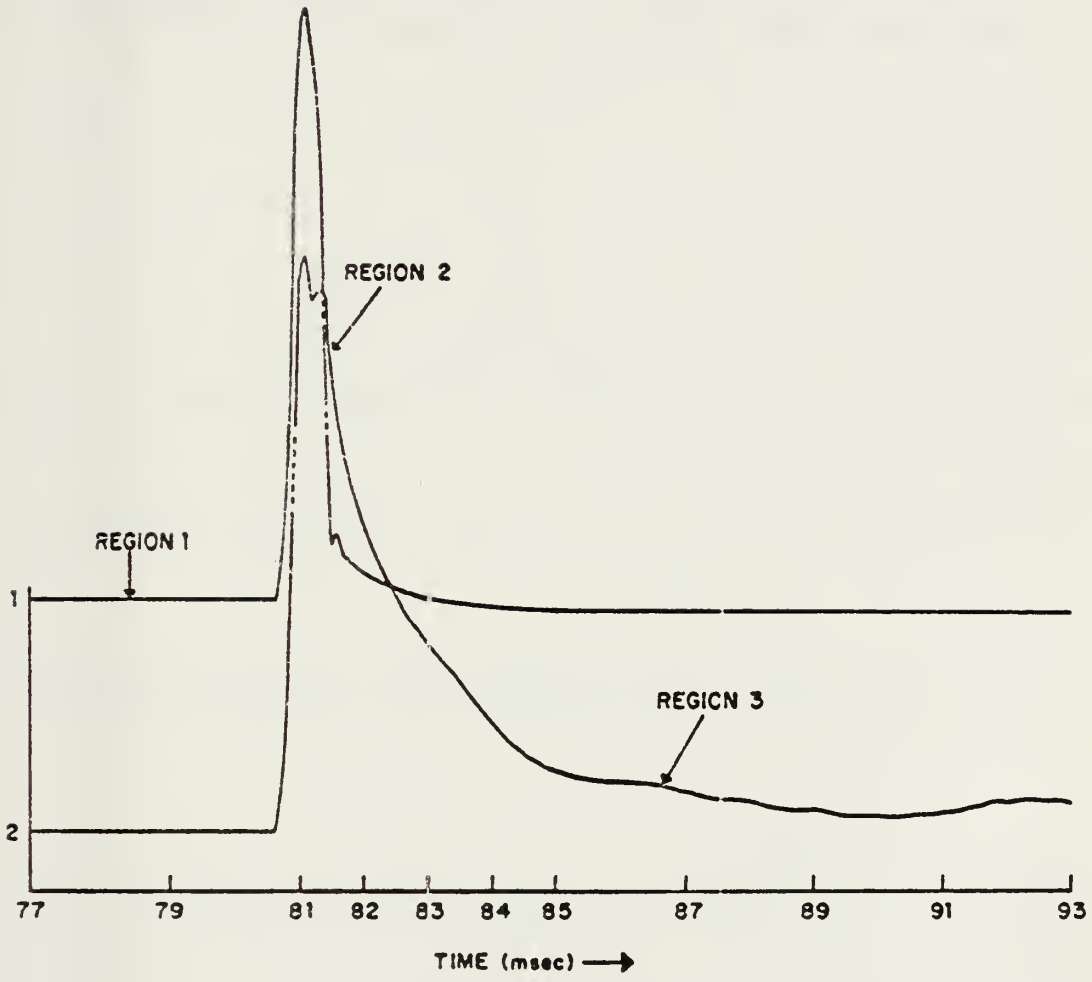

Figure 33. Wave-form Trace of Test Sequence

(1) Filtered "Grey" PMT Response, (2) Unfiltered "Silver" PMT Response.

Figure 34(b) shows wire temperature as a function of distance along the wire, X, at various times t_1, t_2, etc. At time t_2 the local temperature at the crimp in the wire equals the melting temperature of aluminum, T_m. Excessive heating occurs at the crimp due to the peak in R' at the same location.

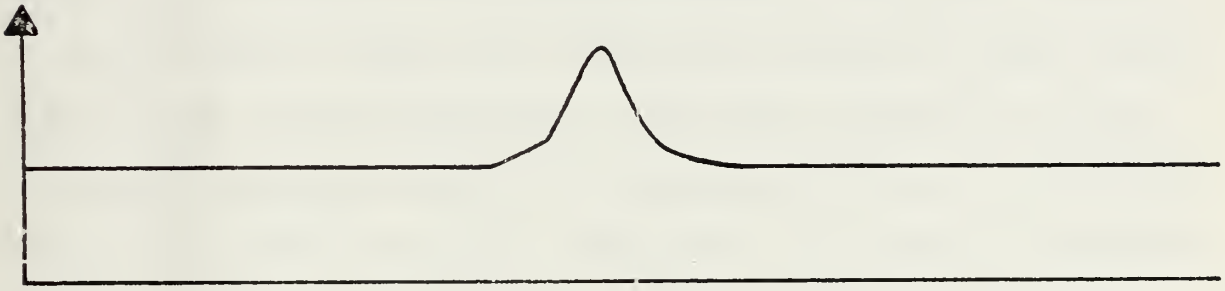

(a) Resistance per unit length within the wire.

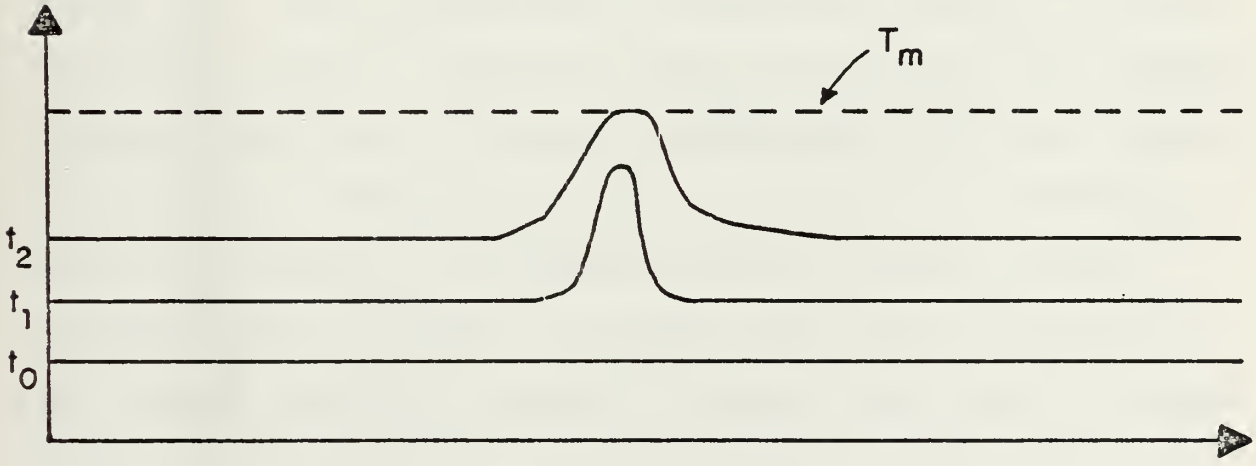

(b) Local temperature distribution along the wire.

Figure 34. Cause of Rupture at the Crimp

Figures 35-40 are a series of sketches of the various phases existing in the aluminum wire during the heating process. After the firing switch is closed the wire begins to heat. The wire continues to heat until portions of the wire begin to melt at a temperature of 933 K; see Figure 35. An aluminum oxide coating, which has a much higher melting temperature (2700 K) surrounds the aluminum wire and prevents the formation of droplets of molten aluminum. Unable to flow in molten form, the aluminum continues to heat until some of the molten aluminum is vaporized, Figure 36. This vaporized aluminum reduces the thickness of the wire through which the current can pass. Addition of a crimp in the wire acts as a local point of higher resistance which further concentrates the electrical current. The resistance of the wire increases, the pressure within the aluminum oxide coating increases, and the current through the wire decreases; see Figure 19. Due to deposition of electrical energy, the wire continues to heat. Unable to escape, the molten and vaporized aluminum continues to thermally expand until the oxide coating is fractured. See points A and C in Figure 37. Conditions exist for formation of a plasma created from the air and aluminum vapor; a plasma is a high temperature, ionized gas. The coating ruptures, releasing aluminum vapor and the liquid aluminum particles which instantly begin to burn; see Figure 37. The burning aluminum particles continue to burn for at least 20 milliseconds or more; see Figure 17.

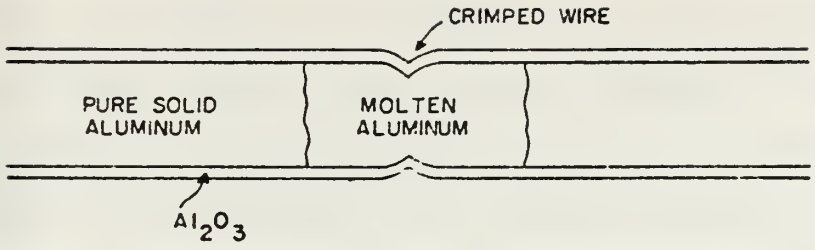

Figure 35. Condition of Aluminum Wire at Time t_2.

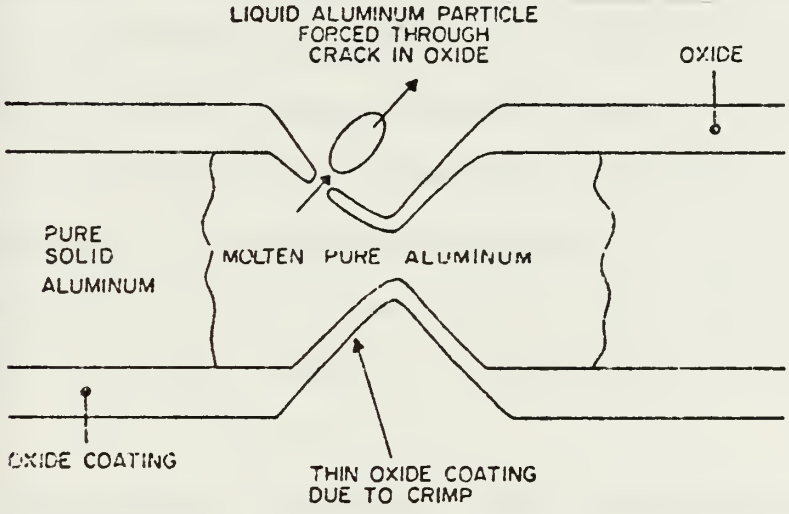

Figure 36. Cracking of Oxide due to Expansion of Molten Aluminum

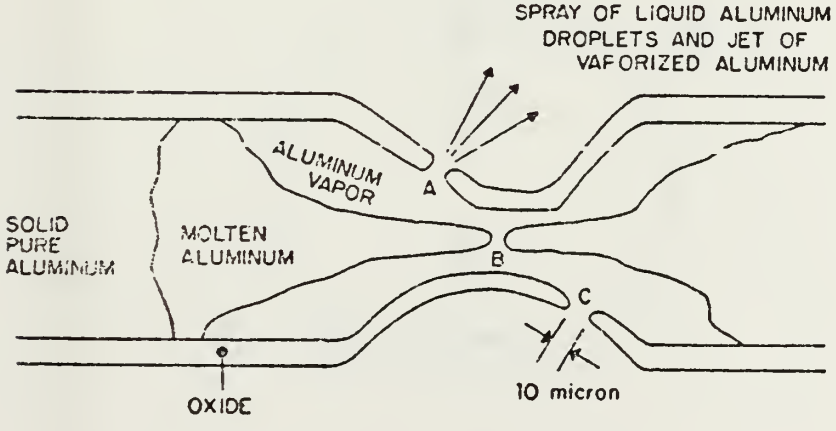

Figure 37. Origin of Plasma and Ejected Particles

A more detailed explanation of the origin of the plasma is warranted. At point B in Figure 37, a gap is shown in the strand of molten aluminum. The gap is caused by the pinching effect of magnetic forces. Refer to Figure 38 which shows a cross section of a conductor. The current density, J, is into the paper. The force F due to J X B is toward the axis of the conductor. The magnetic forces tend to reduce the radius of the conductor; restated, the magnetic forces pinch the conductor, reducing cross sectional area A. For fixed current, I, as the cross sectional area decreases, the current density increases. The relevant equation is J = I/A. Define e as the energy per unit volume added to the molten aluminum; e is related to current density J and electric field E by:

$$e = J \cdot E \qquad (7)$$

Note that e has units of Joule/m^3. When the molten aluminum is pinched to a thread, J is very large. For example, suppose

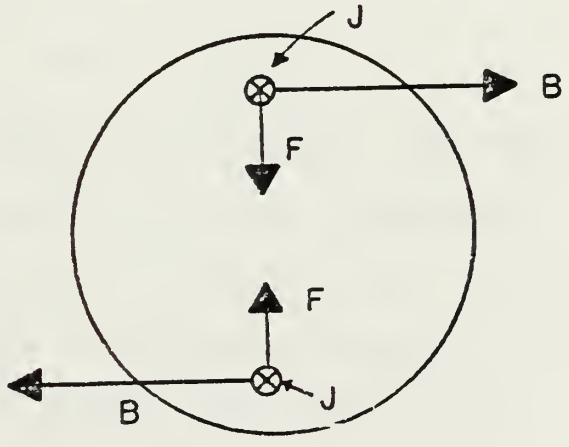

Figure 38. Magnetic Forces within an Electrical Conductor

the strand of molten aluminum has a diameter of 0.1 compared to original wire diameter. Hence:

$$J = I/A = 480 \text{ amperes}/(7.8 \times 10^{-9} m^2) \quad (8)$$

$$= 6 \times 10^{10} \text{ amperes}/m^2$$

As shown in Figure 37, a small gap exists at points A, B, and C. For discussion purposes, assume the gap is 10 micron. For a voltage, ϕ, across the crimped region of the aluminum test wire of 10 volts, the electric field, E, volts/meter is:

$$E = \phi/d = 10 \text{ volts}/10^{-5} m = 10^6 \text{ volts}/m \quad (9)$$

The volume of aluminum in the gap region is small and has a magnitude

$$V = Ad = (10^{-5} m)\ (7.8 \times 10^{-9}\ m^3) \quad (10)$$

The heating rate for the aluminum which fills the gap at point B, in Figure 37, just prior to breakage of the aluminum strand is very large; it is

$$\rho\ CV\ dT/dt = EJV \quad (11)$$

where ρ is the density of aluminum, 2700 kg/m^3; C is the specific heat capacity of molten aluminum, 0.9 kJ/kg K; E is the electric field, 10^6 volts/m; and J is current density, 6×10^{10} amperes/m^2. Canceling volume, V, in equation (11) and inserting the values given above gives:

$$dT/dt = 2.5 \times 10^{10} \text{ K/sec}$$

Extremely high heating rates occur as the molten aluminum is pinched. These heating rates cause the gap and create the plasma.

At a time several tens of microseconds later, the condition depicted in Figure 37 evolves into the situation shown in Figure 39. The plasma region is at high pressure and high temperature. Aluminum particles are expelled from the region by the high pressure of the plasma. The plasma rapidly cools due to two mechanisms: expansion and losses of energy due to copious radiation. The 35 mm slides show the condition existing in Figure 39; see for example Figure 20. The high pressure of the plasma in the gap also causes the molten aluminum on the ends of the wire to begin to flow along the wire. The ejected particles ignite and move away from the gap region.

On occasion, after the burning is complete, the test wire responds to the large magnetic forces involved. Figure 22 shows bent aluminum wire which was displaced by the J X B magnetic force exerted during the surge of current. Figure 40 shows the molten aluminum which flows away from the point of rupture and cools. The wire is glowing red; this fact is based on evidence from 35 mm slides.

Figure 40 also explains the apparent discrepancy in Table 5. The length of missing wire, L, was calculated using

$$L_1 = m/\rho A \qquad (12)$$

where m is the measured mass which is lost in the test, A, is the wire cross sectional area, and ρ is the density of aluminum. Subscript 1 indicates method 1 was used to determine L. The gap shown in Figure 40 was also measured by a feeler gauge and yielded values L_2. In Table 5, L_2 is greater than L_1. Method 1 for determining L does not account for the molten aluminum which flows along the wire away from the gap region in Figure 40.

B. BURNING ALUMINUM PARTICLE DYNAMICS

Equations for range as a function of time, x(t), and for velocity as a function of time, V(t), are given in the notes by Fuhs [Ref. 15]. Equations (13) to (16) were developed for projectiles from guns. Range is

$$x(t) = 2\beta[1 - \exp(t/T)]/\rho g \qquad (13)$$

where ρ is density of ambient gas, g is acceleration of gravity, β is ballistic coefficient, and T is a characteristic time. The ballistic coefficient, β, is

$$\beta = W/C_D A \qquad (14)$$

where W is the weight of the particle, C_D is the drag coefficient, and A is the cross sectional area of particle. The characteristic time is

$$T = 2\beta/\rho V_o \qquad (15)$$

where V_o is the initial particle velocity. The velocity of the particles as a function of time, V(t), is

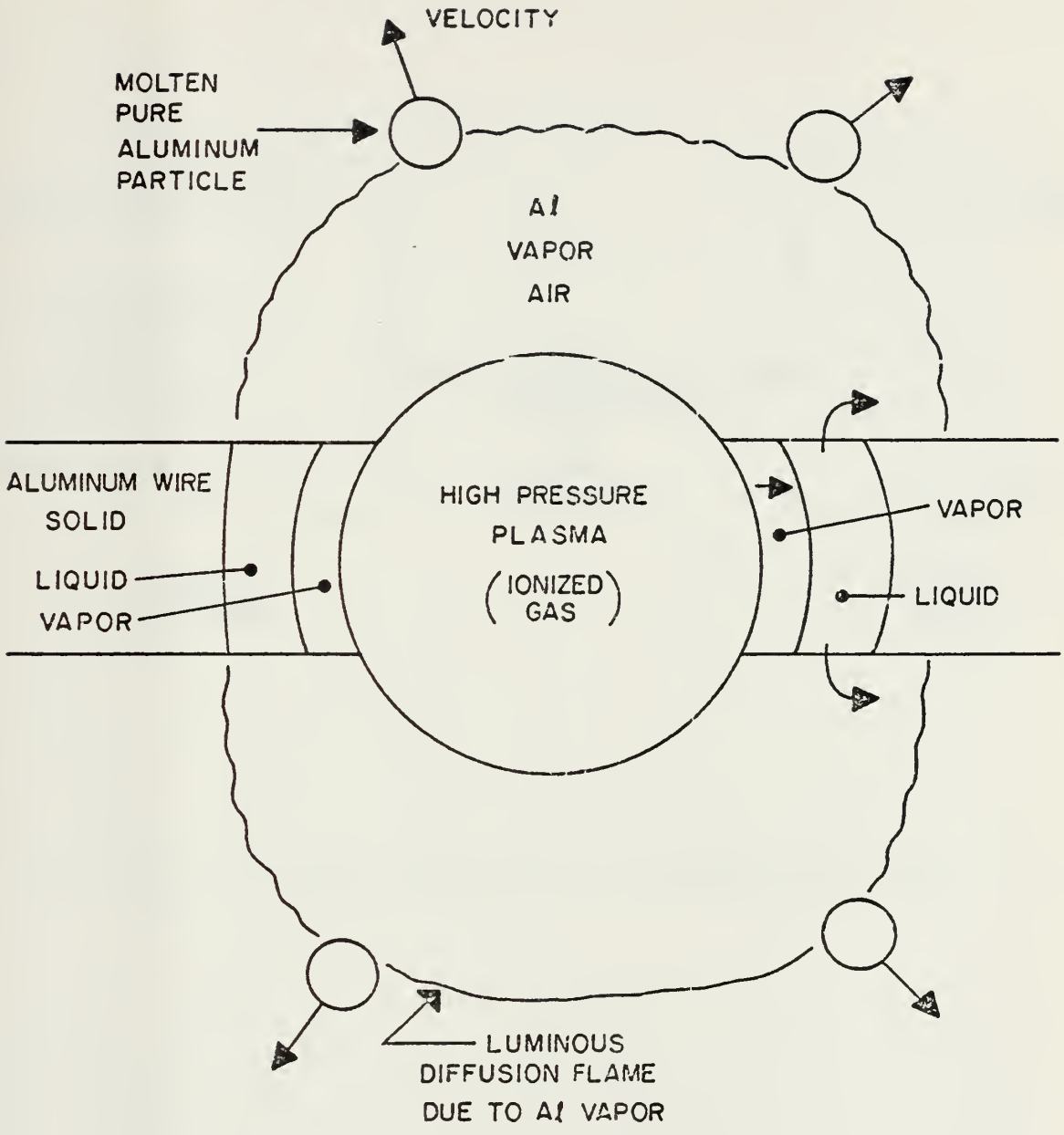

Figure 39. Conditions at Instant of Plasma Flash.

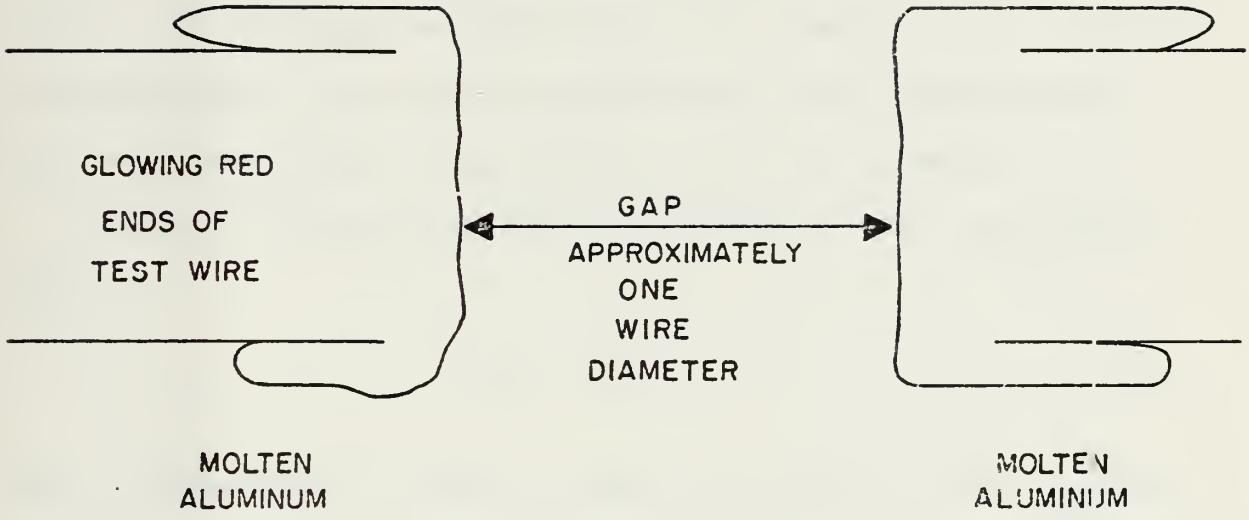

Figure 40. Final Condition of Aluminum Test Wire.

$$V(t) = V_o \exp(-t/T) \tag{16}$$

Equations (13) through (16) apply only if thrust and gravity are inconsequential.

Presumably one could determine x(t) from the high speed movies. An attempt was made to do so; however, the inability to measure x(t) accurately yielded data with considerable scatter. Meaningful conclusions could not be made.

With the limited information available, one can assume that:

$$\beta_s = \beta_a \tag{17}$$

where subscripts "s" and "a" refer to steam and air, respectively. Further, one can assume that the initial velocities V_o for particles ejected in steam or air are the same. If the plasma formation dominates the ejection process, the assumption seems to be plausible. Only density remains in equation (15). The density ratio is

$$\rho_s / \rho_a = (p_s/p_a)(T_a/T_s)(M_s/M_a) \tag{18}$$

where p is the pressure, T is the temperature and M is the molecular weight. Table 6 summarizes the values of p, T, M, and density ratio. Obviously, the density ratio is near unity. Consequently, the characteristic time, T, in equation (15) is nearly the same for tests in air or steam, and the range as $t \to \infty$ from equation (13) should be the same in air or steam.

Table 6. Density Ratio for Steam and Air Tests

Runs	Environment	P(psi)	T (C)	M	ρ_s/ρ_a
1 to 17	Air	14.7	20	29.8	---
First	Steam	31.5	131	18	0.97
Second	Steam	20.3	117	18	0.65

The observed ranges in air and steam are not the same. One can attribute the observation to the "rocket" effect. Another observation concerning the two tests in steam is relevant. The density for the first run in steam is greater than for the second run; see Table 6. Hence, the average range of particles should be greater for the second test than for the first test. The observed results for particle ranges are correct.

Table 7 summarizes the observations concerning tests in steam or air. Marked differences occur; it is these differences which must be explained in order to understand the role of metal-water reactions in underwater explosions.

Figure 41 illustrates the origin of erratic particle paths and particle spin. An oxide coating forms a chamber from which liquid aluminum flows through an opening. Combustion occurs on one side of the particle as shown in Figure 41(a). A thrust is developed of sufficient magnitude to cause the high acceleration turns shown in Figures 20, 21, and 22. If the nozzle or opening in the oxide coating is asymmetrically located, a torque develops about the center of gravity, CG, of

Table 7. Summary of Observations for Tests in Air and Steam

Steam	Observation	Air
Typical Velocity 2 to 4	Particle Velocity m/sec	Typical Velocity 7 to 11
First Test 31.5 Second Test 20.3	Chamber Pressure psia	All tests 14.7
First Test 1.19 Second Test 0.80	Chamber Density kg/m^3	1.23
Smooth Curved Trajectory (curved due to gravity)	Particle Trajectory	Erratic at End of Trajectory (curved due to rockets)
Same	Ballistic Coefficient	Same
Yes, with Pulsation in Intensity	Reignition	None or Rare
Test 1 28.7±22.9 Test 2 37.3±17.8	Range of Particles mm	55.4 ± 39.3
None Evident	Diffusion Flame at the wire	Pale Blue Surrounds Wire, Bright Yellow Above Wire; indicates Convection
Absent; not observed	"Rocket" Effect of Combustion	Major Factor near end of Trajectory

the particle, as shown in Figure 41(b). The spinning particles shown in Figure 20 are a result of the torque.

A model is needed which matches the main features of the observations. Figure 42 is a flow chart which was used to develop the model. The heavy lines around the boxes in Figure 42 are the final results of the model.

It is assumed that the particles are ejected from the wire by the plasma without an oxide coating and at the same average velocity irrespective of the environment, i.e., air or steam.

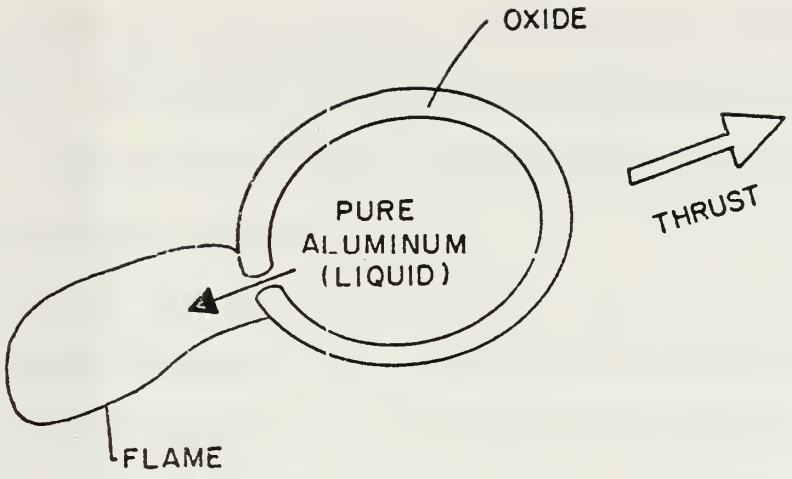

(a) Thrust developed due to "rocket" effect.

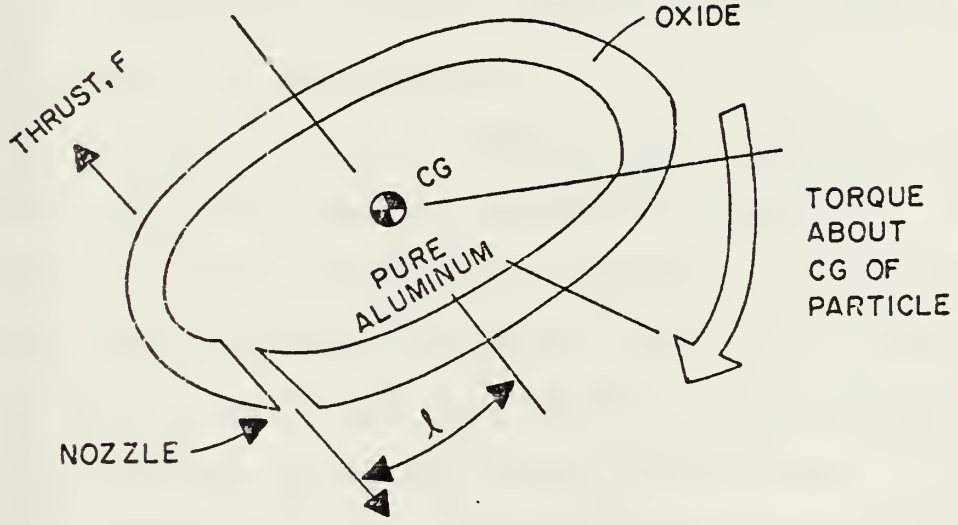

(b) Torque, Fℓ, due to asymmetric nozzle.

Figure 41. Origin of particle dynamics.

For particles in air, the combustion generates an oxide coating as the particle moves along the trajectory. Near the end of the trajectory, the condition illustrated in Figure 41 prevails leading to the erratic trajectories shown in Figures 20, 21, and 22. The oxide coating causes thrust and extends the range of the particles in air.

For particles burning in steam, spin was not observed. Also, sharp changes in the direction of motion were not seen. According to Figure 41, the thrust and torque on the aluminum particles are due to an oxide coating. Either an oxide coating does not develop or else the oxidizer can diffuse evenly through the oxide coating. Macek, Friedman, and Semple [Ref. 13] observed a different diffusion flame structure for aluminum burning in wet or dry oxidizer.

Refer to Figures 25 and 26. Almost every particle trajectory in steam shows the behavior sketched in Figure 43. The film exposure is shown in Figure 43. At point A, the trajectory is narrow and increases in width to point B. If the particle is burning at a fixed rate while the velocity is decaying, the exposure of the film would be as shown.

From point B to C to D, the exposure decreases in spite of the fact the velocity is decreasing. For this to occur, the rate of combustion must be decreased.

At point D, the flame is extinguished with reignition occurring at point E. The reignition occurs sharply. A critical condition for combustion must exist; the critical

condition is undoubtedly related to particle velocity. Following the reignition, the flame is extinguished once again going along the trajectory from point E to F.

Also shown in Figure 43 is an inset depicting pulsating combustion which occurred in test number 2 in steam. Once again this interesting phenomenon is not understood.

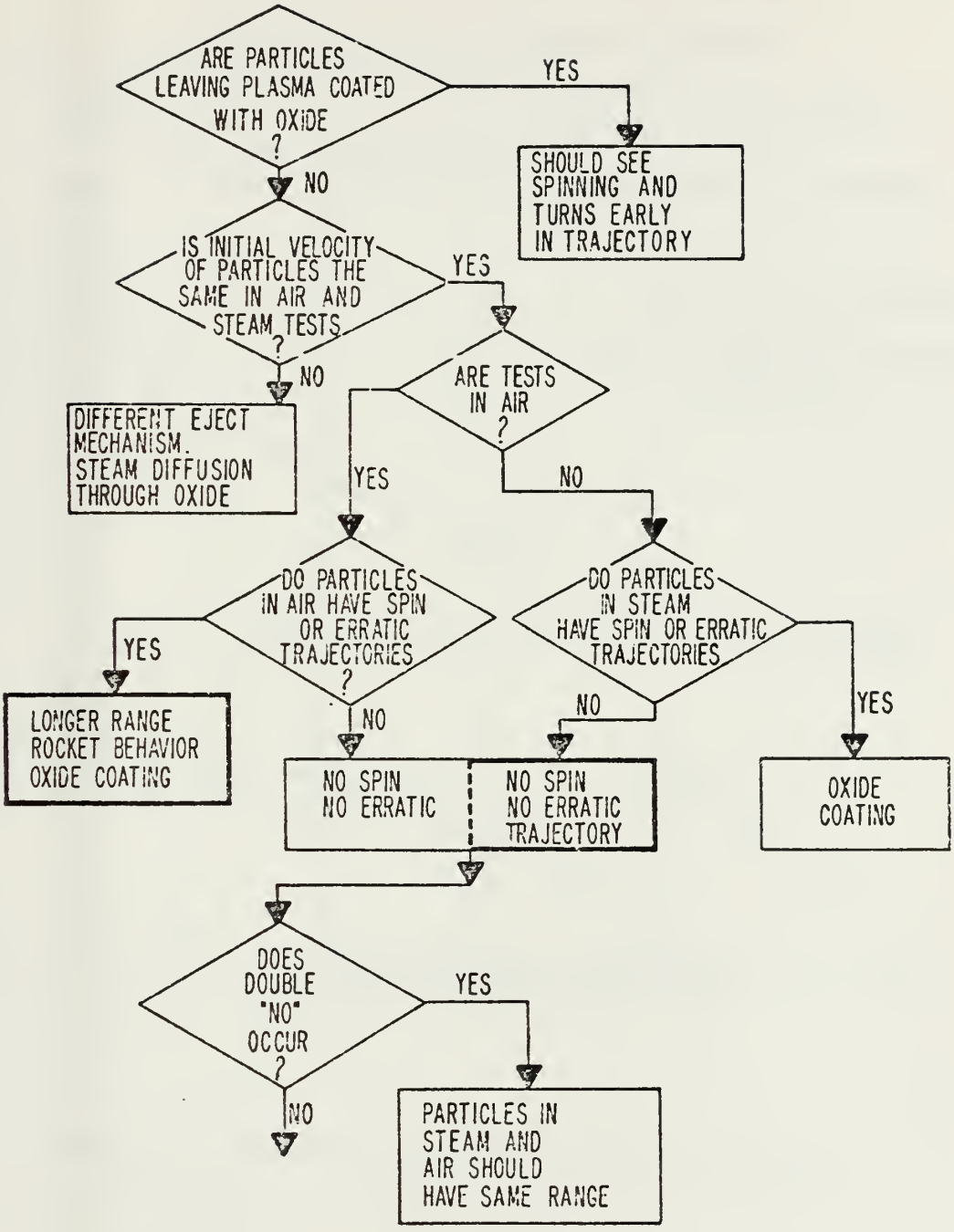

Figure 42. Flow chart for logic used to construct a model of combustion.

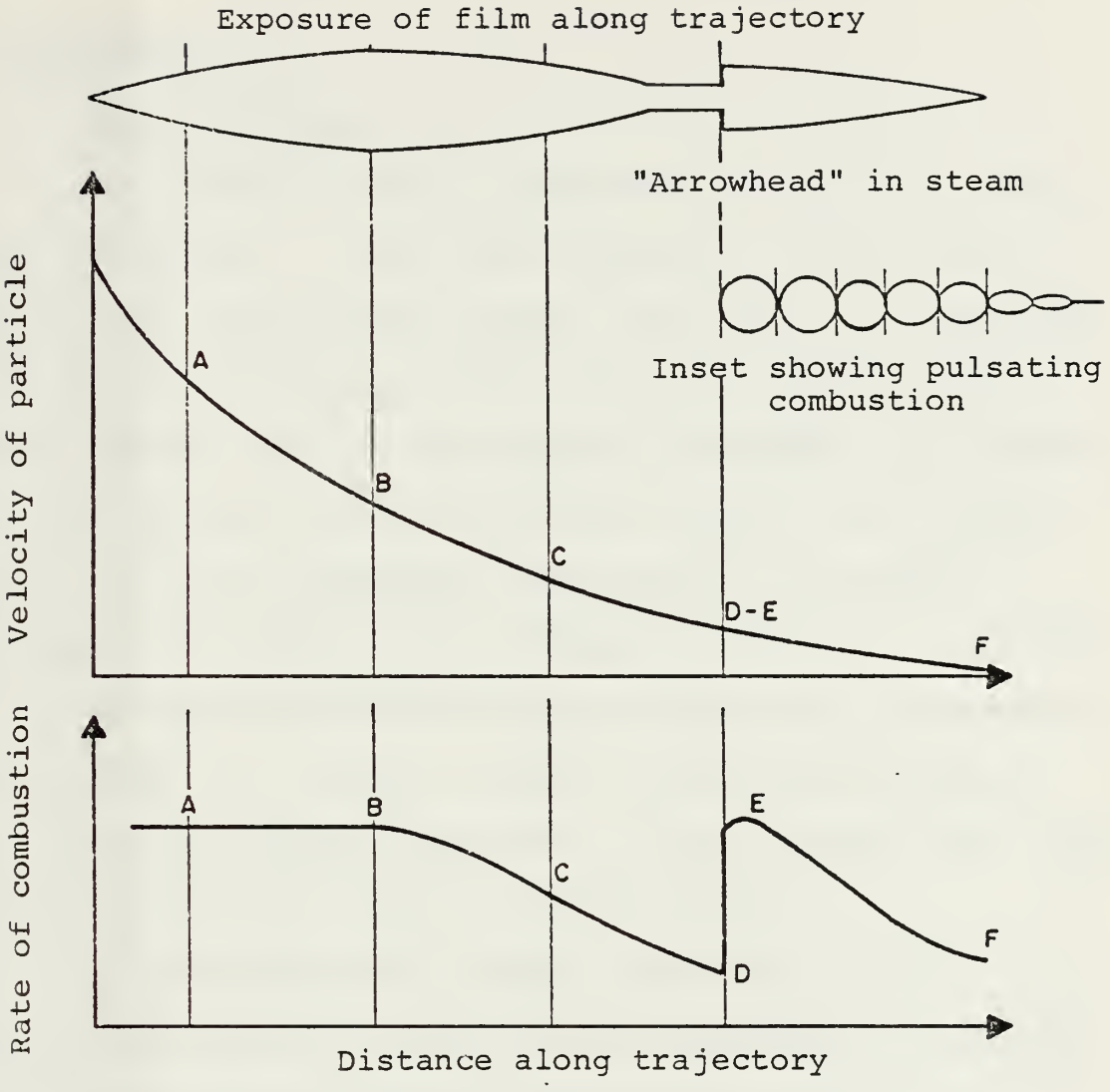

Figure 43. Re-ignition of aluminum particle.

VII. CONCLUSIONS AND RECOMMENDATIONS

A. CONCLUSIONS

1. Test Apparatus

The pressure vessel, described in Section III, functioned as designed. Tests were conducted in nearly pure steam at high temperatures without difficulty. As predicted by the design calculations, the insulation system greatly reduced the heat loss to the outside atmosphere. The observation ports provided clear undistorted views of the testing process; by using appropriate experimental techniques, condensation of steam on the windows was avoided. The flexible, versatile design of the pressure vessel and its accompanying equipment will provide a means of conducting numerous tests under the desired conditions. Much valuable data should become available with the use of this device.

The photomultiplier tubes, described in Section IV, provided qualitatively correct data; measurements involving PMT are difficult and require considerable experimental finesse. Data from the PMT, in conjunction with data from the movie camera, provided excellent information on the multiple flash phenomenon. The high speed movie camera provided data in sufficient quantity to evaluate the average velocity of each particle; however, the high speed movie film did not permit evaluation of equations (13) and (16) which are the range and velocity of the burning aluminum particles as a

function of time. The 35 mm color slides also provided valuable data. The nature of particle trajectories (Figure 20), wire dynamics (Figure 22), wire radiation (Figure 21), and evidence of diffusion flames (Figure 24) was obtained from slides taken of various tests in both air and steam.

Electrical energy measurement equipment operated satisfactorily; improved accuracy of measurement may be desirable. Dual-beam oscilloscopes provided the initial information needed to properly adjust the wave-form recorder for best data collection. The digital thermometer system and the vacuum/pressure systems performed as designed. Temperature control of the apparatus allowed precise setting of the desired steam pressure and temperature.

2. Results

Many of the results cited in this report are pioneering and preliminary in nature. Aluminum combustion in steam has been demonstrated; see Figures 25 and 26. Plasma was formed using 480 amperes of current. A spray of burning aluminum particles was ejected in the testing prccess in both air and steam. The spray of aluminum particles is relevant since previous research by Strott and Buck [Ref. 2] has provided evidence of the particles in underwater shaped charge experiments. Hence, the results of these experiments should provide useful information on the behavior of aluminum particles in steam. Thorough study of Tables 2 and 7 will provide several important, useful facts about aluminum combustion in various atmospheres.

As stated, this research was preliminary in nature. An investigative approach to evaluation of the results was made. Figure 42 is a flow chart of the logic used in developing a model to explain the observed combustion phenomenon. Conjecture, speculation, and intuition were used at times to reach plausible conclusions where data were not available. Table 7 lists those facts that were verifiable by the data collected. Figures 25, 26, and 43 contain data which has provided more questions than answers. What makes the particles in steam? Why do the particles appear to pulse? Why is there very little evidence of a diffusion flame along the wire in steam? Further research should provide the answers.

Additional information which was not obtained, due to a lack of time, was data on transient temperatures and pressures at the instant of plasma flash. The transducers and test equipment are available but were not used for these tests. Additionally, an infrared thermometer system was ordered but did not arrive in time to be used in these experiments. The infrared system is sensitive in the 2.0 to 2.6 micron region and has a time response of 100 milliseconds.

B. RECOMMENDATIONS

The most useful data from these experiments was collected when several of the instruments were operational for the same test. Simultaneous use of all of the instrumentation provides more information for screening and checking hypotheses. Synergistic results are available by cross correlation between

measurement methods. Multiple plasma flashes were observed on 3 separate occasions by different instruments. In none of the 3 cases were multiple instruments in use.

Use of color high speed movie film may provide more evidence of diffusion flames in steam. Use of a spectrograph can complement the results available from the PMT. A system to measure the quantity of hydrogen gas evolved due to combustion would provide a measurement of the extent of combustion. A more accurate scale, with 10 microgram accuracy, is needed to improve measurement of before/after aluminum wire mass; see Table 5.

Multiple test runs of the pressure vessel might damage the vacuum pump; installation of a cold trap in the vacuum pump piping could prevent water damage to the vacuum pump. See Figure 13 for the vacuum pump piping. The shunt used for measurement of the current in the test wire circuit was rated at 300 amperes for 50 millivolts; calibration of the shunt could provide answers to the whereabouts of some of the "missing" Joules, see Section II. Calibration of the shunt was not accomplished in these tests due to lack of time.

Finally, the performance of tests involving slow heating of the aluminum wire in both air and steam could provide additional information and better understanding of the ignition process. Slow heating provides better control and measurement of wire temperature. The diffusion flame may be apparent before the plasma flash occurs.

APPENDIX A

ENERGY CALCULATIONS

Calculation of total energy required to change aluminum at 200 C into vapor at the boiling point of aluminum (2494 C)

Define:
- ℓ, the length of aluminum test wire
- x, the length of "missing" aluminum test wire
- T_o, initial temperature of test wire, 200 C
- T_m, melting temperature of aluminum, 660 C
- T_b, boiling temperature of aluminum, 2494 C
- C_{p1}, specific heat of solid aluminum, 0.9 J/gm K
- C_{p2}, specific heat of liquid aluminum, 1.18 J/gm K
- h_f, heat of fusion of aluminum, 397 J/gm
- h_v, heat of vaporization of aluminum, 10.78 kJ/gm K
- h_c, heat of combustion of aluminum, 31.05 kJ/gm
- m_ℓ, mass of aluminum test wire, 0.138 gms
- m_x, mass of "missing" aluminum wire, 0.000212 gms

Assume:
(1) ℓ = 65 mm
(2) x = 1 mm
(3) all of the sample ℓ melted
(4) all of the "missing" sample x vaporized
(5) all of the "missing" sample x burned

$$e_m = m_\ell \int_{T_o}^{T_m} c_{p1}\, dT$$

$$e_m = 0.138 \int_{473}^{933} 0.9\, dT = 78.6 \text{ Joules}$$

$$h_f = 0.84 \text{ Joules}$$

$$e_b = m_x \int_{T_m}^{T_b} c_{p2}\, dT$$

$$e_b = 0.000212 \int_{933}^{2967} 1.18\ dt = 4.59 \text{ Joules}$$

$$h_v = 22.9 \text{ Joules}$$

$$e_t = e_m + h_f + e_b + h_v = 106.9 \text{ Joules}$$

$$e_c = m_x h_c = 65.8 \text{ Joules}$$

Electrical Energy Transferred to the Wire

Define: t, the time for rupture of wire to occur

V, the voltage in the circuit, volts

I(t), the current in the circuit, as a function of time (t)

Assume: (1) $t = 76.0$ msec

(2) $V = 8$ volts

(3) $I(t) = 480 - 60t/.076$

$$e_e = \int_0^t VI\ dt$$

$$e_e = V\int_0^t (480 - 60t/.076)\ dt$$

$$= 274 \text{ Joules}$$

Energy "Lost" in Resistance of Test Wire Circuit

Copper resistivity = 16.73 nanoohm meters

Stainless Steel resistivity = 72 nonoohm-meters

Total resistance Copper and Stainless Steel

$$R = .00263 \text{ ohms}$$

$$e = R\int_0^t I^2\ dt$$

$$= 40.6 \text{ Joules}$$

APPENDIX B

ESTIMATION OF WIRE TEMPERATURE

Estimation of Wire Temperature Using Time History of Electrical Current

A simplified circuit is shown in Figure B-1.

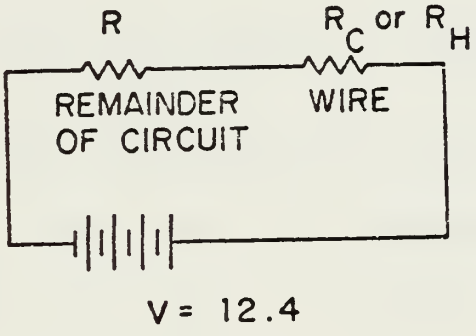

Figure B-1. Simplified Circuit for the Test Specimen

Define the following symbols:

R_C = wire resistance, cold, ohms

R_H = wire resistance, hot, ohms

R = resistance of remainder of current which includes shunt, battery internal resistance, copper cables, and stainless steel test holder, ohms

R_O = total circuit resistance, cold, ohms

R_1 = total resistance circuit, hot, ohms

ρ_C = resistivity of pure aluminum, cold, 2.62×10^{-6} ohm cm

ρ_H = resistivity of pure aluminum, hot, ohm cm

C = temperature coefficient for resistivity of aluminum, 0.0039 per degree C.

L = length of test wire, 6.5 cm

r = radius of test wire, 0.05 cm

V = battery potential, volts

I_C = current in circuit, cold, amperes

I_H = current in circuit, hot, amperes

When the battery is charged, V has a value of 12.4 volts. From Section V, the values for I_C and I_H are 480 and 420 amperes, respectively. Hence, the total circuit resistance when the aluminum wire is cold is

$$R_O = V/I_C = 12.4/480 = 0.02583 \text{ ohms} \qquad \text{(D-1)}$$

The total circuit resistance, hot, R_1 is

$$R_1 = 12.4/420 = 0.02952 \text{ ohms}$$

$$R_H - R_C = R_1 - R_0 = 0.02952 - 0.02483$$

$$R_H - R_C = 0.00396$$

$$R_C = 0.00167$$

$$R_H = 0.00396 + 0.00167 = 0.00536$$

$$R_H/R_C = \rho_H/\rho_C = 1 + C\Delta T$$

$$\Delta T = (\rho_H/\rho_C - 1)/C$$

$$\Delta T = 566 \text{ C}$$

$$273 + 566 = 839 \text{ K} = \text{near melting point}$$

APPENDIX C

MAGNETIC FORCE ON THE WIRE

The magnetic field at the center of a square loop of wire is

$$H = \sqrt{2}\, I/\pi a \qquad \text{(C-1)}$$

where the current in the wire is I, amperes, and the length of one side of the wire is 2a, meters. Equation (C-1) is from Lawden [Ref.17]. The value of H calculated from equation (C-1) is not the value at the wire; however, the order of magnitude of the force, F, Newtons on the wire can be estimated using H as calculated.

The current density in the wire is

$$J = I/A \qquad \text{(C-2)}$$

where A is the cross sectional area of the wire. The force per unit volume is

$$F/V = JB = \mu JH \qquad \text{(C-3)}$$

where the wire volume is V, m^3. The relation between the magnetic flux density, B, and magnetic field H has been introduced into equation (C-3) through the magnetic permeability, μ. The value of μ in air is $4\pi \times 10^{-7}$ Henry/meter. The wire volume is

$$V = LA \qquad \text{(C-4)}$$

where L is the length of the wire, meters.

Combining the preceding equations and noting that $L = 2a$, one obtains

$$F = \mu\sqrt{8}\, I^2 / \pi \qquad \text{(C-5)}$$

Inserting current of 480 amperes into equation (C-5) yields a force of 0.26 N. The aluminum wire has a mass of approximately 0.1 gram. The weight of the wire is

$$w = mg = (0.0001 \text{ kg})\ (918 \text{ m/sec}) = 0.00098 \text{ N}$$

The ratio of F to w is of interest; the value is

$$F/w = 260$$

Obviously, the magnetic force greatly exceeds the weight of the wire.

APPENDIX D

DETERMINATION OF PARTICLE SPEED

Determination of Particle Speed from High Speed Movie in Air.

Define: a, length from lens to image, mm
b, length from lens to object, mm
f, the focal length of the lens, mm

$$f = ab/(a+b)$$

Assume: f = 75 mm
b = 330 mm

$$a = bf/(-f + b)$$

$$= (330)\ (75)/(330 - 75) = 97 \text{ mm}$$

Magnification, M = dimension of object/dimension of image

$$= b/a$$

$$M = 330/97 = 3.4$$

Define: d_p, distance on film print
d_f, distance on film (image)
d_s, distance of object

$$d_p / d_f = 94/10 = 9.4$$

$$d_s = d_f M = d_p M/(d_p/d_f)$$

$$m = 3.4 d_p/9.4$$

Frame	d_p(mm)	Δd_p	d_s	Δd_s	V m/sec
	0	7.0	0	2.53	
1	7.0		2.53		10.9
		4.5		1.63	
2	11.5		4.16		7.0
		4.5		1.63	
3	16.0		5.79		7.0
		5.0		1.81	
4	21.0		7.60		7.8

APPENDIX E

TEST PROCEDURE - EXPLODING WIRE CASE

1. Weigh and install test wire in holder.
2. Install test wire holder in top of test assembly.
3. Install windows.
   a. Insure gaskets are clean.
   b. Place gasket on each side of glass.
   c. Put flange, glass, and gasket assembly in position and tighten bolts hand tight.
   d. Close drain valve and open pressure gage and vacuum pump valves.
   e. Turn on vacuum pump and pump down 10 psi.
   f. Turn off vacuum pump and close vacuum valve.
   g. Sequentially tighten each flange bolt to 1 foot pound of torque.
4. Install sides and top of box including observation port covers.
5. Close all valves.
6. Open Nitrogen drain valve.
7. Open Nitrogen supply valve.
8. Open drain tube valve and fill water pipe including syringes.
9. Close valves.
10. Check battery voltage.
11. Connect battery cable to top of test wire lead.
12. Open pressure gage valve.
13. Open vacuum pump pipe valve.
14. Turn on vacuum pump, monitor pressure gage and digital multimeter.
15. Close vacuum pump valve and turn off vacuum pump.
16. Plug in 220 volt heater line.
17. Turn on heater control and all monitoring devices.
18. Load high speed camera.
19. Open water valve under base and close syringes.
20. Close water valve under base.
21. Monitor temperature and pressure until desired conditions are established.
22. Turn on oscilloscopes.
23. Turn on wave-form recorder.
24. Turn on high voltage power supply for photomultiplier tubes.
25. Turn on Variac, set voltage for desired camera speed.
26. Ensure equipment warm-up is complete and lenses are properly positioned.
27. Monitor temperature and pressure until desired conditions are reached.

28. Record highest temperature indicated. (Thermocouple #8)
29. Record maximum pressure indicated by digital multimeter.
30. Close Heise pressure gage valve.
31. Depress High Speed Camera, wait for camera to reach maximum speed.
32. Depress trigger switch.
33. Photograph oscilloscope traces.
34. Unplug 220 volt heater line.
35. Allow apparatus to cool.
36. Record test data.
    a. Make plot of voltage change with wave-form recorder.
    b. Remove and develop high speed film.
37. Open base water valve and drain valve allowing pressure to stabilize.
38. Disconnect battery cable.
39. Remove top port cover.
40. Remove test wire holder assembly.
41. If additional runs are desired, return to step 1.
42. If final run of series, remove top and sides of box to allow further cooling.
43. When device returns to normal temperature level, remove windows.
44. Clean window surfaces with distilled water.
45. Check battery voltage, hook-up battery charger at end of last run for the day or whenever battery voltage is low.

APPENDIX F

SAFETY PROCEDURES

1. CAUTION: Apparatus is designed for high temperature and pressure.
2. Ensure all switches are OFF and drain valves are OPEN before approaching apparatus.
3. Ensure high voltage heaters are UNPLUGGED at the wall receptable.
4. Check all thermocouple readings before removing any portion of apparatus.
5. Battery circuits and the vacuum pump are GROUNDED to the metal table. Ensure the positive lead of the battery remains above the table top when circuits are energized.
6. Observation port glass is very hard and will BREAK if OVERSTRESSED.
7. SAFETY GOGGLES should be worn when tightening flange bolts.
8. All FLANGE bolts should be installed finger tight only initially.
9. Follow window installation procedures completely.
10. Photomultiplier tubes are EXTREMELY light sensitive. Ensure high voltage power to the Photomultiplier Tubes is turned OFF before opening Photomultiplier tube box.

LIST OF REFERENCES

1. Naval Surface Warfare Center Report 81-490, The Reflection of Oblique Shock Waves in Water, by F. D. Hains, 1981.

2. Strott, J. B. and Buck, J. A., Underwater Shaped Charges, Master of Science Thesis, NPS 67-82-005, June 1982.

3. Baker, L., Jr. and Liimatainen, R. C., The Technology of Nuclear Reactor Safety, Volume 2, Chapter 17, Massachusetts Institute of Technology Press, 1973.

4. United States Atomic Energy Commission Report ANL-6379, Metal-Water Reactions: Levitation Method, by R. E. Wilson and P. Martin, Argonne National Laboratory, 1961.

5. Webb, F. H., Jr., and others, "The Electrical and Optical Properties of Exploding Wires," Exploding Wires, Volume 2, p. 37-76, Plenum Press, 1962.

6. Long, G., "Explosions of Molten Aluminum Water-- Cause and Prevention," Metal Progress, 71, 107, 1957.

7. Atomic Energy Commission Report AECS-3664, A Study of the Reactions of Metals and Water, by H. M. Higgins, Hanford Atomic Product Operations, 1955.

8. Chace, W. G. and Moore, H. K., [eds.], Exploding Wires, Volume 1, p. 7-13, Plenum Press, 1959.

9. Metals Handbook, Ninth Edition, Volume 2, Properties and Selection: Nonferrous Alloys and Metals, p. 137, American Society for Metals, 1979.

10. Metals Handbook, Ninth Edition, Volume 3, Properties and Selection: Stainless Steels, Tool Materials and Special Purpose Metals, American Society for Metals, p. 195, 1980.

11. Brzustowski, T. A. and Glassman, I., "Vapor-Phase Diffusion Flames in the Combustion of Magnesium and Aluminum: Part II, Experimental Observations in Oxygen Atmospheres," Heterongeneous Combustions, Progress in Astronautics and Aeronautics Volume 15, p. 117-158, Academic Press, 1964.

12. Mark's Standard Handbook for Mechanical Engineers, Eighth Edition, p. 4-111, McGraw-Hill, 1978.

13. Macek, A., Friedman, R., and Semple, J.M., "Techniques for the Study of Combustion of Beryllium and Aluminum Particles," Heterogeneous Combustions, Progress in Astronautics and Aeronautics Volume 15, p. 3-16, Academic Press, 1964.

14. Landshoff, P. and Metherell, P., Simple Quantum Physics, p. 140, Cambridge University Press, 1979.

15. Fuhs, A. E., Notes on Exterior Ballistics, unpublished notes for AE 4705, p. 1-4, Naval Postgraduate School, January 1983.

16. Reference Data for Radio Engineers, Sixth Edition, p. 421, Howard V. Sims & Company, 1975.

17. Lawden, D. F., Electromagnetism, p. 64-66, George Allen and Unwin Limited, 1973.

INITIAL DISTRIBUTION LIST

		No. Copies
1.	Defense Technical Information Center Cameron Station Alexandria, Virginia 22314	2
2.	Library, Code 0142 Naval Postgraduate School Monterey, California 93940	2
3.	Department Chairman, Code 67 Department of Aeronautical Engineering Naval Postgraduate School Monterey, California 93940	1
4.	Distinguished Professor Allen E. Fuhs Code 67Fu Naval Postgraduate School Monterey, California 93940	2
5.	Professor Richard A. Reinhart, Code 61Ri Naval Postgraduate School Monterey, California 93940	1
6.	Mr. Donald E. Phillips, Code R102 White Oak Laboratory Naval Surface Weapons Center Silver Springs, Maryland 20910	1
7.	Mr. Nathaniel L. Coleburn, Code R13 White Oak Laboratory Naval Surface Weapons Center Silver Springs, Maryland 20910	1
8.	Dr. Franklin D. Hains, Code R14 White Oak Laboratory Naval Surface Weapons Center Silver Springs, Maryland 20910	1
9.	Mr. Wayne K. Reed, Code R14 White Oak Laboratory Naval Surface Weapons Center Silver Springs, Maryland 20910	1
10.	Information Services Division, Code X20 White Oak Laboratory Naval Surface Weapons Center Dahlgren, Virginia 22448	1

11. Dr. Don Kubose, Code R11 — 1
White Oak Laboratory
Naval Surface Weapons Center
Silver Springs, Maryland 20910

12. Captain Robert M. Wellborn, Jr., PMS 406 — 1
Naval Sea Systems Command
Washington, DC 20360

13. Mr. Francis J. Romano, SEA 63R3 — 1
Naval Sea Systems Command
Washington, DC 20360

14. Dr. William Sykes, Code 175 — 1
David W. Taylor Naval Ship Research
and Development Center
Bethesda, Maryland 20084

15. Mr. Raymond P. Gogolewski — 1
Defense Advanced Research Project Agency
1400 Wilson Boulevard
Arlington, Virginia 22209

16. Mr. Charles Beatty — 1
Naval Undersea Center
San Diego, California 92132

17. Mr. Robert Whitman, PMS 406 — 1
Naval Sea Systems Command
Washington, DC 20360

18. LCDR Amos E. Hallenbeck, Jr., — 2
3293 Edinburgh Drive
Virginia Beach, Virginia 23452

19. Jonathan L. Minner — 1
Naval Surface Weapons Center
Dahlgren, Virginia 22448

20. Zernow Technical Services — 1
Attn: Louis Zernow
425 W. Bonita
San Dimas, California 91773

21. Dr. Louis Baker, Jr. — 1
Argonne National Laboratories
9700 South Cass Avenue
Building 207
Argonne, Illinois 60439

22.	Professor Irvin Glassman Department of Mechanical and Aeronautical Engineering Princeton University Princeton, New Jersey 08540	1
23.	R. G. S. Sewell Code 3835 Naval Weapons Center China Lake, California 93555	1
24.	R. R. Durrell Code R12 Naval Surface Weapons Center Silver Springs, Maryland 20910	1
25.	LT Jerome Buck USS Goldsborough (DDG-20) FPO, San Francisco 96666	1
26.	LT John Strott USS Radford (DD-968) FPO New York 09586	1
27.	D. R. Kennedy Associates, Inc. 4940 El Camino Real, Suite 209 P.O. Box 4003 Mountain View, CA 94040	1
28.	Mr. J. M. McNerney Battelle Columbus Laboratories 505 King Avenue Columbus, OH 43201	1
29.	Dr. G. E. Jensen Chemical Systems Division United Technology Corporation P.O. Box 358 Sunnyvale, CA 94086	1

Thesis
H1613 Hallenbeck
c.1 Preliminary investigation on aluminum combustion in air and steam.